ARI-RR-152

AD A067900

DDC FILE COPY
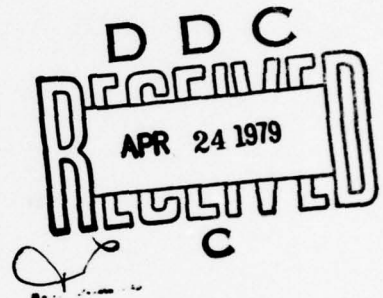
GENERATION OF DENSE FOGS FOR INFRARED
MULTIPLE SCATTERING APPLICATIONS

Final Technical Report

By

W. Cheng, J. Ebersole, M. Camac,
M. Martinez-Sanchez, and S. Kallelis

February 1979

Prepared for

Office of Naval Research
800 North Quincy Street
Arlington, Virginia 22217

79 04 24 063

SECURITY CLASSIFICATION OF THIS PAGE *(When Data Entered)*

REPORT DOCUMENTATION PAGE		READ INSTRUCTIONS BEFORE COMPLETING FORM
1. REPORT NUMBER	2. GOVT ACCESSION NO.	3. RECIPIENT'S CATALOG NUMBER
4. TITLE *(and Subtitle)* GENERATION OF DENSE FOGS FOR INFRARED MULTIPLE SCATTERING APPLICATIONS		5. TYPE OF REPORT & PERIOD COVERED Final Technical Report 9/1/77 - 8/31/78
		6. PERFORMING ORG. REPORT NUMBER ARI-RR-152
7. AUTHOR(s) W. Cheng, J. Ebersole, M. Camac, M. Martinez-Sanchez, S. Kallelis		8. CONTRACT OR GRANT NUMBER(s) N00014-77-C-0591
9. PERFORMING ORGANIZATION NAME AND ADDRESS Aerodyne Research, Inc. Bedford Research Park, Crosby Drive Bedford, MA 01730		10. PROGRAM ELEMENT, PROJECT, TASK AREA & WORK UNIT NUMBERS
11. CONTROLLING OFFICE NAME AND ADDRESS Office of Naval Research - Attn: Dr. R. Junker 800 North Quincy Street Arlington, Virginia 22217		12. REPORT DATE February 1979
		13. NUMBER OF PAGES 116
14. MONITORING AGENCY NAME & ADDRESS *(If different from Controlling Office)*		15. SECURITY CLASS. *(of this report)* Unclassified
		15a. DECLASSIFICATION/DOWNGRADING SCHEDULE

16. DISTRIBUTION STATEMENT *(of this Report)*

Approved for public release; distribution unlimited.

Final technical rept. 1 Sep 77-31 Aug 78,

17. DISTRIBUTION STATEMENT *(of the abstract entered in Block 20, if different from Report)*

18. SUPPLEMENTARY NOTES

19. KEY WORDS *(Continue on reverse side if necessary and identify by block number)*

Fog	Sonic Spray Nozzles	Multiple Scattering
Haze	Droplet Shattering	Infrared
Aerosol Generation	Agglomeration	Atmospheric Propagation
Condensation Nuclei		
Mie Scattering		

20. ABSTRACT *(Continue on reverse side if necessary and identify by block number)*

A continuous flow fog chamber was built with the fog generated by a commercially available spray nozzle. The droplet size spectrum produced resembles that of natural fog and is 10 to 100 times denser. An optical depth of 3 to 5m was obtained with the present setup, and it is feasible to decrease the optical depth (i.e., increase the fog particle density) by an order of magnitude by using multiple spray nozzles.

The spectral shape was found to be insensitive to the operating parameters of the commercially available spray nozzle. Preliminary experiments were carried out

DD FORM 1473 EDITION OF 1 NOV 65 IS OBSOLETE
1 JAN 73

S/N 0102-LF-014-6601

SECURITY CLASSIFICATION OF THIS PAGE *(When Data Entered)*

(Continued)   *micrometers*

to produce fog with a variable size spectrum. The amount of small droplets
(radius < 2 μm) produced by the nozzle can be increased or decreased by an order of
magnitude by mixing steam or hot air with the spray.   *micrometers*

Experiments were carried out to grow sodium chloride nuclei in steam by passing
the mixture through a cooled pipe. Preliminary results were very encouraging as
a significant amount of large particles (5 to 10 μm radii) were obtained by changing
the temperature of the coolant in the heat-exchanger pipe. Fog densities achieved
with these controllable, large-particle spectra were up to 100 times greater than
natural fog.

ACCESSION for

NTIS   White Section
DDC   Buff Section
UNANNOUNCED
JUSTIFICATION

BY
DISTRIBUTION/AVAILABILITY CODES
              SPECIAL

TABLE OF CONTENTS

Table of Contents (Continued)

APPENDIX A

TURBULENCE EFFECTS ON DROPLET COAGULATION

APPENDIX B

CONDENSATION OF WATER VAPOR BY MIXING WITH AIR OF LOWER TEMPERATURE

APPENDIX C

PREPARATION OF FOG DROPLETS BY COOLING OF WATER VAPOR VIA A HEAT EXCHANGER: COMPUTER SIMULATION

LIST OF ILLUSTRATIONS

List of Illustrations (Continued)

List of Illustrations (Continued)

1. INTRODUCTION

There are several technology areas of interest to the Navy for which an understanding of multiple scattering of infrared radiation by fog is an important consideration. One application is in the field of electro-optics meteorology (EO-Met), the limitations of electro-optical systems due to water. Based on this information, the Navy can determine the utility of electro-optical systems under various field conditions.

An example is optical communications between a satellite and a ship. The light beam must traverse atmospheric scenes with clouds and fog. The communication system could use laser heterodyne techniques, as discussed by Yura,[1] Lutomirski and Buser,[2] and J.P. Gollub et al.,[3] for example. However, since the usefulness depends upon the laser beam coherence, it is essential to know its degradation by multiple scattering. *It would be useful to correlate* multiple scattering data taken at different wavelengths under different weather conditions. It is important to relate visibility to atmospheric transmittance at $3.8\ \mu$m and 10.6 laser radiation in order to know the propagation characteristics of DF and CO_2 laser beams.

Another useful application is in covert communications where beam blowup by multiple scattering (in addition to atmospheric turbulence, such as described by Lutominski and Yura[4] could permit the opposition to intercept information that is

---

[1]H.F. Yura, "Optical Heterodyne Signal Power Obtained From Finite Sized Sources of Radiation," Appl. Opt. 13, 150-157 (1974).

[2]R.F. Lutomirski and R.G. Buser, "Mutual Coherence Function of a Finite Optical Beam and Application to Coherent Detection," Appl. Opt. 12, 2153-2160 (1973).

[3]J.P. Gollub et al., "Optical Heterodyne Measurement of Cloud Droplet Size Distributions," Appl. Opt. 12, 2838-2842 (1973).

[4]R.F. Lutomirski and H.T. Yura, "Propagation of a Finite Optical Beam in an Inhomogeneous Medium," Appl. Opt. 10, 1652-1658 (1971).

being transmitted. Alternatively, knowledge of multiple scattering would be useful in applications where it is desired to intercept or monitor the transmission of information by an adversary.

At present, the Navy resorts to theoretical calculation for predicting multiple scattering of infrared radiation in fogs and clouds, using experimentally determined data on refractive index and particle size distribution. (See, for example, the detailed IRIA state-of-the-art review performed for ONR by A. J. LaTocca and R.E. Turner.[5]) However, theoretical models of multiple scattering should be checked with experimental results, especially in the infrared beyond 1 μm where data is lacking. (For instance, multiple scatter data on clouds and fog have been done at 0.694 μm radiation by S.R. Pal and A.I. Carswell[6] and at 0.9 μm by J.V. Sinstanley and C. Wigmore.[7]) A multiple scattering measurement facility would also provide a means for comparing the accuracy and practicality of scattering theories and calculational methods.

An additional area of potential practical importance is knowledge of the multiple scattering properties of fog particles with different concentrations of salts from the ocean. The salt could significantly affect beam scattering, the extinction of a beam, and the multiple scattering signal. (See, for example, single scattering data by W.C. Wells et al.,[8] and by H.R. Calon et al.[9]) The method discussed in this report has the potential capability of generating sea-spray-like fogs.

---

[5] A.J. LaRocca and R.E. Turner, "Atmospheric Transmittance and Radiance: Methods of Calculation," IRIA State-of-the-Art Report, June 1975, pp. 30-33, 54-84, 441-467.

[6] S.R. Pal and A.I. Carswell, "Multiple Scattering in Atmospheric Clouds: Lidar Observations," Appl. Opt. 15, 1990-1995 (1976).

[7] J.V. Winstanley and C. Wigmore, "A Multiple Scattering Correction For Lidar Systems," AGARD Conf. Proc. No. 183 (Oct. 1975), pp. 27-1 to 27-13.

[8] W.C. Wells et al., "Aerosol Distributions in Maritime Air and Predicted Scattering Coefficients," Appl. Opt. 16, 654-659 (1977).

[9] H.R. Carlon et al., "Infrared Extinction Spectra of Some Common Liquid Aerosols," Appl. Opt. 16, 1598-1605 (1977).

It is well known (see for instance articles by Zuev et al.[10-12]) that the Soviets are doing a large amount of research, both theoretical and experimental, in the field of light scattering in fogs, hazes, and the atmosphere (both single and multiple).

In summary, because multiple scattering is difficult to predict theoretically, although it is a tractable problem, experimental data would be useful in understanding the phenomenon.

Section 2 briefly reviews field measurements of fog parameters. Section 3 discusses absorption and single and multiple scattering of fog. Section 4 examines requirements on fog generation for multiple scattering applications, including analyses on particle agglomeration causes. Section 5 gives a detailed discussion of the Aerodyne fog facility, included automated particle counting data acquisition, fog-jet spray nozzle operating parameters, fog chamber, and unique particle counter dilution technique. Data analysis is provided in Section 7, especially variation of nozzle parameters on fog generation in relation to natural fog measurements. Section 8 discusses two other main fog generation mechanisms investigated: fog particle condensation on nuclei by either mixing with cold air or by cooling with a cold-wall heat exchange. The latter method appears to hold the greatest potential for controllable generation of large fog particles ($\gtrsim 5\mu$m radius)

[10] V.E. Zuev, "Laser-Light Transmission Through the Atmosphere," Laser Monitoring of the Atmosphere, E.D. Hinkley, Ed. (New York, Springer Verlag, 1976).

[11] V.E. Zuev, Propagation of Visible and Infrared Radiation In The Atmosphere, (New York, Wiley, 1974).

[12] V.E. Zuev, M.V. Kabanov, and B.A. Savelov, "Propagation of Laser Beams In Scattering Media," Appl. Opt. 8, 137-141 (1971).

2. NATURAL FOG MEASUREMENTS IN THE FIELD

Table 1 gives a listing of some measurements which have been made on natural fog. The average particle radius lies somewhere between 0.1 - 10 μm, and the mean or most probable particle radius is somewhere between 4 - 6 μm. The typical particle concentration is on the order of 100 to 500 cm^{-3}, with a maximum mass loading on the order of 0.9 g/m^3.

Table 1

Natural Fog Measurements In The Field

	Particle Radius Range (μm)	Most Probable Particle Radius (μm)	Maximum Concentration (cm^{-3})	Maximum Mass Loading (g/m^3)
Institute d'Optique (Arnulf and Bricard)[13]	1 to 8	4 to 6	Unknown	Unknown
Rand Corporation (Deirmendjian)[14]	1 to 9	4	100	Unknown
Atmospheric Sciences Laboratory (WSMR) (Pinnick, et al.)[15]	1 to 10	5	Unknown	0.002 - 0.9
Review (by Zuev)[16]	Unknown	5	Unknown	10^{-4} - 0.6
M. Diem (Referenced by Yamamoto, et al.)[17]	1 to 3	4	450	0.28

[13] A. Arnulf and J. Brichard, "Transmission By Haze and Fog In The Spectral Region 0.35 to 10 Microns," J. Opt. Soc. Am. 47, 491-498 (1957).

[14] D. Deirmendjian, "Scattering and Polarization Properties of Water Clouds and Hazes In The Visible and Infrared," Appl. Opt. 3, 187-196 (1964).

[15] R.G. Pinnick, J.D. Lindberg, and E.B. Stenmark, "Vertical Inhomogeneity In Wintertime Atmospheric Fog and Haze In West Germany and the Effects on IR Transmission," Unclassified report of the Atmospheric Sciences Laboratory, White Sands Missile Range (1976).

[16] V.E. Zuev, Propagation of Visible and Infrared Radiation In The Atmosphere, (New York, Wiley, 1974), pp. 168-177.

[17] G. Yamamota, M. Tanaka, and S. Asano, "Radiative Transfer In Water Clouds In The Infrared Region," J. Atm. Sci. 27, 282-292 (1970).

A typical fog particle distribution as given by Deirmendjian[14] is:

$$N(R) = 0.024 \, N_D \, R^6 \, e^{-1.5 \, R} \qquad .$$

(2-1)

Here, $N(R)$ is in units of $cm^{-3} \, \mu m^{-1}$, N_D is in cm^{-3}, R is in μm. Figure 1a shows a typical fog particle distribution according to Deirmendjian; note the peak at $R = 4 \, \mu m$. More realistically, fog is composed of a superposition of two or more modes, as shown in Fig. 1b.
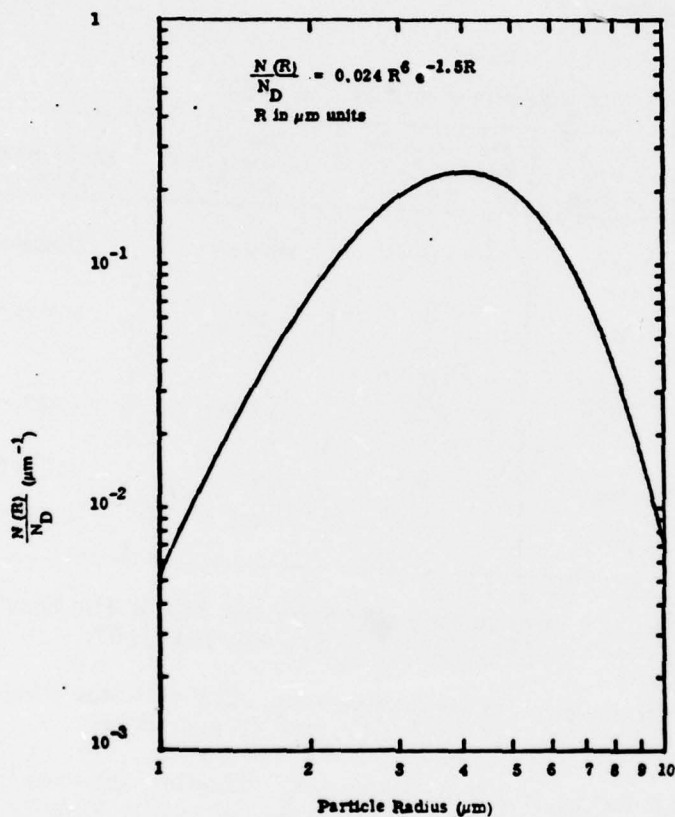
Figure 1a. Typical Single-Mode Fog Particle Distribution (Deirmendjian).[14]

Figure 1. Fog Particle Distributions.

2-2
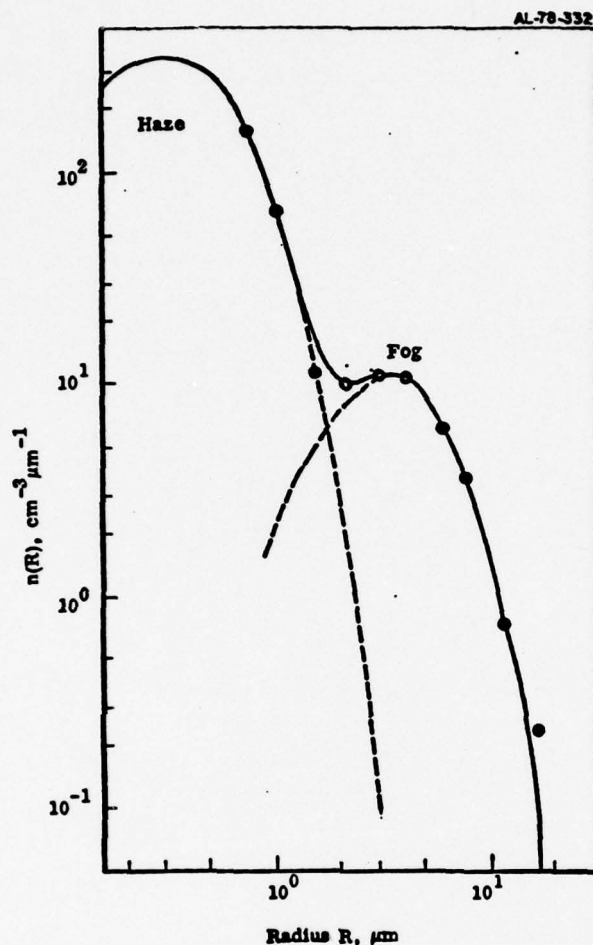
Figure 1b. Typical Bimodal Fog and Haze Particle Size Distribution.[18]
The Circles Represent Actual Measurements. The Solid Line
Represents a Bimodal Curve Fit Through the Data. The Haze
and Fog Modes Are Similar to "Haze M" and "Cloud" Models
of Deirmendjian.

Figure 1. (Continued)

[18]C. Tomasi and F. Tampieri, "Size Distribution Models of Small Water Droplets
in Mist and Their Volume Extinction Coefficients at Visible and Infrared
Wavelengths," Atm. Environ. 10, 1005-1013 (1976).

3. MULTIPLE SCATTERING

Multiple scattering occurs when the scattering mean free path Λ_{mfp} is much less than the optical path L, and the scattering dominates absorption. It is convenient to set the optical depth of the medium, which is the reciprocal of the scattering coefficient k_{scat}, equal to Λ_{mfp}, i.e.,

$$\Lambda_{mfp} = 1/k_{scat} \qquad . \tag{3-1}$$

For example, for a monodisperse distribution of aerosols of radius $\overline{R}$,

$$1/\Lambda_{mfp} = k_{ext} = N_D \, \pi \overline{R}^2 \, Q_{scat} \qquad , \tag{3-2}$$

where N_D is equal to the number of particles per unit volume and Q_{scat} is the Mie scattering efficiency.

In order to understand the angular effect of multiple scattering, it is useful to first perform calculations for single scattering. Figures 2 through 5 show the proportion of scattering due to four different radii water aerosols as a function of angle from 0 to 180°. The refractive index used was m = 1.363 - 0.00345i for a wavelength $\lambda = 3.8 \, \mu$m (interpolated from Irvine and Pollack[19]). The quantity $(I_1 + I_2)/2$ represents the average of the proportional amount of light scattered for vertical and horizontal polarizations, as calculated from Mie scattering theory.

It may be seen that the back scattering at 180° is virtually nonexistant for fog particles with a radius greater than 1 μm; it is well known that most single scattering for larger particles is in a forward lobe near $\theta = 0^o$.

---

[19]W.M. Irvine and J.B. Pollack, "Infrared Optical Properties of Water and Ice Spheres," Icarus 8, 324-360 (1968).
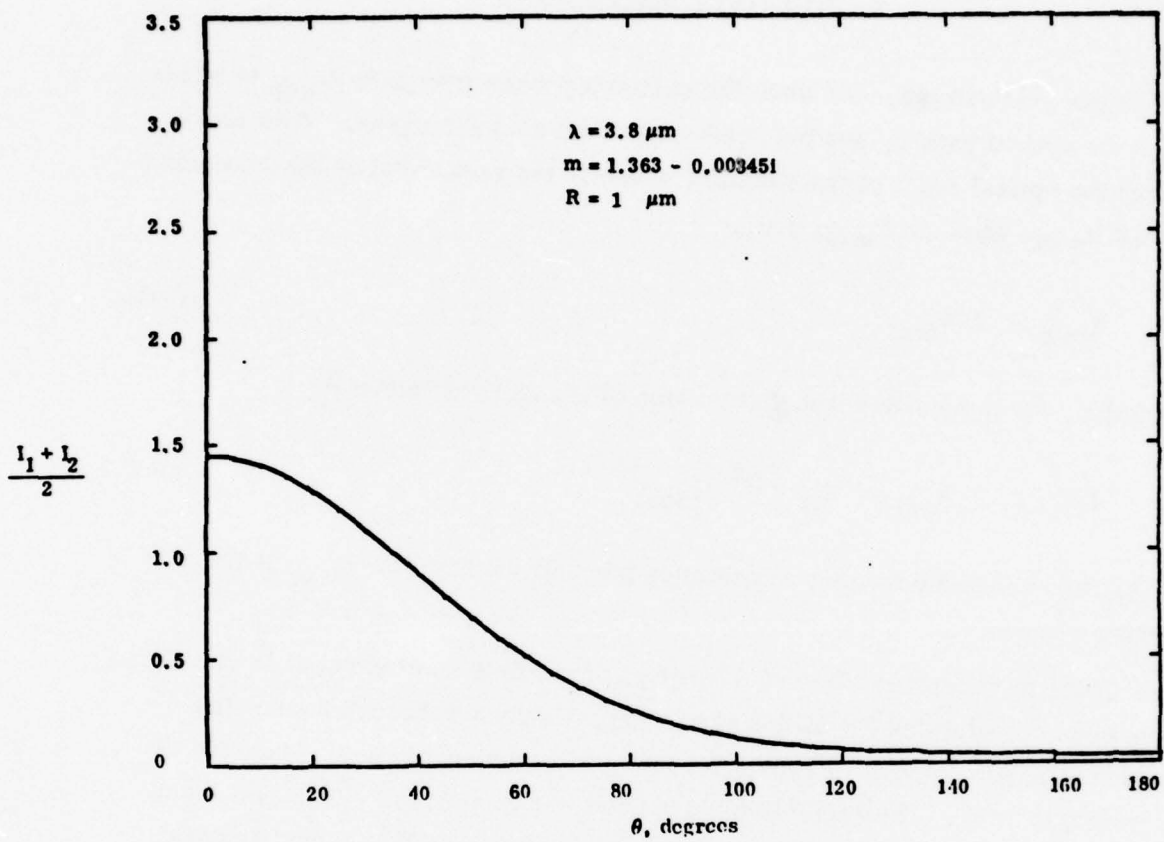
Figure 2. Single Scattering as a Function of Angle for Particle
Radius R = 1 μm

$$\lambda = 3.8 \ \mu m$$
$$m = 1.363 - 0.00345i$$
$$R = 2 \ \mu m$$
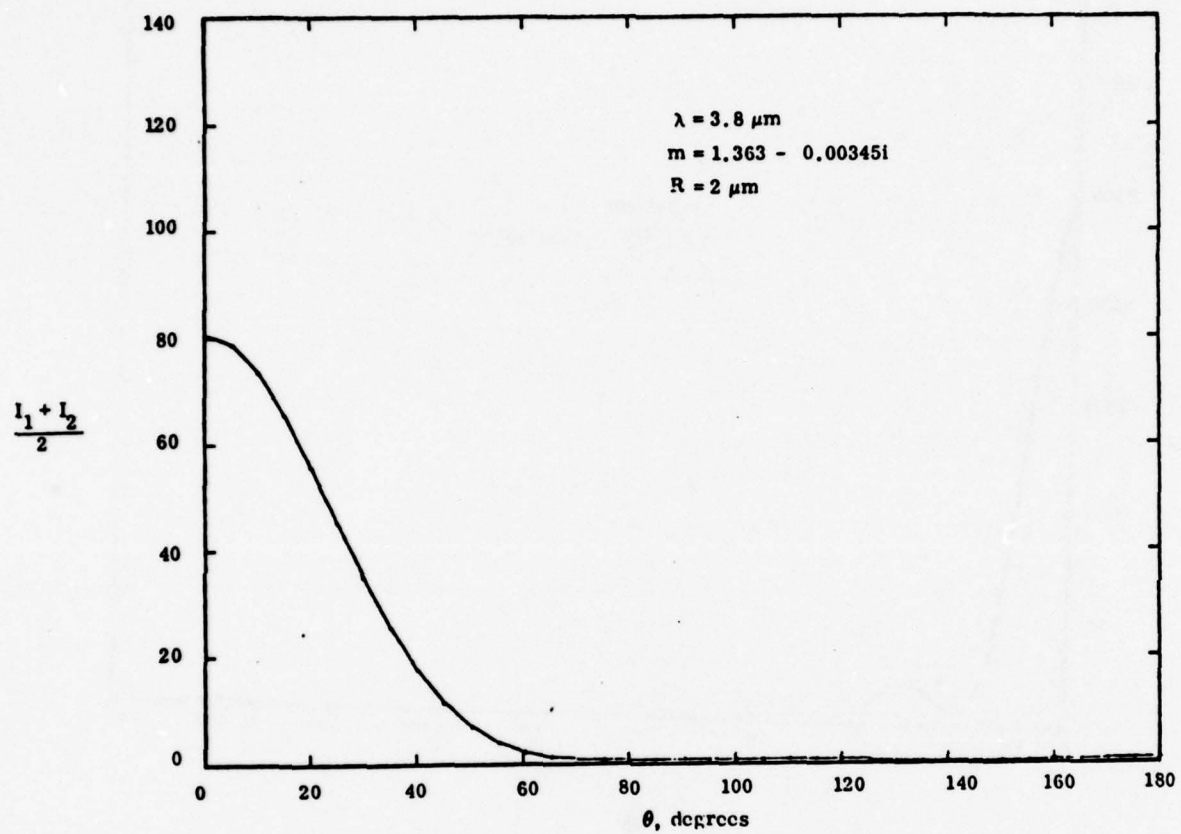
Figure 3. Single Scattering as a Function of Angle for Particle Radius R = 2 μm
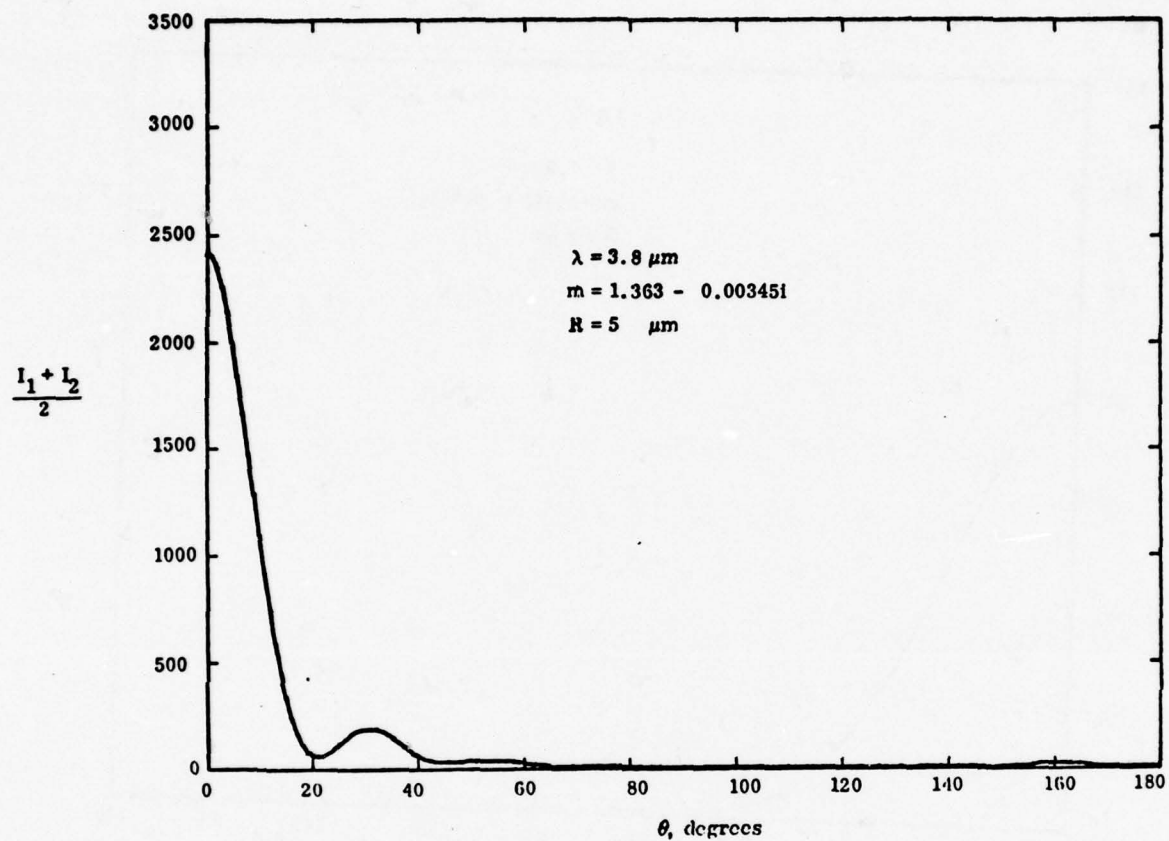
Figure 4. Single Scattering as a Function of Angle for Particle
Radius R = 5 μm
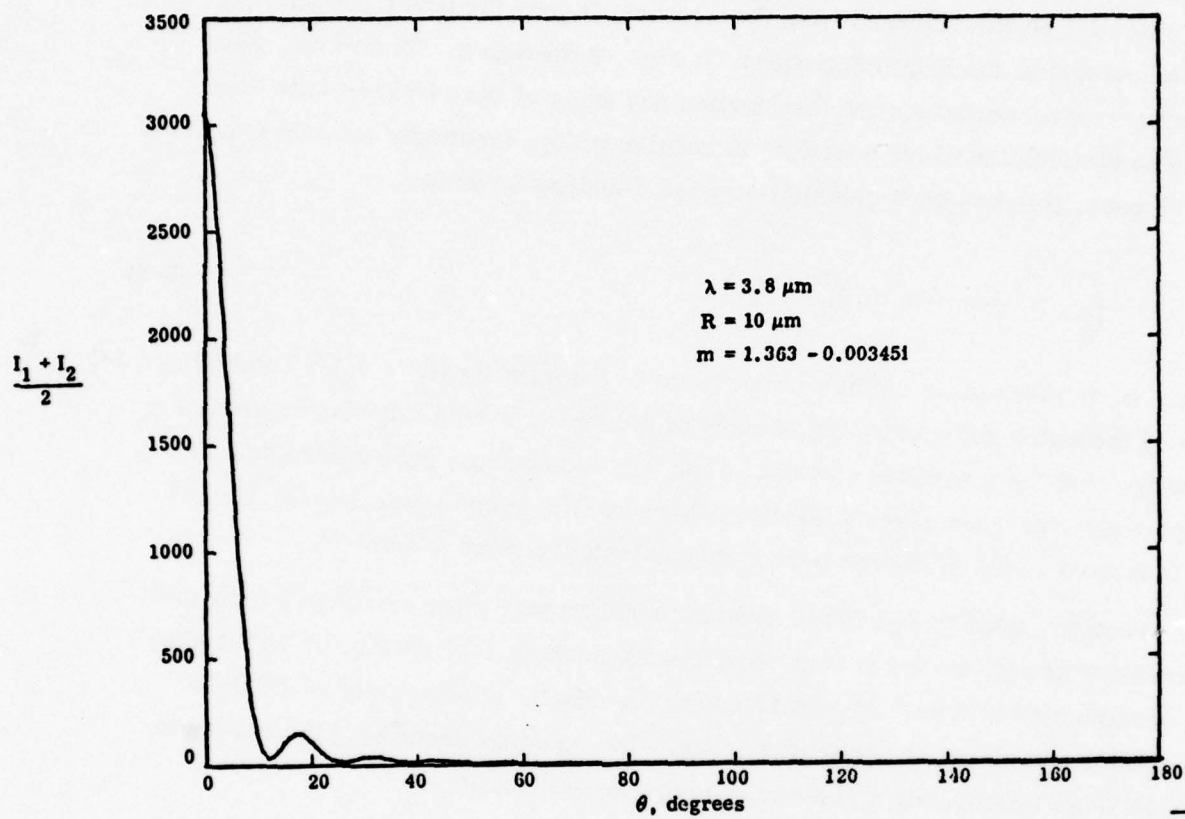
Figure 5. Single Scattering as a Function of Angle for Particle
Radius R = 10 μm

Figures 6 through 9 are plots of the relative angular scattering for what might be considered a multiple scattering situation. In this case, the assumption has been made that as a photon scatters from the aerosol, it goes through a random walk process subject to the scattering shown on Figs. 2 through 5. Therefore, after suffering several collisions the distribution and angle of the radiation take on a Gaussian distribution which broadens in angular width, eventually extending to 180°. In each case, this has been calculated by the following formula:

$$\frac{I}{I_0} = \exp\ (-\theta^2/n\theta_0^2) \qquad .\qquad\qquad (3-3)$$

Here, θ_0 is taken to be the half power point of the quantity $(I_1 + I_2)/2$, and n in Figs. 6 through 9 represents the number of scattering events. It may be seen, for instance, that for a particle radius of 5 μm (which is a most probable radius for a fog particle) that even after 50 scatters there is almost no backscattering at 180° and that most of the scattered light is concentrated between 0 and 90°.

Further, even though fog is almost nonabsorbing, after much scattering and traversals through the fog in this random walk method, the laser beam absorption can become appreciable. Figure 10 shows the results of absorption of DF laser radiation due to multiple scattering in fog. The equation describing the curves in Fig. 10 is as follows (for a given monodisperse distribution):

$$\frac{I_n}{I_0} = \exp\ (-k_{abs} L) = \exp\ (-\pi\bar{R}^2 Q_{abs} N_D\ n\Lambda_{mfp}) \qquad . \qquad (3-4)$$

From Eq. (3-2) $N_D = 1/\pi\bar{R}^2 Q_{scat}\Lambda_{mfp})$; therefore, Eq. (3-4) becomes:

$$\frac{I_n}{I_0} = \exp\ (-n\ Q_{abs}/Q_{scat}) \qquad . \qquad (3-5)$$

3-6

Relative Angular Scattering

1.0

0.8

0.6

0.4

0.2

0

n = 50

n = 20

n = 10

$R = 1 \ \mu m$

$\theta_o = 44^o$

$\left[\dfrac{(I_1 + I_2)}{2}\right]_{\theta = 0^o} = 1.45$

0   20   40   60   80   100   120   140   160   180

θ, degrees
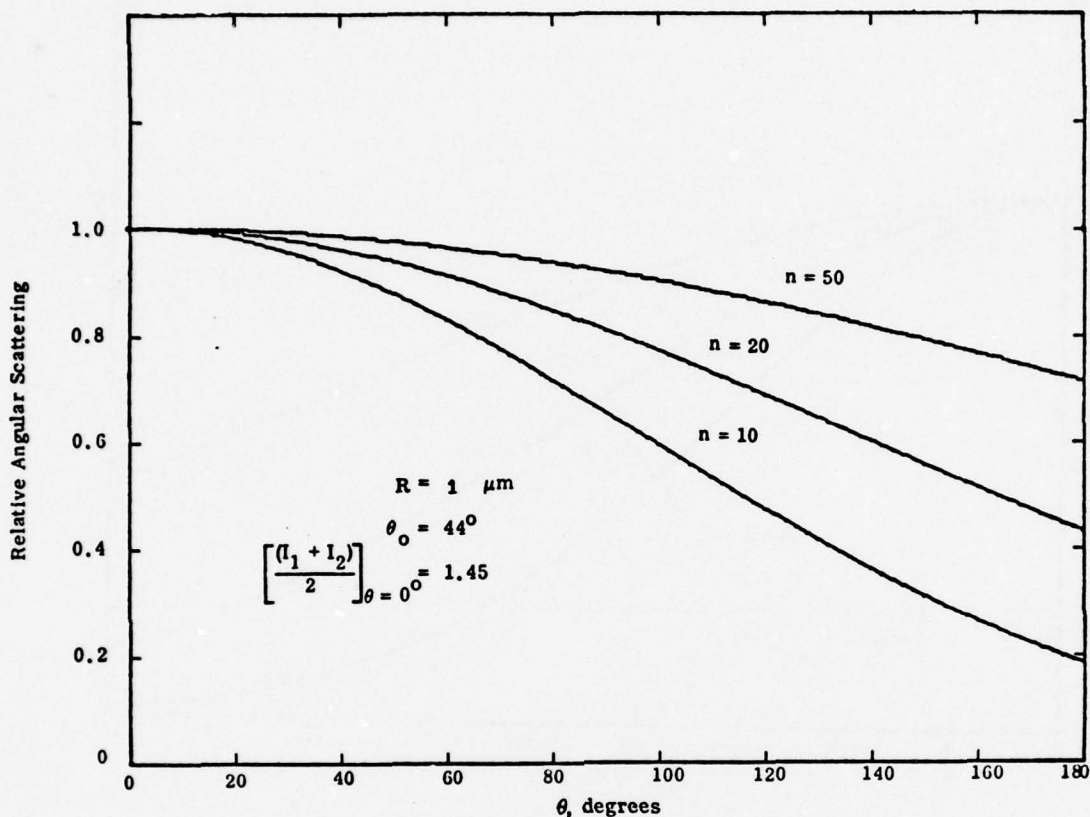
Figure 6. Multiple Scattering for Particle Radius $R = 1 \ \mu m$;
n is the Number of Scattering Events

It may be noticed that for a particle radius of 5 μm and n = 50 scatterings, the light
is attenuated to about 10%. In fact, the value of I_n/I_0 never exceeds 30 - 40% for
any particle radius for n = 50 particle scatterings. This information taken together
with Figs. 6 through 9 suggests that virtually no light at DF laser radiation wave-
lengths will be backscattered at 180° without severe attenuation, and that what light
does get backscattered due to multiple scattering will be due primarily to the smaller
radius particles.
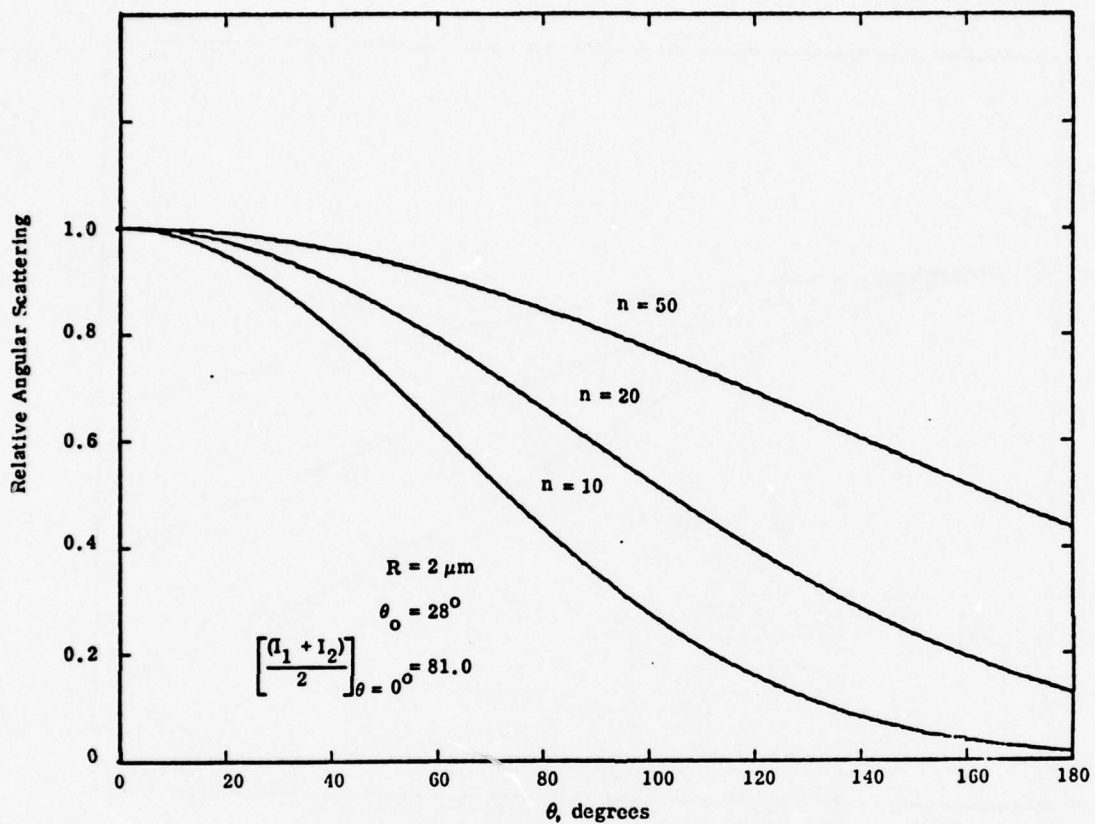
Figure 7. Multiple Scattering for Particle Radius R = 2 μm; n Is the Number of Scattering Events
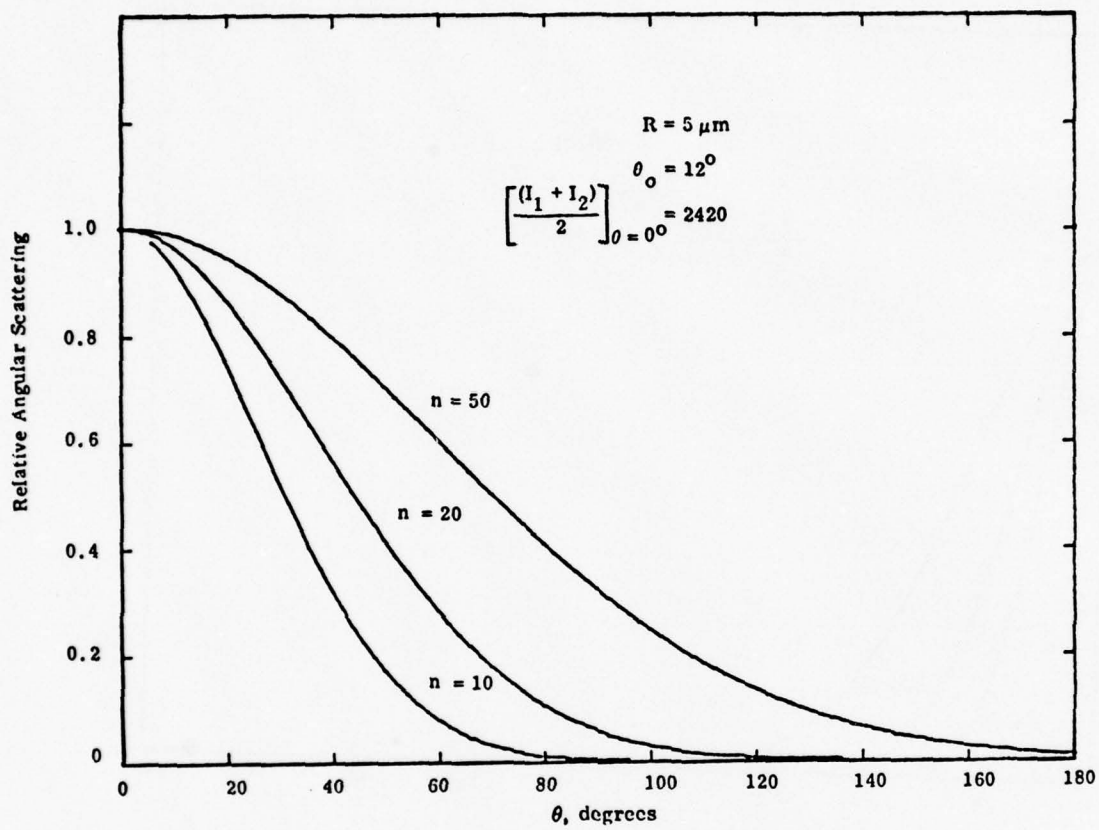
Figure 8. Multiple Scattering for Particle Radius R = 5 μm; n Is the Number of Scattering Events

3-9
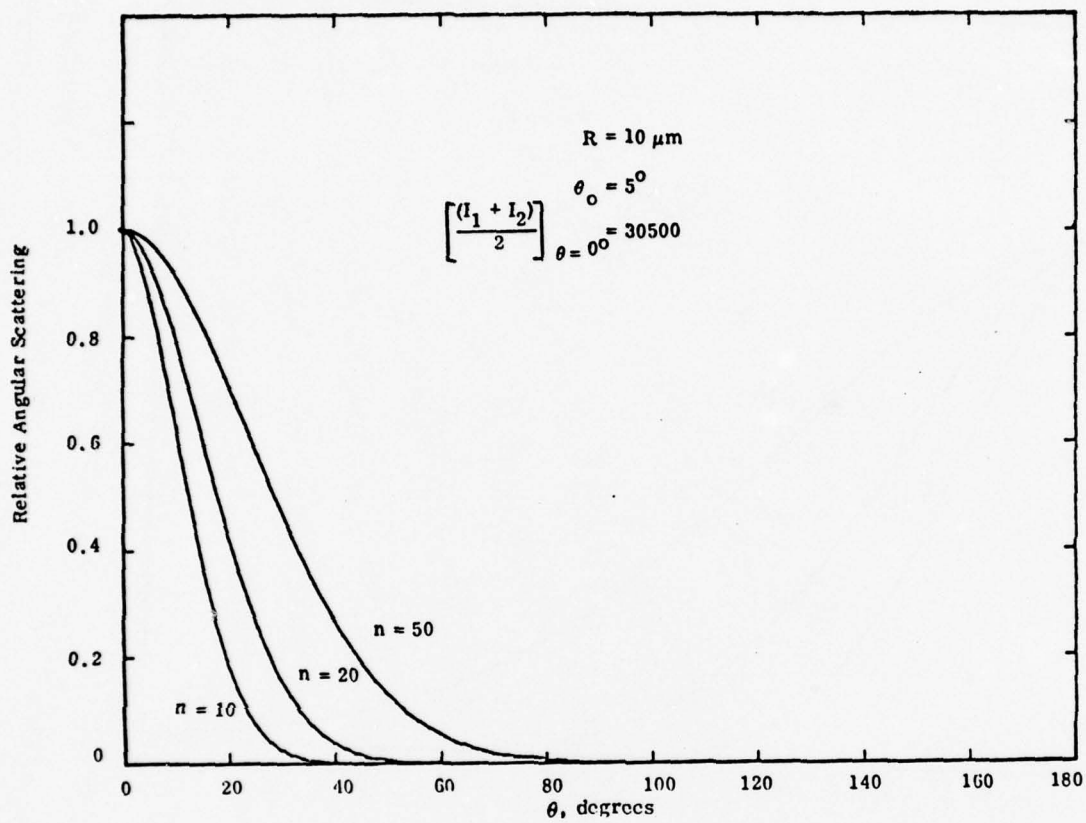
Figure 9. Multiple Scattering for Particle Radius R = 10 μm; n Is the Number of Scattering Events

The figure shows transmission I_N/I_O versus Monodisperse Particle Radius (μm) on log-log scale, with curves labeled n = 10, n = 20, and n = 50.

Labels within plot:
H_2O
$m = 1.36 - 0.003i$
$\lambda = 3.8\ \mu m$
(n = number of times light is scattered)

Y-axis: Transmission, I_N/I_O

X-axis: Monodisperse Particle Radius (μm)
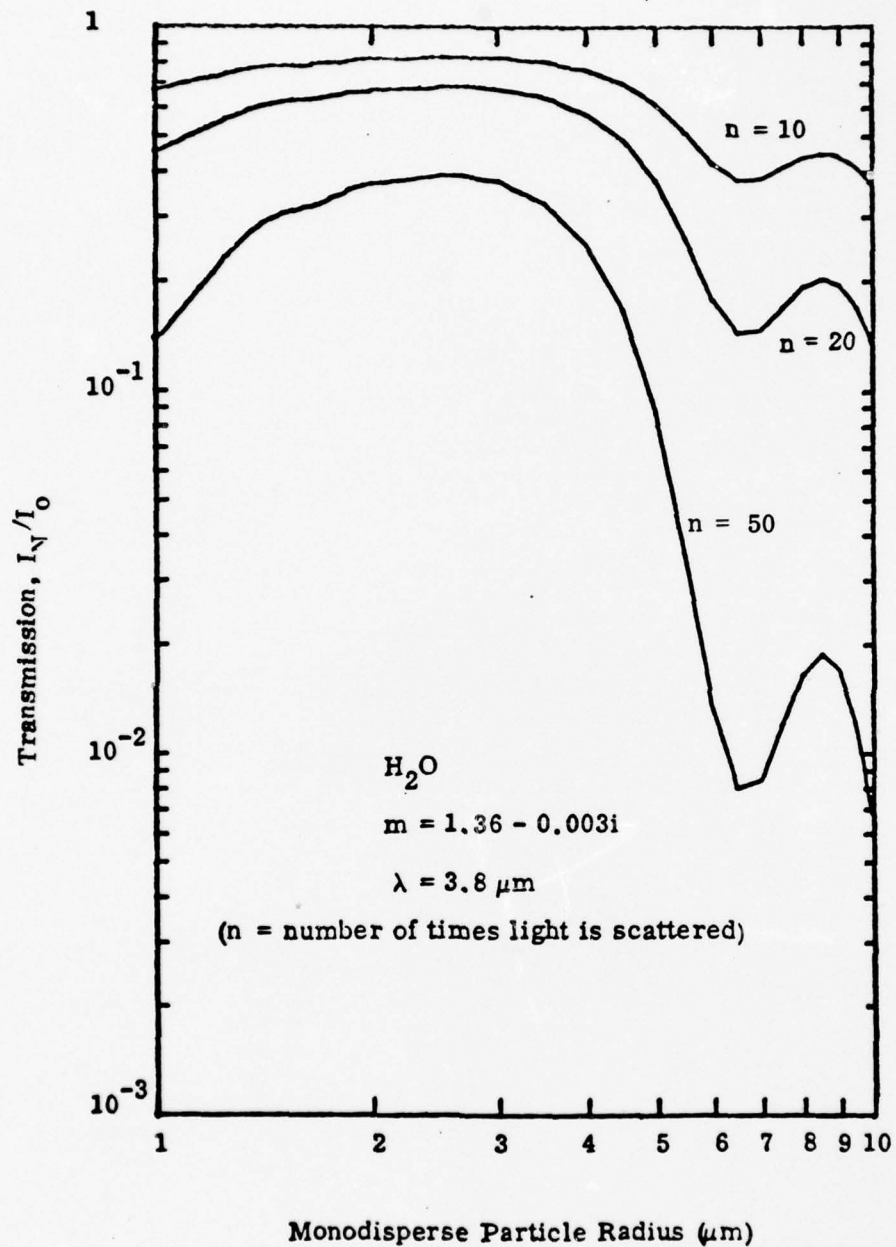
Figure 10. Effect of Absorption on the Transmission of DF Laser Radiation Due to Multiple Scattering in Fog; Here, the Loss in Transmission Due Only to Absorption After (n) Scattering Events Is Included

3-11

4. FOG GENERATION

Table 2 presents a summary of some of the known techniques for artificially generating fog for experiments. Perhaps the most important thing to note is that none of the chambers were capable of generating a fog which could last more than 20 minutes, i.e., the fog dissipated in time. It may be seen at the bottom of Table 1 that use of an aerosol spray, which will be continuously flowing, has the potential for producing a nondissipating fog.

A description is given below of the required parameters for generating fog in order to perform multiple scatter experiments. The essential design criterion is that the density of particles be sufficient to produce an optical depth $1/k_{scat}$ which is about one-tenth the dimension (in a given direction) of the fog chamber.

4.1 Required Particle Density

Figure 11 shows a plot of number of particles per cm^3 required to perform multiple scatter experiments for two different mean free paths as a function of particle radii, with the assumption of monodisperse particle distribution. For particle radii in the 4 to 5 μm radius region, it may be seen that for a mean free path of about 50 cm, approximately 10^4 cm^{-3} would be required at $\lambda = 3.8\,\mu m$; for a mean path of 10 cm, approximately 5×10^4 cm^{-3} would be required. Those curves were generated from Eq. (3-2).

Figure 12 shows the required mass loading for the multiple scatter experiment. This was obtained from Fig. 11 by multiplying the particle density by mass density and particle volume. It may be seen that for particle radii on the order of 4 to 5 μm, anywhere from 3 to 30 g/m^3 is required for a multiple scatter experiment. It may be noted that the published value mass loading from commercially available sonic spray nozzles is on the order of 1000 g/m^3. More will be said later on this value.

Table 2

Artificial Fog Generation

Laboratory	Technique	Size of Chamber (m^3)	Particle Radius Range (μm)	Most Probable Particle Radius (μm)	Maximum Concentration (Particles/ cm^3)	Mass Loading (g/m^3)	Comments
Army Corps of Engineers (N.H.) (Munis and Delaney)[20]	Cooling of steam to -4°C	4	1 to 10	3.5	260	Unknown	Dissipated in 10 to 15 minutes after initial injection
Army Corps of Engineers (N.H.) (Munis and Delaney)[21]	Cooling of steam to -43°C	4	2 to 12	6.5 (ice fog)	170	Unknown	Dissipated in 10 to 15 minutes
Siberian Physics – Technical Institute USSR (Zuev, et al.)[22]	Unknown	15	2 to 12	4 to 6	900	0.6	Dissipated
Aeronutronic-Ford (Reisman, et al.)[23]	Cooling of saturated air	0.4	Unknown (1 to 9 estimated)	2 to 4	Unknown	Unknown	Dissipates in 10 to 20 minutes
Aerodyne Laboratory Experiment	Aerosol Spray	250	Unknown (1 to 10 estimated)	5	5×10^4 (equivalent mono-disperse density)	3 - 30	Non dissipating

[20] R.H. Munis and A.J. Delaney, "Simultaneous Measurement of Laser Extinction in Warm Fog at Wavelengths of 0.6328, 1.15 and 10.6 Microns," Army Research Report 343, October 1975, Army Corps of Engineers, Hanover, N.H.

[21] R.H. Munis and A.J. Delaney, "Measurements of Laser Extinction in Ice Fog for Design of SEV Pilotage System," Army Research Report 302, August 1972, Army Corps of Engineers, Hanover, N.H.

[22] V.E. Zuev et al., "Attenuation of Visible and Infrared Radiation by Artificial Water Fogs," Izv., Atm. and Ocean. Phys. Ser. 1, 509-516 (1965), trans.

[23] E. Reisman, G. Cumming, and C. Bartky, "Comparison of Fog Scattered Light and Monochromatic Incoherent Light," Appl. Opt. 6, 1969-1972 (1967).

Figure 11. Required Particle Density, N_D, for Multiple Scatter Experiment

4-3
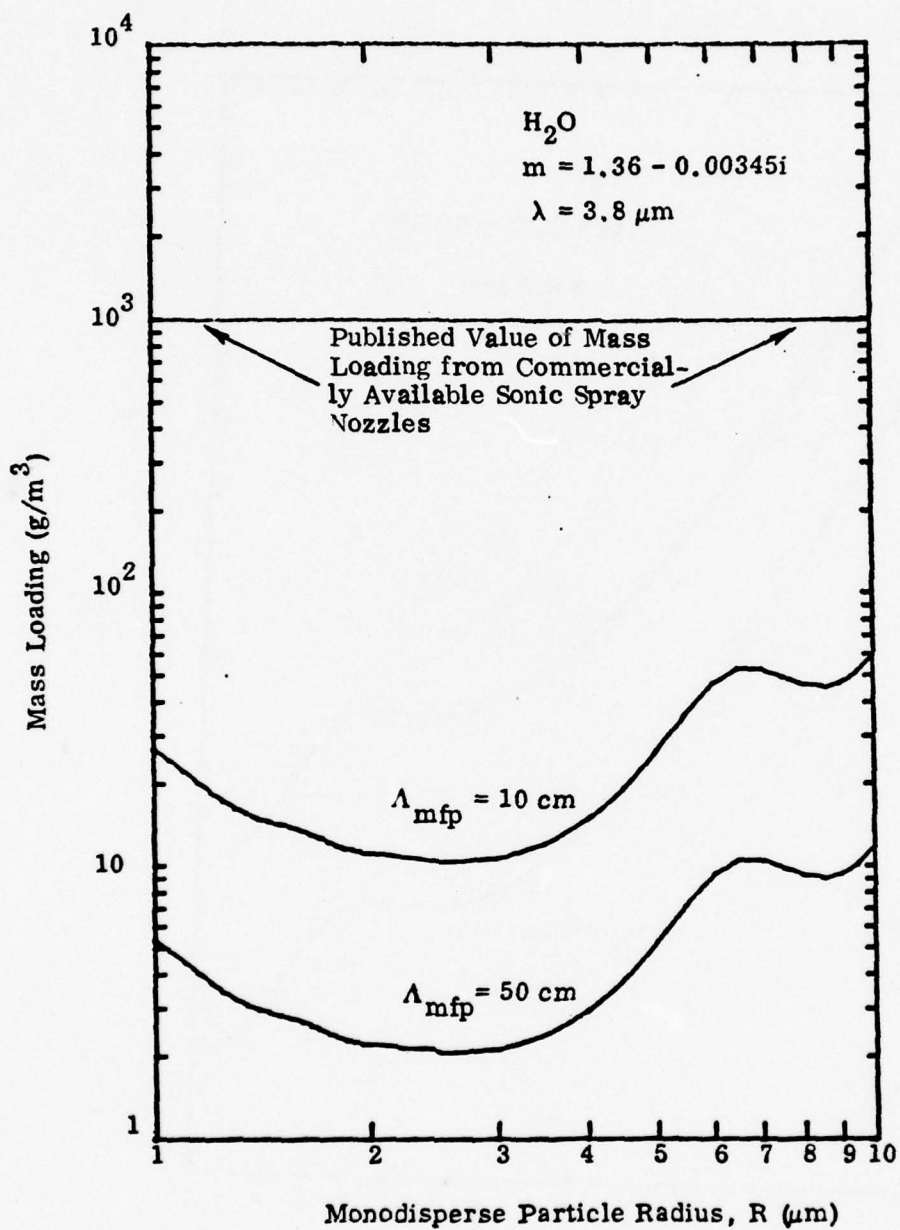
Figure 12. Required Mass Loading for Multiple Scatter Experiment

4.2 Agglomeration

4.2.1 Rate of Agglomeration

If one defines the mean time τ_2 between collisions of particle radius R_2 and velocity V_2 in a cloud of particles of R_1, V_1, and density N_{DI}, then

$$\tau_2^{-1} = \sigma_{21} \, V_{21} \, N_{DI} \qquad , \tag{4-1}$$

where $\sigma_{21} = (R_2 + R_1)^2$ and $V_{21} = \left| V_2 - V_1 \right| = $ the relative velocity between particles. For this case, the rate of agglomeration of particle R_1 in a cloud of R_2 particles of density N_{D2} is given by:

$$\frac{dN_{D1}}{dt} = \frac{N_{D2}}{\tau_2} \qquad , \tag{4-2}$$

or

$$\frac{d \log N_{D1}}{dt} = \tau_2^{-1} \; \frac{N_{D2}}{N_{D1}} = \frac{1}{\tau_1} \qquad . \tag{4-3}$$

Thus, the agglomeration time τ_1 (for the e^{-1} point of agglomeration) is:

$$\frac{1}{\tau_1} = \sigma_{21} \, V_{21} \, N_{D2} \qquad . \tag{4-4}$$

4.2.2 Turbulence

Appendix A gives a detailed description and analysis of the effects of turbulence on agglomeration of fog particles. The results of that analysis show that turbulence effects will not be significant in either the region near the spray nozzle or far away from the nozzle in the fog chamber. If anything, gravitational settling may possibly have a more significant impact.

4.2.3 Brownian Motion

According to the equipartition theorem, the mean square velocity of a particle of radius R_i and mass m_i is given by:

$$\langle V_i^2 \rangle = \frac{3kT}{m_i} \tag{4-5}$$

where

$$m_i = \rho \frac{4}{3} \pi R_i^3 \quad , \tag{4-6}$$

and ρ is the mass density, k is Boltzmann's constant, T is the temperature.

In this case, using Eq. (4-4) and the approximation $\langle V_i \rangle \cong \langle V_i^2 \rangle^{1/2}$, the agglomeration rate is described by the following equation

$$\frac{1}{\tau_1} = \frac{3}{2} \left(\frac{\pi kT}{\rho} \right)^{1/2} (R_2 + R_1)^2 \left| R_2^{-3} - R_1^{-3} \right|^{1/2} N_{D2} \quad . \tag{4-7}$$

Figure 13 is a plot of Brownian motion agglomeration of a Deirmendjian distribution for $\Lambda_{mfp} = 50$ cm. The agglomeration time τ_1 is plotted on the verticle axis, the particle radius R_1 on the horizontal axis. It may be seen that the agglomeration time for a particle of $R_2 = 1$ μm falling in a fog will be no less than 10^4 sec. For a particle size of $R_2 = 4$ μm, which is a maximum particle radius for many fogs, the agglomeration occurs no faster than 10^3 sec. With a transit time of the fog through the chamber of about 50 sec, Brownian motion will be negligible as a cause for water droplet agglomeration in a fog chamber.

4.2.4 Gravitational Settling

The equation for the terminal or settling velocity V_s is given by:

$$mg = \rho \frac{4}{3} \pi R^3 = 6 \pi \eta R V_s \quad , \tag{4-8}$$

4-6
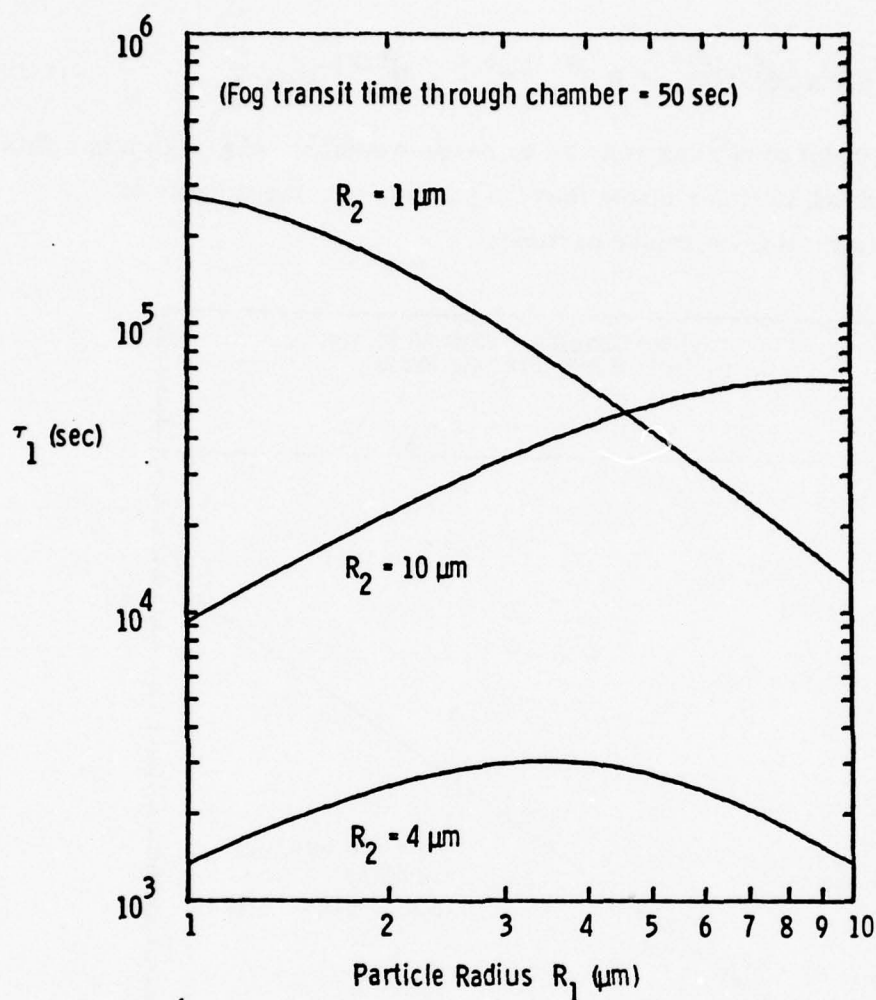
Figure 13. Brownian Motion Agglomeration Rate for Λ_{mfp} = 50 cm

where m is the mass of the particle, g is acceleration of gravity, ρ is the density of water, η is the viscosity of air. Solving for the settling velocity produces:

$$V_s = \frac{2R^2 g\rho}{9\eta} \qquad . \qquad (4-9)$$

Empirically (from the Stanford Research Institute Chart on the Characteristics of Particles) $V_s = 6.8 \times 10^5 R^{1.9}$ for V_s in cm/sec, and R in cm. For this situation, using Eq. (4-4), the agglomeration time is described by the following equation;

$$\frac{1}{\tau_1} = 6.8 \times 10^5 \ \pi (R_1 + R_2)^2 \ \left| R_2^{1.9} - R_1^{1.9} \right| \ N_{D2} \quad . \tag{4-10}$$

Figure 14 is a plot of settling velocity vs particle radius. Also shown is a flow velocity, which is about 10 times faster than the particle settling velocity of 10 cm/sec, which is for a 5 μm radius particle.
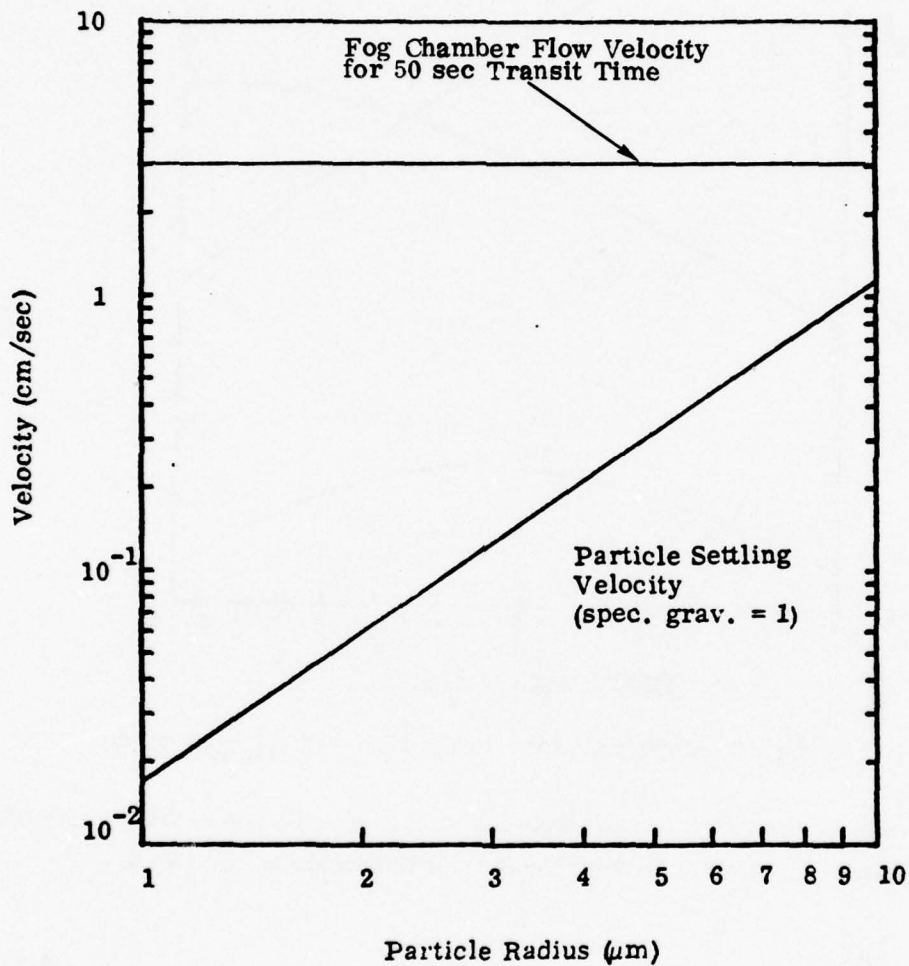
Figure 14. Gravitational Settling. (Source for particle settling velocity: Stanford Research Institute Chart on the Characteristics of Particles, 1961.)

4-8

Figure 15 shows the gravitational agglomeration time for a mean free path of 50 cm. The curves in this figure describe the effect of a larger particle of radius R_2 falling through a particle distribution described by Deirmendjian. For instance, it may be seen that as the size of particle R_2 approaches R_1, the time of agglomeration approaches infinity since both particles are falling at the same rate and one never catches up to the other. It turns out for this situation that as one goes to larger and larger particle radii R_2, one might expect a larger amount of agglomeration due to faster settling velocities. However, this is offset by the fact that larger and larger
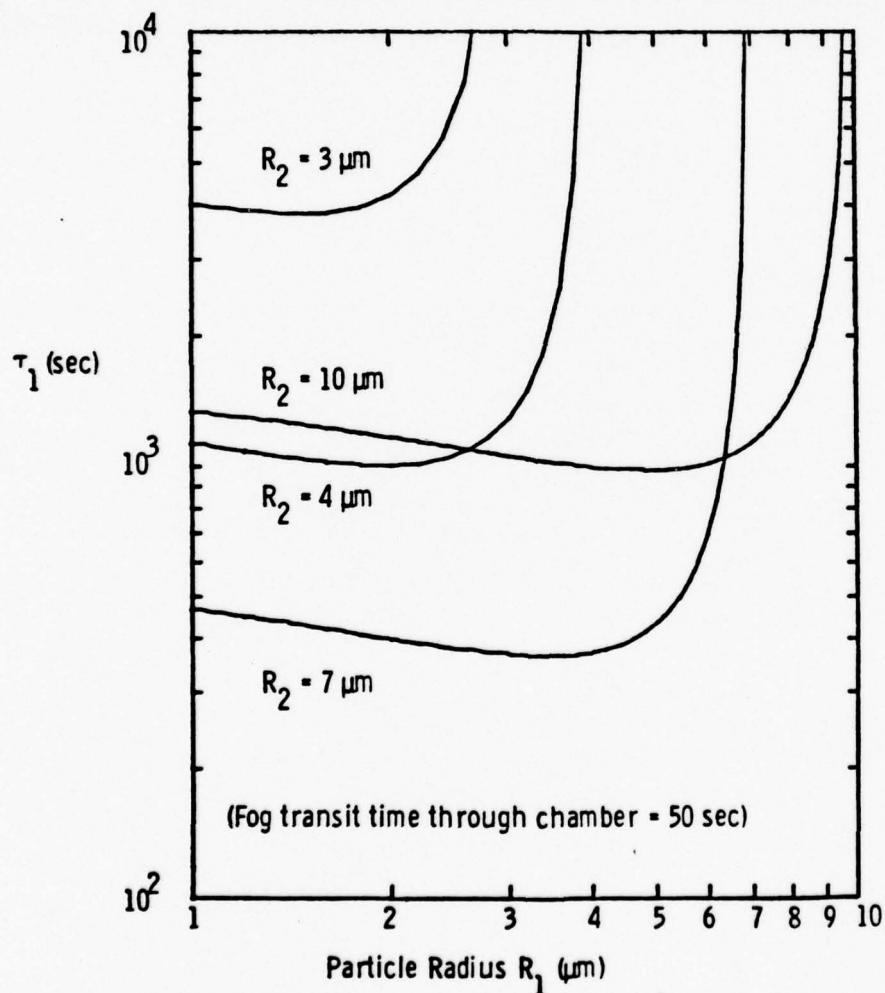
Figure 15. Gravitational Agglomeration Rate for Λ_{mfp} = 50 cm

particle radii are less frequent in number according to a typical fog particle distribution. The point at which a combination of the two produces the greatest amount of agglomeration occurs for a value of R_2 equal to about $7 \, \mu m$. In this case, as shown in Fig. 15, agglomeration occurs in about 400 sec. Again, it is worth pointing out the fog transit time through the chamber can be made to occur on the order of 50 sec, or almost 10 times faster than this agglomeration rate. Actually, the situation is even better than this; it says that approximately 10% of the fog has agglomerated only by the time it reaches the bottom. At the top, of course, there is virtually no agglomeration, and at the middle there is at most 5%, so this may be an overly conservative estimate of the effective agglomeration time due to gravitational settling.

5. DESCRIPTION OF APPARATUS

5.1 Concept

The key concept in the design of the fog chamber is to obtain a continuous flow of fog so that steady state operation is achieved. The components involve a fog generator from which the fog droplets are mixed with and carried away by a continuous stream of air to obtain a continuous flow of fog. By employing air of relative humidity equal to 1, no evaporation or condensation of the fog droplets takes place, thus the original particle size spectrum of the generated fog can be preserved.

The spray nozzle is used to generate the fog. By adjusting the parameters of the nozzle, some control of the size spectrum can be achieved. This will be described in further detail in Subsection 5.2.

The overall schematic of the experiment is shown in Fig. 16. The different components will be described in the following sections.
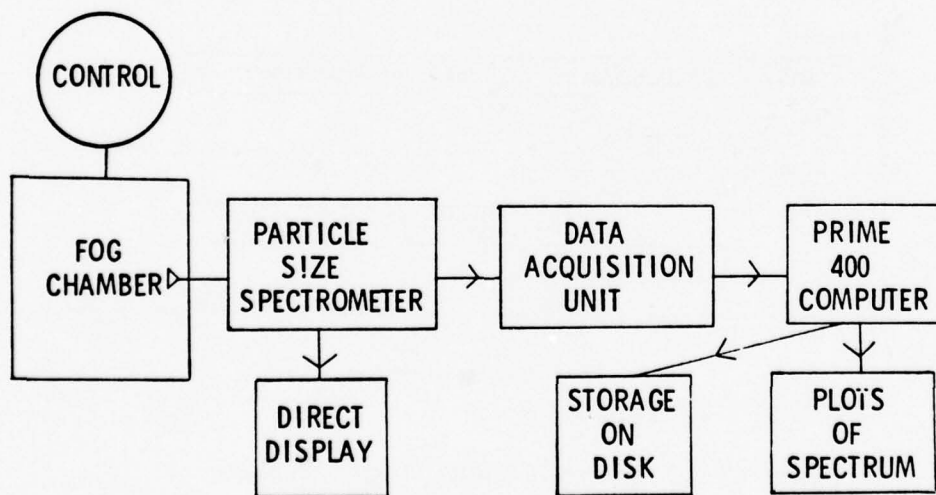
Figure 16. Overall Schematic of Fog Experiment

5.2 Sonimist Spray Nozzles

The fog is generated by a spray nozzle with the droplet size spectrum controlled by the characteristic of the nozzle. Nozzles from a line called Sonimist, manufactured by Heat Systems Ultrasonics, Inc. (38 East Mall, Plainsview, NY 11803) are used. According to the manufacturer, this series of nozzles can give adjustable droplet sizes of 1 to 30 μm (Fig. 17). The operating conditions of these nozzles are shown in Fig. 18. Two nozzles of different throughput rates were purchased - the Model 700-1 with water flow rate of 20 to 100cm^3/min and the Model 900-3 with rate of 600 to 900cm^3/min. The basic design of the nozzle is shown in Fig. 19. The

(a)

GAP

LOCK RING   STEM   RESONATOR   FLUID ORIFICE

(b)

| SONIMIST SPRAY NOZZLES | CONVENTIONAL SPRAY NOZZLES |

TOBACCO SMOKE

BACTERIA

FUMES   CLOUDS

FOGS   MIST   DRIZZLE   RAIN

DUST

PARTICLE SIZE (MICRONS)

0.1   1.0   10.   100   1000   10000

Figure 17.   Operation of Sonimist Spray Nozzle

(a) Schematic of nozzle;

(b) Particle size distribution

(Source: Product information sheet, Heat Systems Ultrasonics, Inc.)

5-2

AL-78-789

Figure 18. Operating Conditions of Various Sonimist Spray Nozzles
(Source: Product Information Sheet, Heat Systems
Ultrasonics, Inc.)

AL-78-790

Figure 19. Schematic of Sonimist Nozzle (Model 700-1)
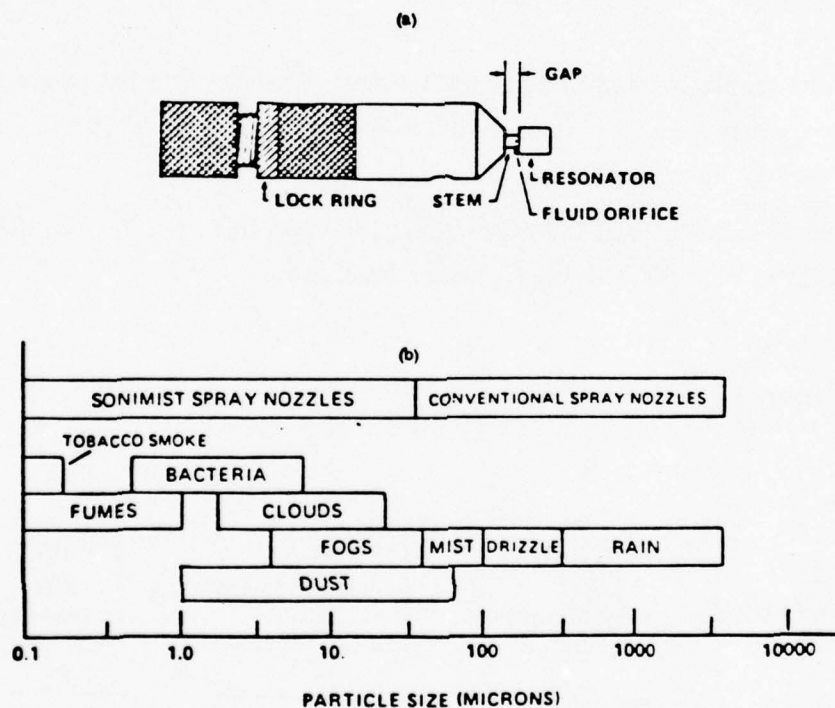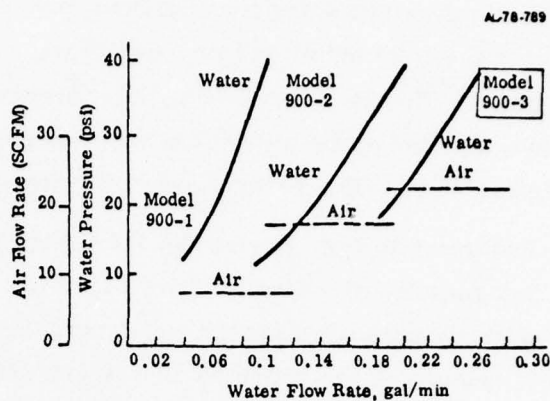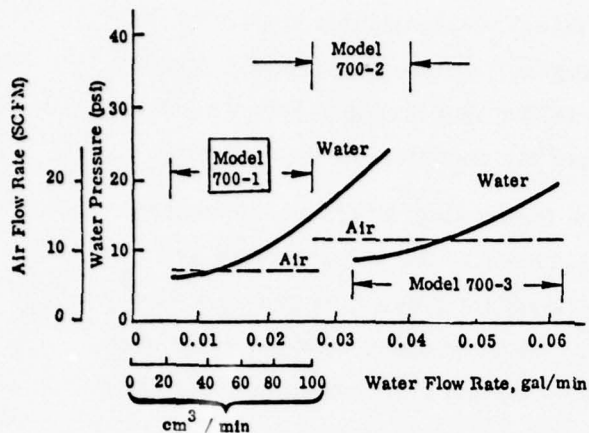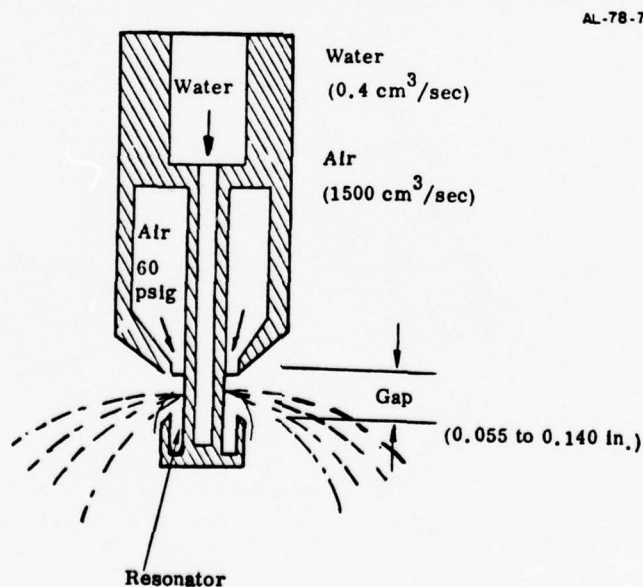
5-3

adjustable parameters are air pressure, water flow rate, and gap setting (distance between the air jet outlet and the resonator). The spray pattern is sensitive to the gap setting. This is shown in Fig. 20. According to the manufacturer, the droplet size is a function of the water flow rate and gap setting and is rather independent of the air pressure. The recommended air pressure for operation is 55 to 60 psig.

Referring to Fig. 19 (for the 700-1 nozzle), water enters through the central stem and goes out of 4 small holes of 1/32 in. diameter at the side. (There are 8 holes of the same size for the 900-3 nozzle.) Based on water flow rate ($\sim$0.4cm^3/sec) the exit velocity of the water jet is $\sim$20 cm/sec. These streams of water encounter a high velocity air jet coming out from the orifice between the central stem and the outer jacket. (The clearance is about 1 mm.) Since the air pressure is $\sim$60 psig, the air stream must be choked at the orifice, and the air velocity coming out should be approximately sonic. This jet of air further interacts with the resonator to give a violent oscillating flow. The frequency is given by the gap size divided by the sonic velocity, and amounts to $\sim$100 kHz. The water stream interacts with this oscillating flow for a distance of $\sim$1 mm (dimension of the annular opening of the

AL-79-11

| Gap size .070 in. | 0.104 in. | 0.112 in. |
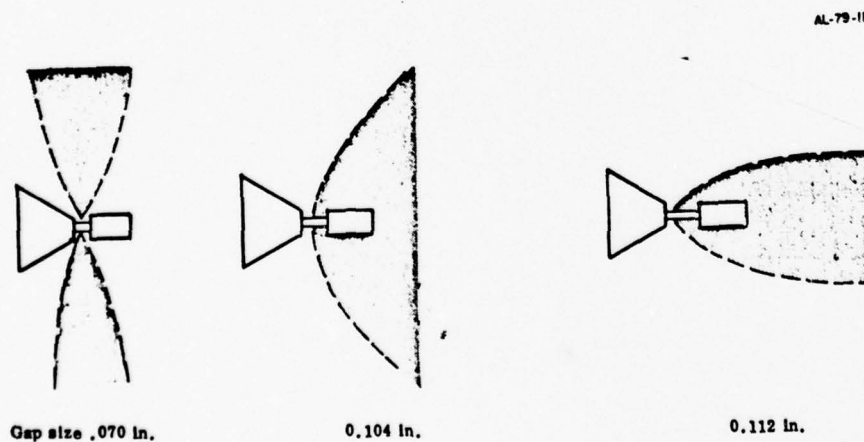
Figure 20. Spray Pattern of Sonimist (Model 700-1)

resonator) and is shattered into water droplets. The residence time τ in this shattering region is:

$$\tau \sim 1 \text{ mm}/20 \text{ cm/sec} = 5 \text{ ms} \qquad .$$

Hence, the water droplets are "hit" approximately 500 times before they come out. Therefore, the Sonimist is a very efficient liquid shattering device.

5.2.1 The Fog Chamber

The fog chamber is designed as a closed circuit wind tunnel driven by a 1000 scfm blower (Fig. 21). There is also the capability of throttling the blower to give a lower flow rate. Because the Sonimist delivers $\sim 1500 \text{ cm}^3/\text{sec}$ of extra air into the circuit, balancing ports were introduced to let this extra air bleed out. The cross section at the test section is 75 cm x 75 cm which gives an unthrottled flow velocity of ~ 80 cm/sec.

AL-78-791

Figure 21. Schematic of Fog Chamber

The Sonimist is located at the top of the chamber and is adjusted so that it gives a horizontal spray pattern (Fig. 20). The spray is mixed with the chamber air and flows through the test section. The return path of the air goes through two filters to remove the water droplets. By running the air in a closed loop, it is ensured that the relative humidity of the air is equal to 1. Excess water is drained out at the bottom of the chamber.

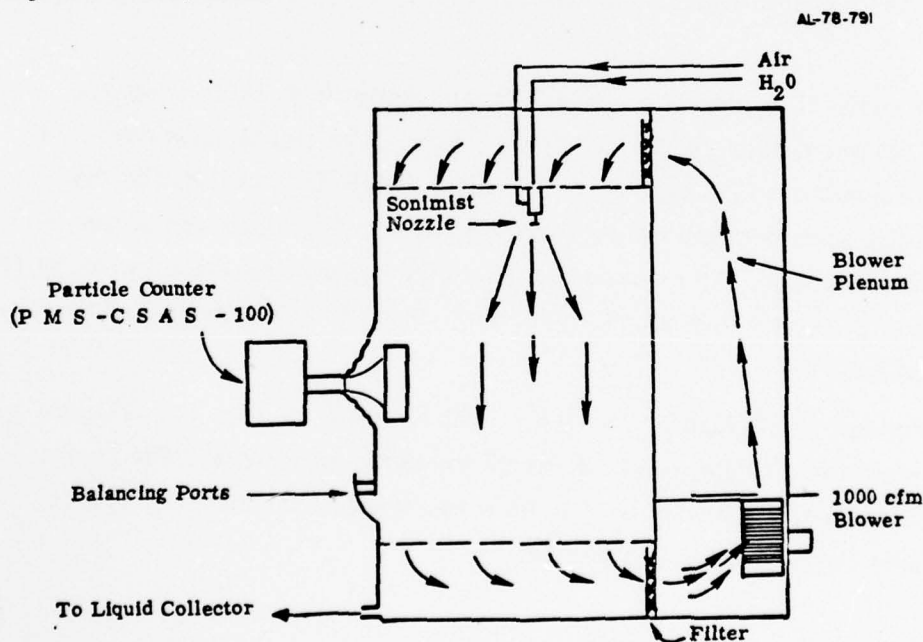The sampling cone of the PMS particle size spectrometer is mounted on the side wall with provision of limited travel in both the vertical and horizontal directions so that different parts of the fog chamber can be sampled.

5.2.2 The PMS CSAS-100 Particle Size Spectrometer

The fog droplet size distribution is measured by the particle size spectrometer model CSAS-100 (Classical Scattering Aerosol Spectrometer) manufactured by Particle Measuring Systems, Inc. (PMS) (1855, 557th Court, Boulder, Colorado 80301). The apparatus is described in detail in the literature.[24] It is briefly discussed here for continuity.

The spectrometer measures forward scattered light at $0.63\ \mu$m wavelength collected from a volume defined by the receiving optics. The signal, received by a PM tube is sent to a pulse height analyzer. The pulse height is correlated to the particle size, and the number of pulses corresponds to how many particles of the particular size are recorded. The saturation limit of the system is reached when more than one particle is present in the sampling volume. The CSAS-100 is limited to a particle density of $\sim 2 \times 10^4/\text{cm}^3$.

The spectrometer is divided into 4 size ranges as shown in Fig. 22. The bin size is constant within one range, but is different for different ranges. The ranges also overlap. Therefore, the counts have to be normalized by the bin sizes before the different ranges can be combined together.

---

[24]R.G. Knollenberg, Preprint Volume, International Conference on Cloud Physics, July 1976, Boulder, Colorado. Published by the Am. Met. Soc., Boston, Mass.
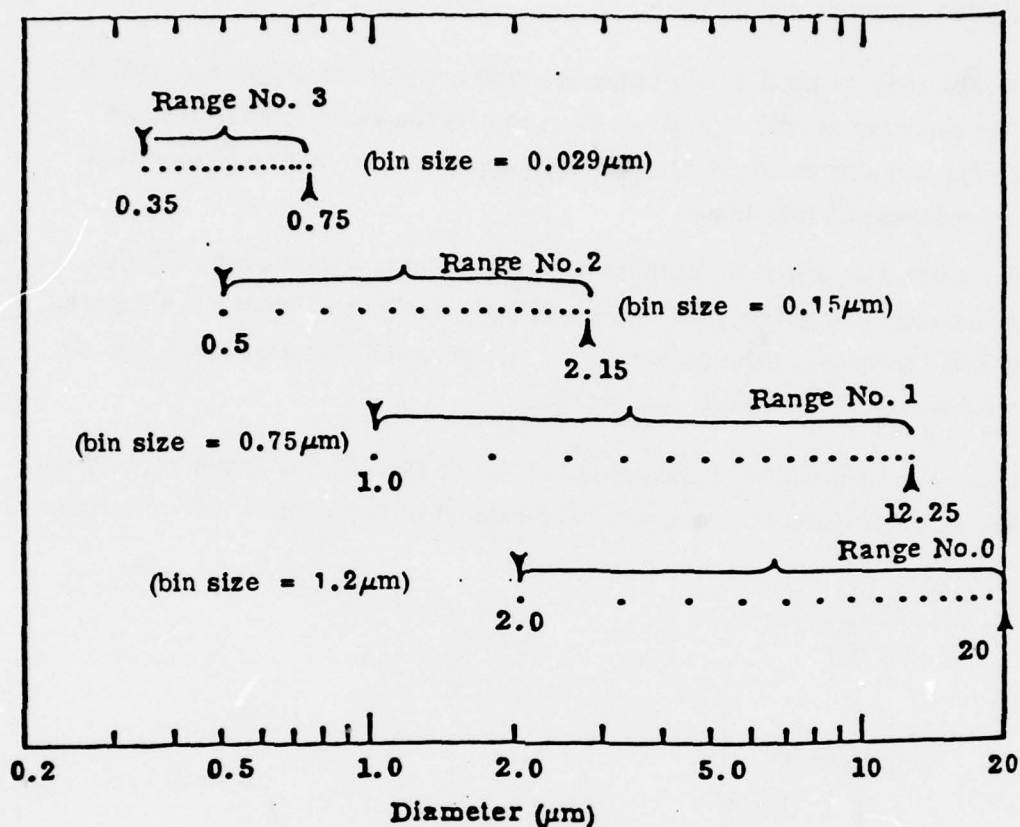
Figure 22. PMS – CSAS Particle Measuring System
(4 ranges with 15 bins each)

For low particle concentration, a long counting period is required for good statistics. The spectrometer automatic counting time per range is selectable from 1 sec to 15 min.

5.2.3 Dilution Scheme

In order to achieve multiple scattering at infrared wavelengths, fog droplet desnities of $10^5 - 10^6/cm^3$ are necessary. This is a factor of $10 - 100$ greater density than the PMS spectrometer can handle. Therefore, the sampled fog should be diluted with a known amount of air so as not to saturate the spectrometer.

The requirements for dilution are:

1.   The dilution air should not change the size distribution of the sampled fog. This requires the dilution air to be precisely the same temperature as the fog and also be of relative humidity equal to 1 so that no evaporation or condensation take place.

2.   The amount of dilution should be precisely known. Since a high dilution is desired (~10 to 100), the volume of fog sampled will be small compared with the volume of dilution air. This requirement indicates that a fog/air valve bleed-off system is appropriate.

The schematic of the dilution scheme is shown in Fig. 23. A closed circulation loop driven by a compressor is employed. The amount of fog sampled is controlled
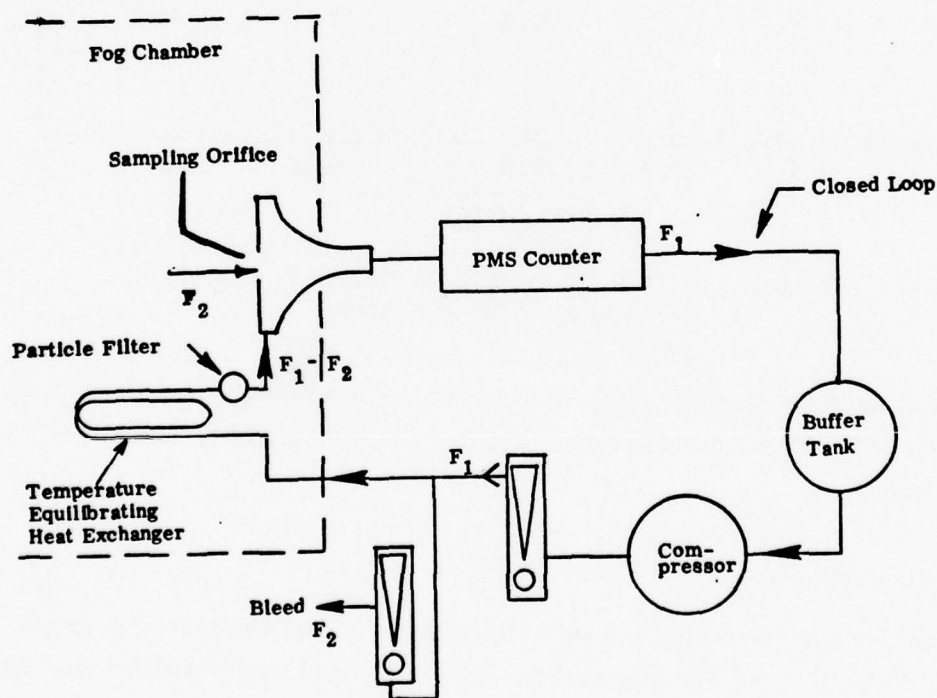
AL-79-7

Figure 23.   Schematic of the Particle Counter Dilution Scheme. Here the Dilution Factor Is Given by the Ratio F_1/F_2

by bleeding an amount of air F_2 out of the loop. The sampled fog is mixed with an amount $(F_1 - F_2)$ of air which has been equilibrated in temperature with the fog chamber through a heat exchanger. At the start of a run, F_2 is turned to maximum so as to saturate the air in the closed loop with moisture. Any excess water droplets are removed by a filter in the loop. Then the desired F_2 is set while F_1 is adjusted to a fixed value of 400 SCFH, the flow rate at which the PMS counter is calibrated. Under these settings the number of particles the spectrometer measures should be scaled by a dilution ratio:

$$\text{Actual count} = \text{measured count} \times \frac{F_1}{F_2} \quad .$$

Figure 24 shows the performance of the dilution scheme. The fact that counts do not reach zero when F_2 is shutoff is entirely due to leakage in the plumbing. This leakage is estimated to be 6 SCFH from the intercept of the figure and may be used as a correction offset to F_2.

The lower limit to F_2 may be discussed on three grounds.

1. Nonisokinetic sampling error: From Fig. 25, for particle diameters less than 20 μm, an acceptable bound is that the ratio of the mean velocity of the fog to the sampling velocity (U_m/U_s) should be less than 1.5. At present, the mean flow velocity at the chamber is $\lesssim$ 1 m/sec and the sampling orifice diameter is 0.25 in. Therefore, F_2 should not be lower than 6 SCFH and F_1/F_2 should be less than 66. However, one can always decrease the orifice diameter to increase U_s. It is the next two considerations which set a lower limit to F_2.

2. Leakage: When F_2 is small, the leakage in the system may completely overshadow F_2, and an accurate dilution ratio cannot be obtained.

3. Thermal and humidity control of the dilution air: When F_2 is small, the total amount of fog droplets is small. Therefore, precise control of the dilution air temperature and humidity is very important, otherwise the fog droplets may evaporate or be subject to further condensation, thus altering the size distribution.
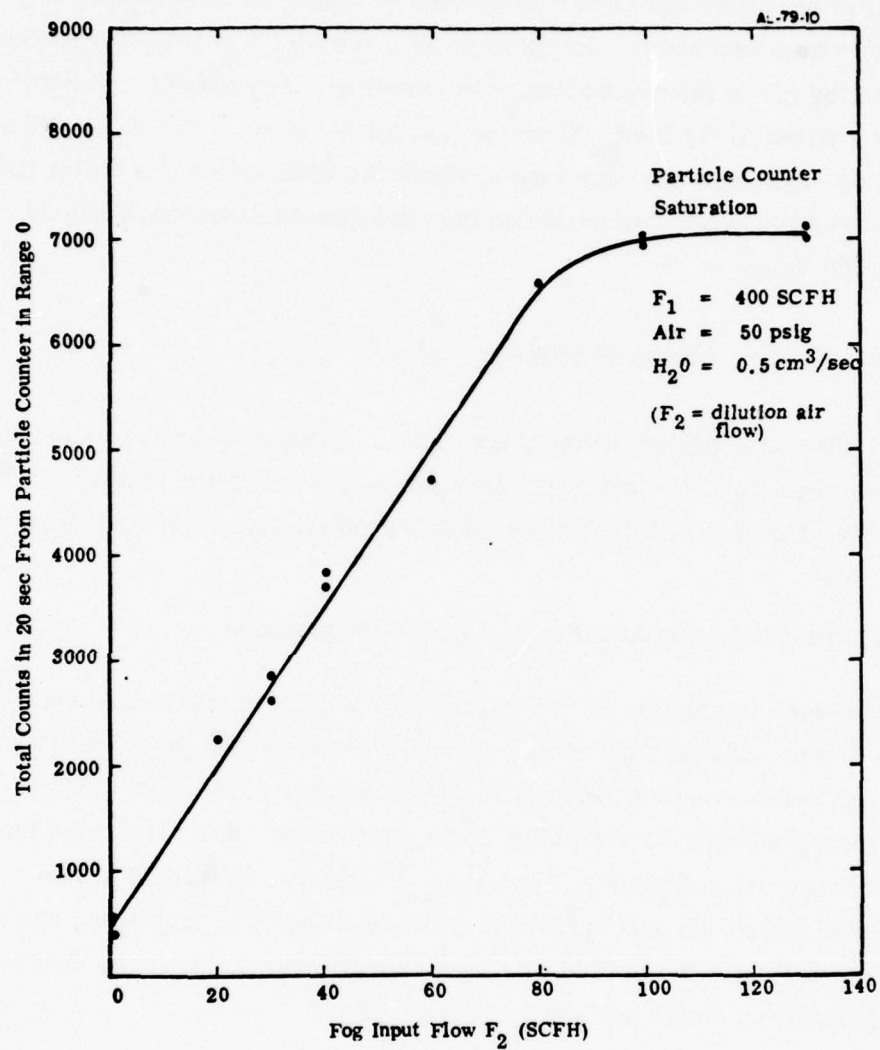
Figure 24. Performance of Dilution Technique
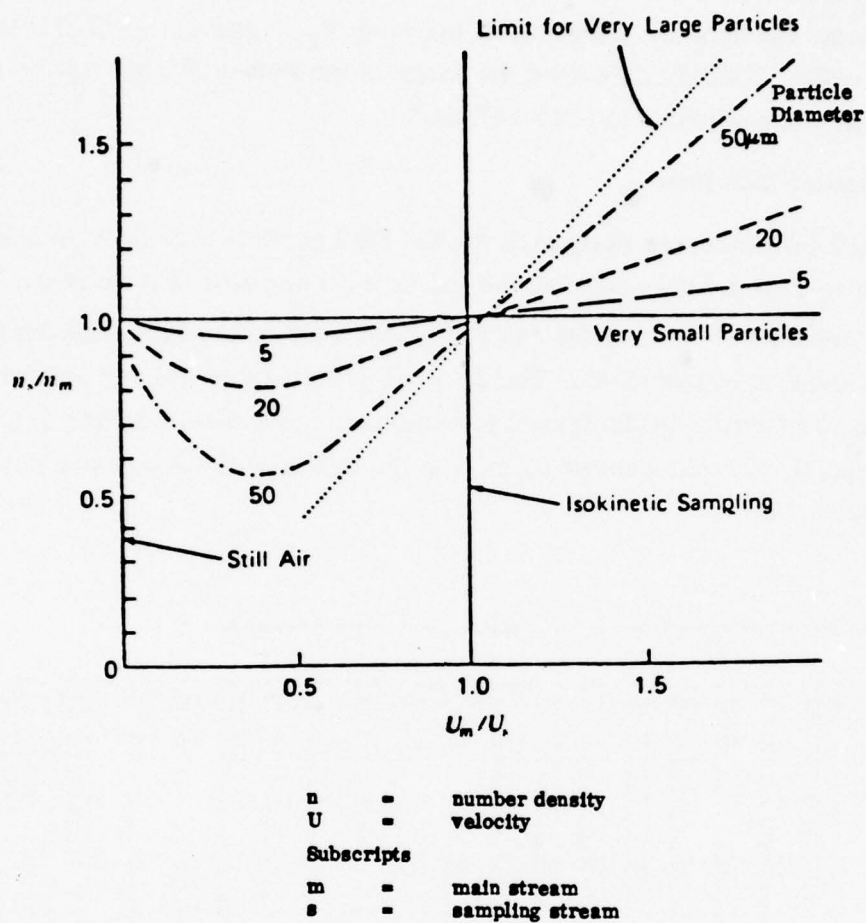
Figure 25. Nonisokinetic Sampling Error for Particle Density of 1 gm/cm^3 (From Ref. (25))

(25)S.K. Friedlander, <u>Smoke, Dust, and Haze</u>, (Wiley, New York, 1977).

Based on the above considerations, it may be seen from Fig. 24 that a dilution ratio of $F_1/F_2 \sim 20$ was actually achieved; by lowering F_2, a dilution ratio of ~ 100 should be achievable. This would extend the range of the PMS-CSAS spectrometer to measure particle densities up to $\sim 2 \times 10^6/\text{cm}^3$.

5.2.4 The Computer Interface

An RS232C interface was purchased for the PMS particle size spectrometer so that data can be directly interfaced to the Prime 400 computer at Aerodyne. Each data record contains the raw data, the settings on the PMS instrument, and the time of the day the measurement is taken. The data are processed to provide printer plots of the size distribution at the terminal on site and more detailed plots at a later time. Typical records, printer plots, and final plots of the result are shown in Figs. 26 through 28.

Figure 26. Typical Record From PMS CSAS Particle Counter
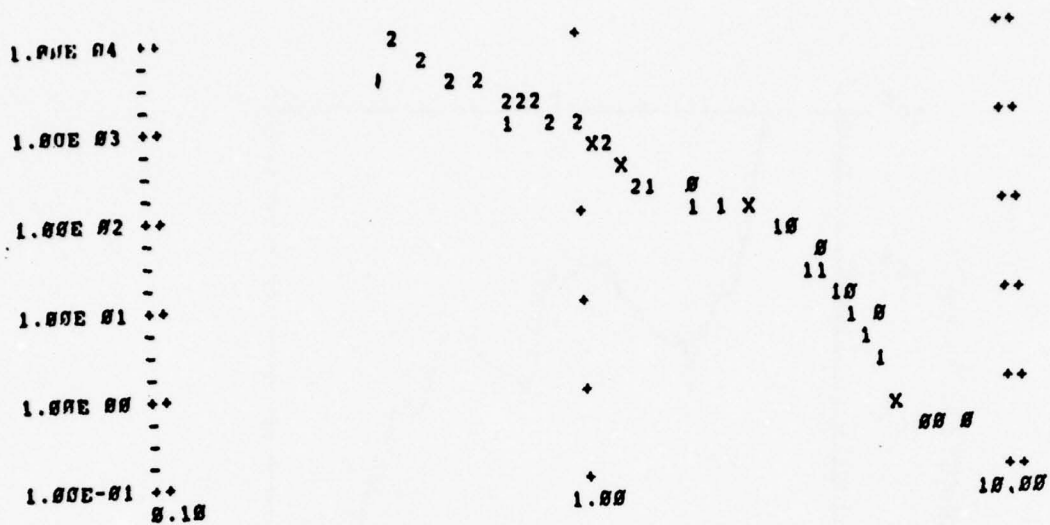
Figure 27. Printer Plot of Spectrum From PMS CSAS Particle Counter as Displayed on Computer Terminal. The vertical axis represents particle number density ($\mu m^{-1} - cm^{-3}$); the horizontal axis represents particle radius (μm).
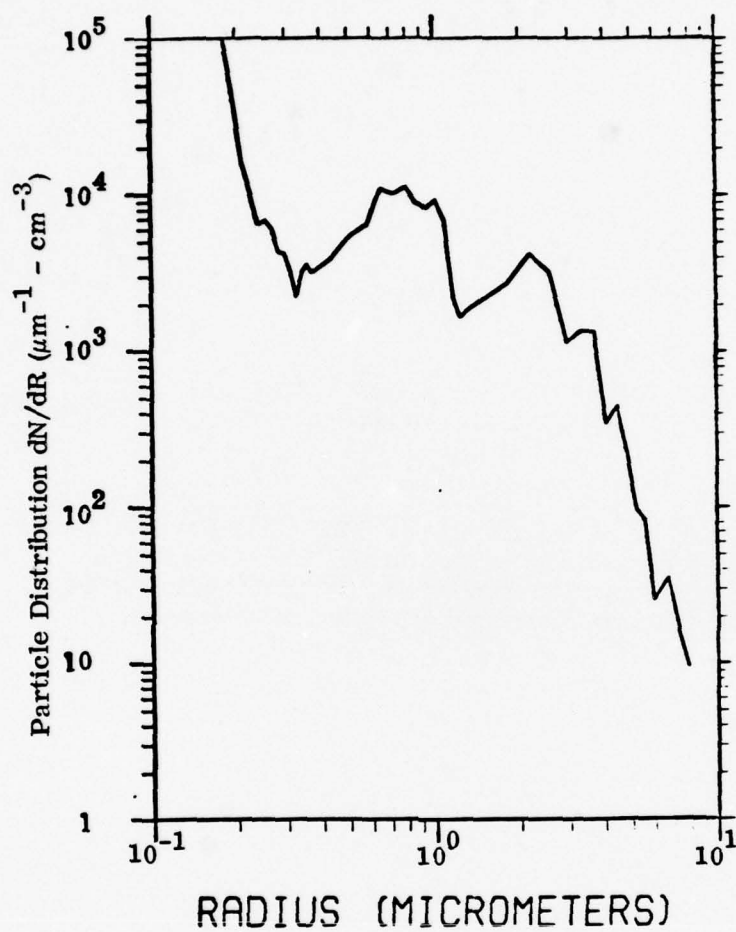
Figure 28. Typical Plot of Fog Spectrum

6. RESULTS AND DISCUSSION

6.1 Data Collection

The parameters of the 700-1 Sonimist were extensively varied. Figure 29 shows a map of the operating gap sizes and water flow rates being studied. In addition, the air pressure supply was varied from 30 to 70 psig at a water flow rate of 60 cm^3/min and 0.085 in. gap setting. The test results are summarized in Figs. 30 through 32 which are plots of the particle size distributions obtained for the different operating parameters.

(Air Pressure 60 psig)

Water Flow Rate (cm^3/min)
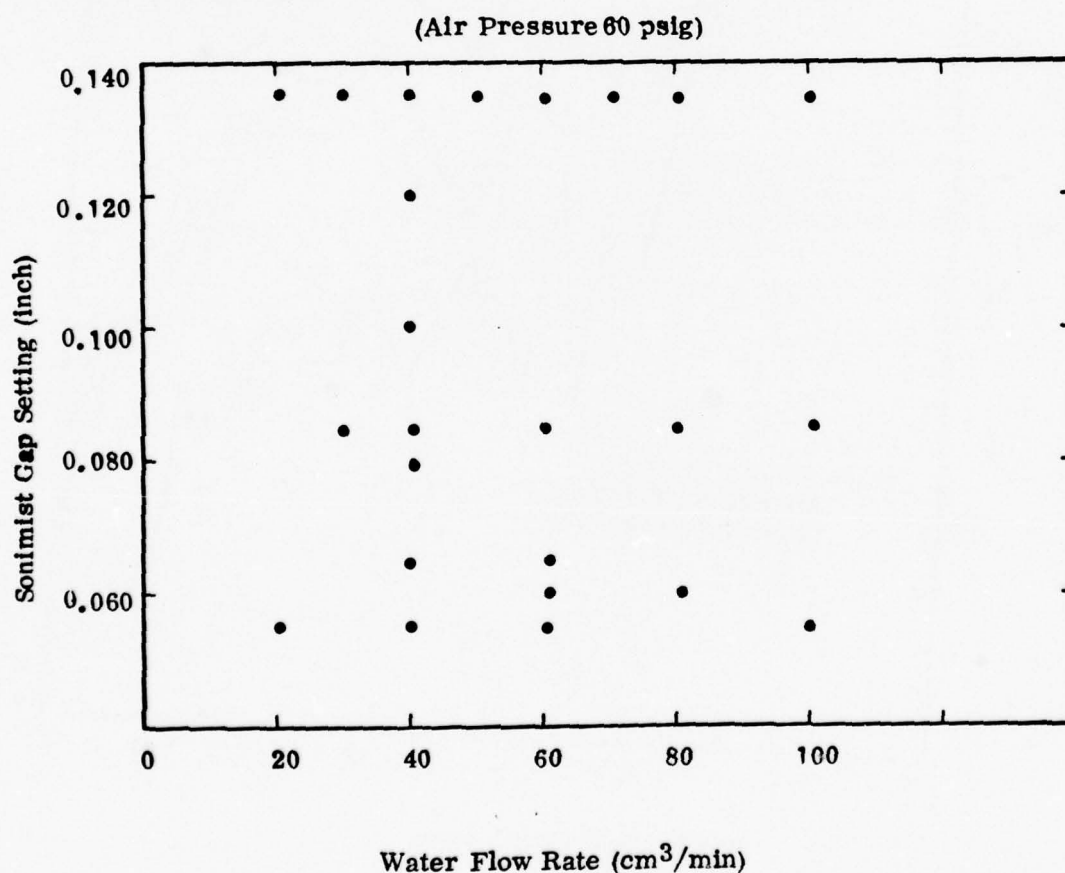
Figure 29. Test Matrix of Gap Size versus Water Flow Rate
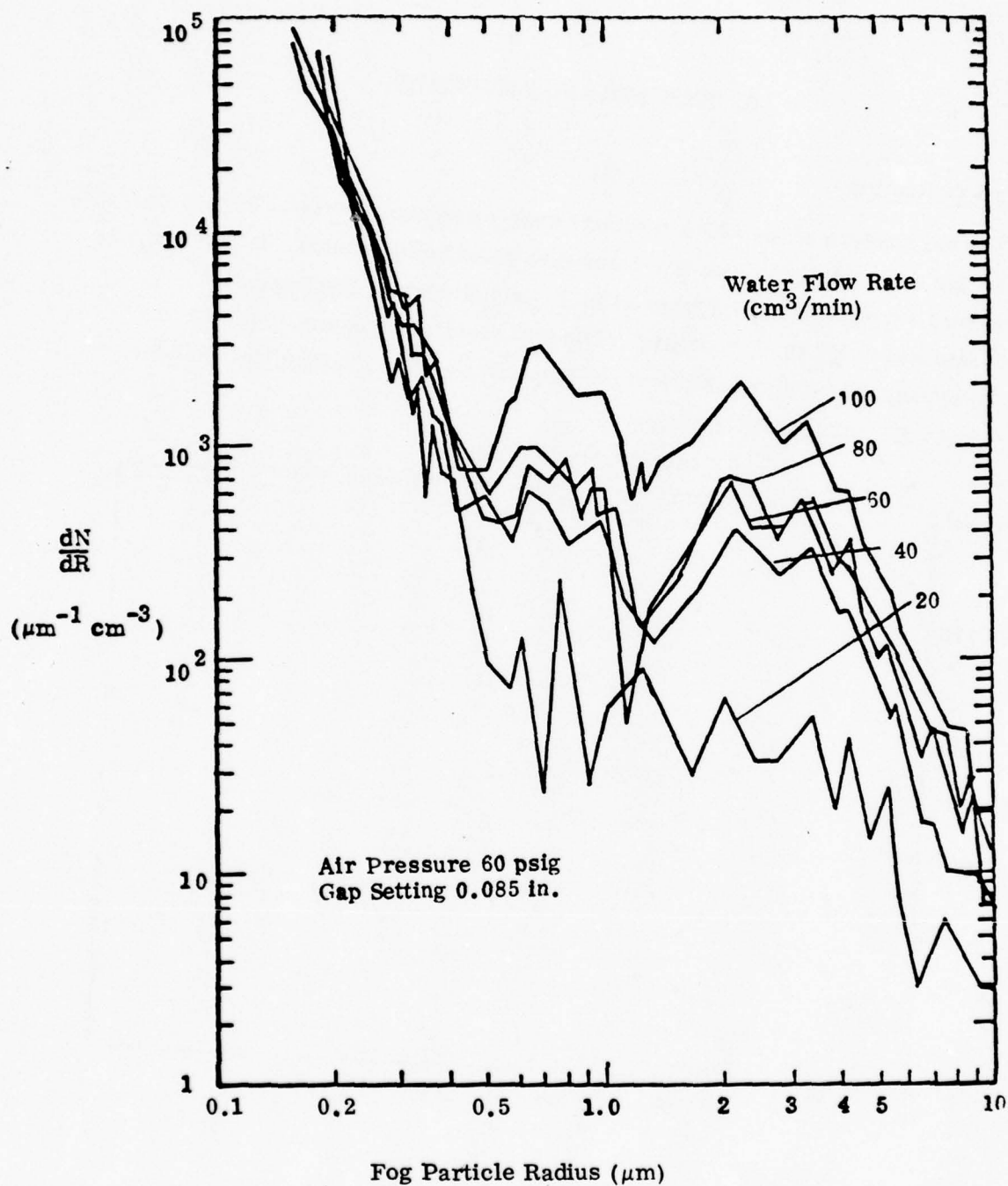
Figure 30. Spectra Variation with Liquid Flow Rate
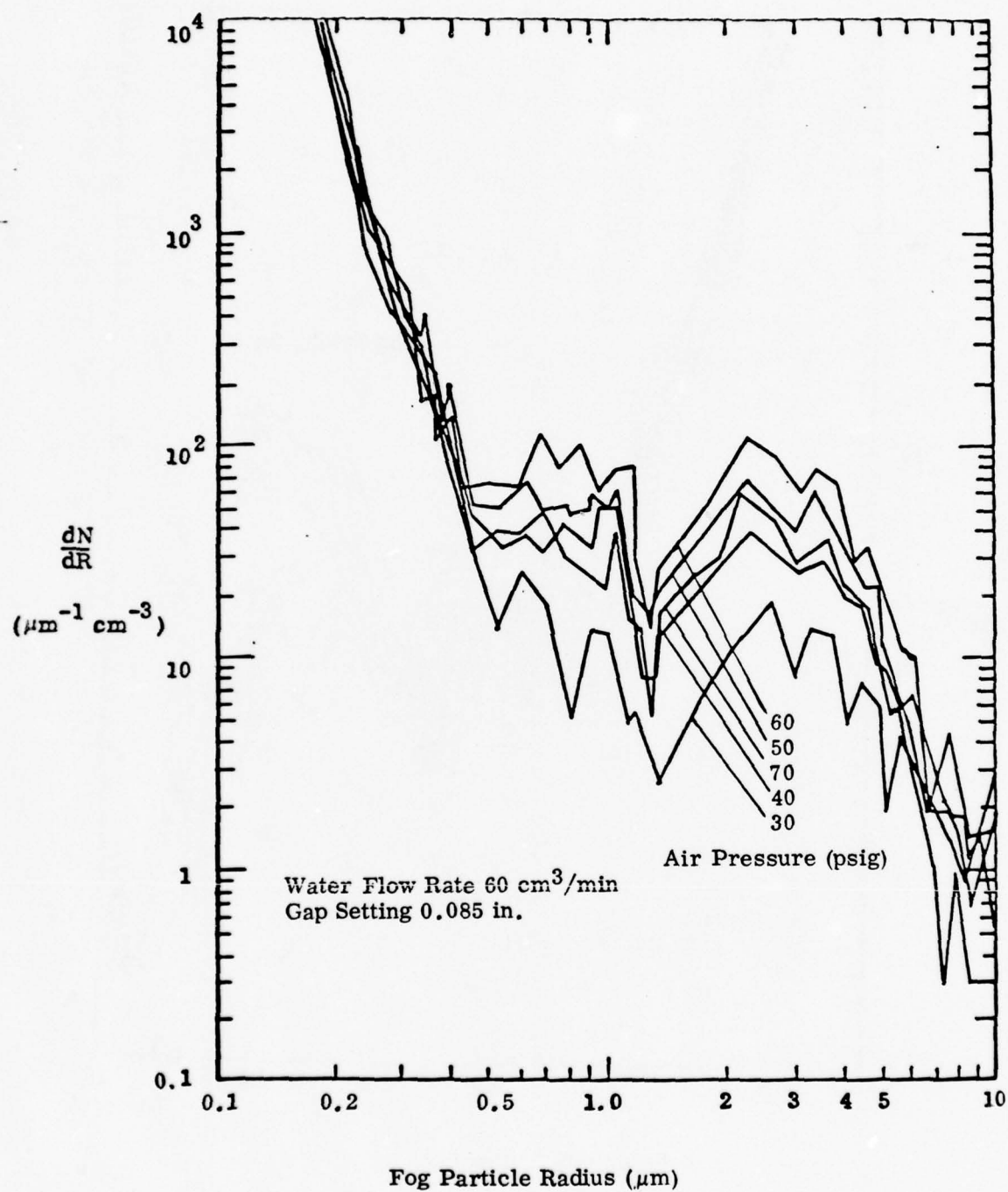
Figure 31. Spectra Variation with Air Pressure
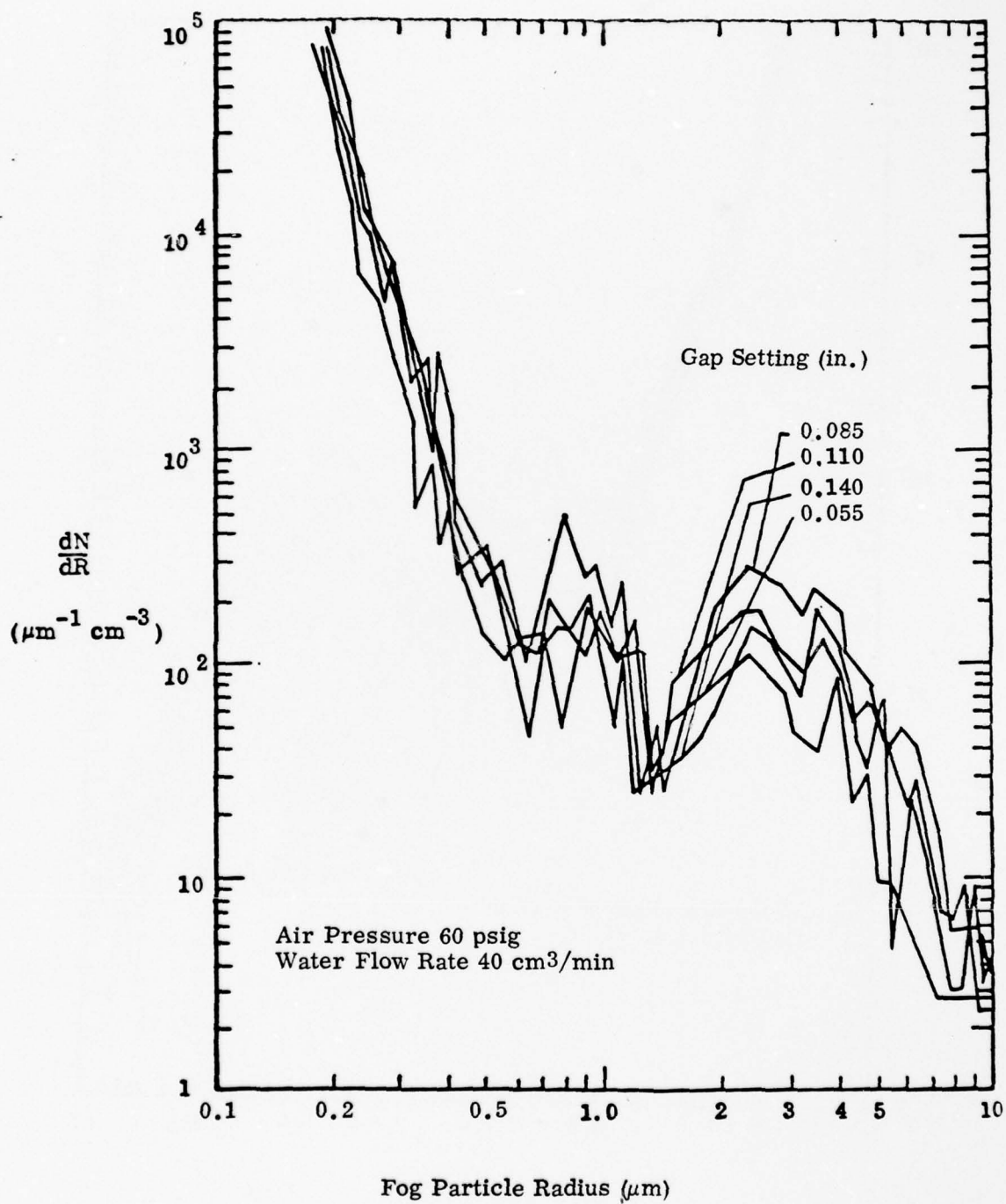
Figure 32. Spectra Variation with Gap Setting

6.2 Test Results and Comparison with Fog Data

The test results show that the particle size spectrum generated by the Sonimist has a distinctive bimodal distribution which peaks at around 0.8 and 3 μm radii. The valley is at around 1 μm radii. Figure 33 is an overlay of Figs. 30 through 32. By changing the water flow rate, gap setting, and applied air pressure, the dN/dR curves move up and down by more than an order of magnitude. However, there is little change of the bimodal shape in the spectrum.

The obtained spectrum does resemble that of natural fog. Figure 34 is the result of typical measurement of natural fog by Trusty.[26] In the 0.2 to 0.6 μm radius region, both spectrums have about the same power law dependence.

In the 0.6 to 4 μm region, the Sonimist spectra has peaks at 3 μm. Trusty's data also shows a slight peak at 1 μm which is followed by a flat region at 2 μm. The particle number density produced by the Sonimist, depending on the operating parameter, is 10^2 to 10^3 times denser than that of Trusty's natural fog data. Beyond 4 μm, both the Sonimist and Trusty's spectra take the same form again (dN/dR varies as the inverse fifth to sixth power of radius).

Figure 35 shows the range of optical depths produced by the Sonimist for wavelengths 0.63, 1.06, 3.8, and 10.6 μm. The optical depth is obtained from integration of the product of the spectra and the total scattering cross section. The minimum optical depth of the present system is around 3 to 5 m. This is about an order of magnitude larger than what one would like to achieve for a laboratory-scale multiple scattering experiment. A smaller optical depth can be obtained by using a number of sonimists spraying together. The present system is, however, suitable for studying the single scattering optical properties of liquid droplets.

---

[26] G. Trusty, Naval Research Lab., Code 8586, Washington, DC 20375. Private communication (1978).
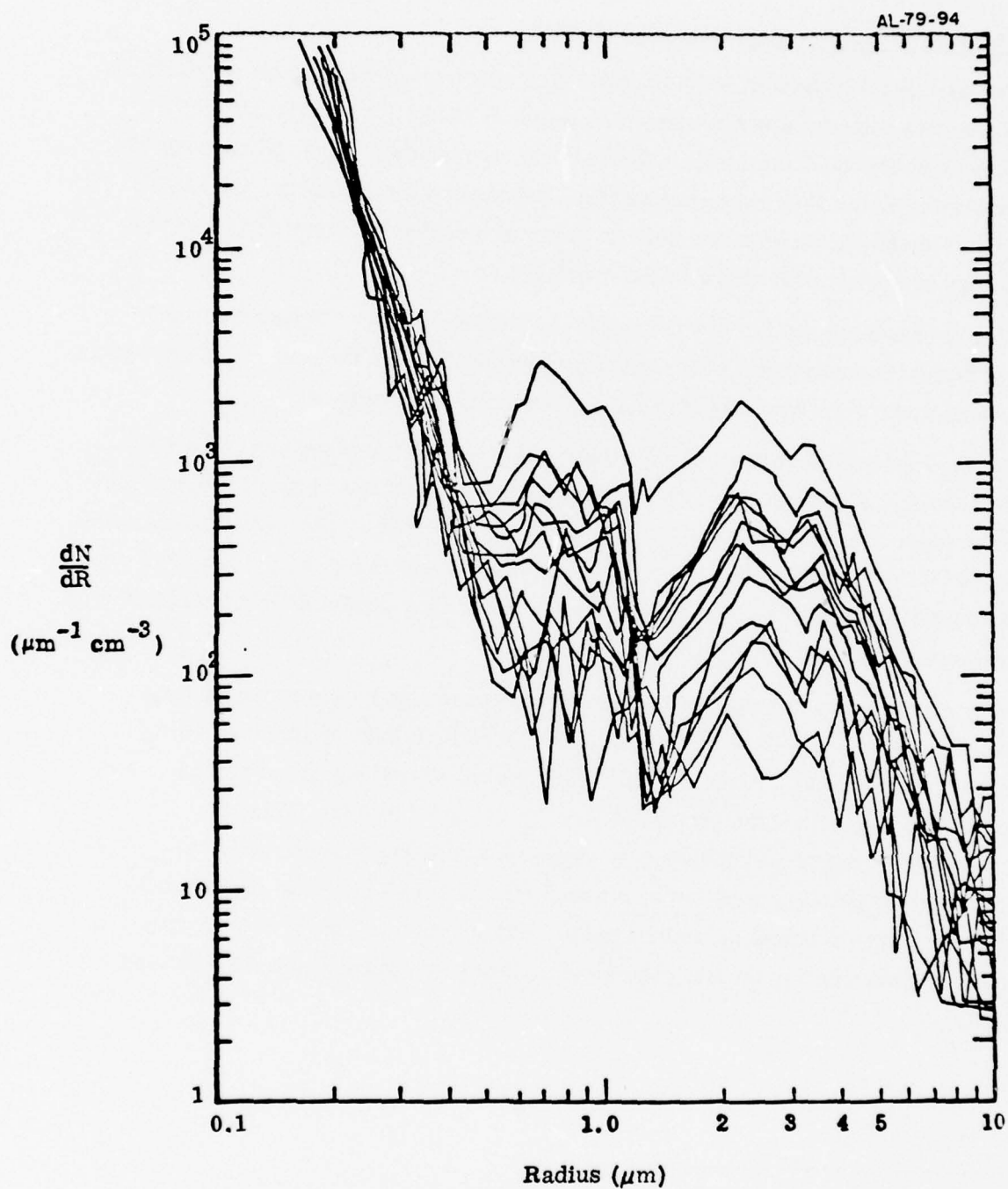
Figure 33. Overlay of PMS CSAS-100 Droplet Spectra From Figs. 30 through 32
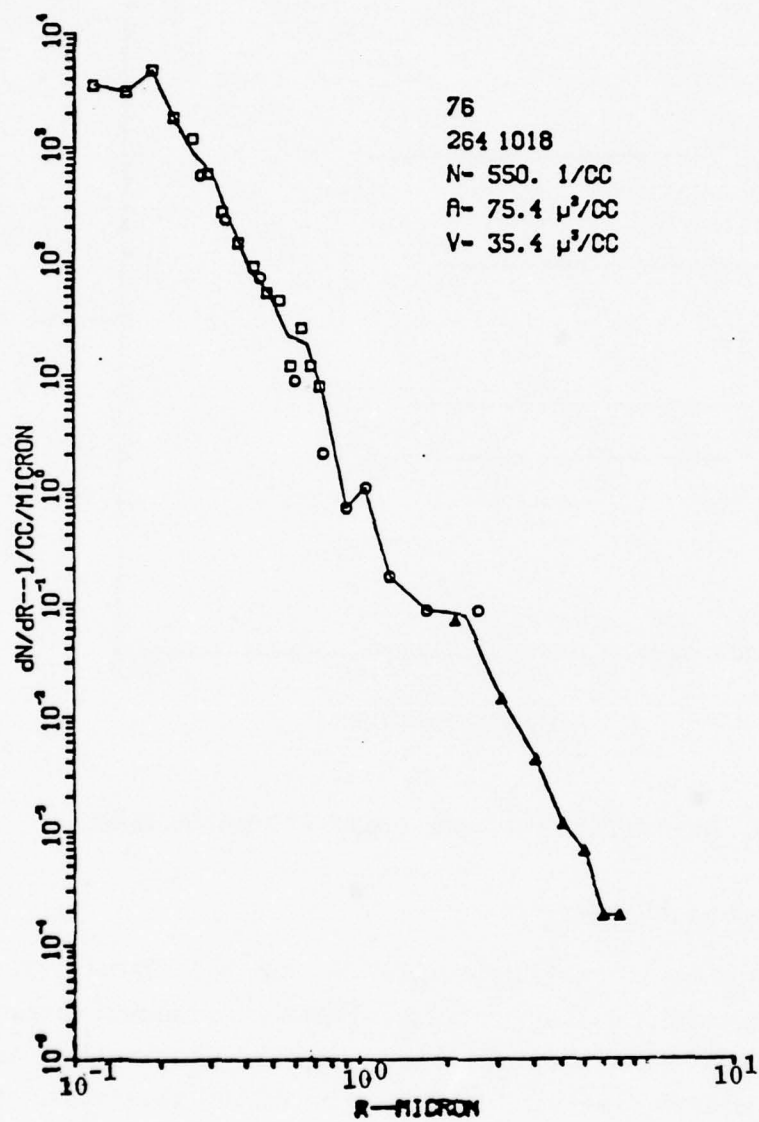
Figure 34. Natural Fog Spectrum (Ref. 26)
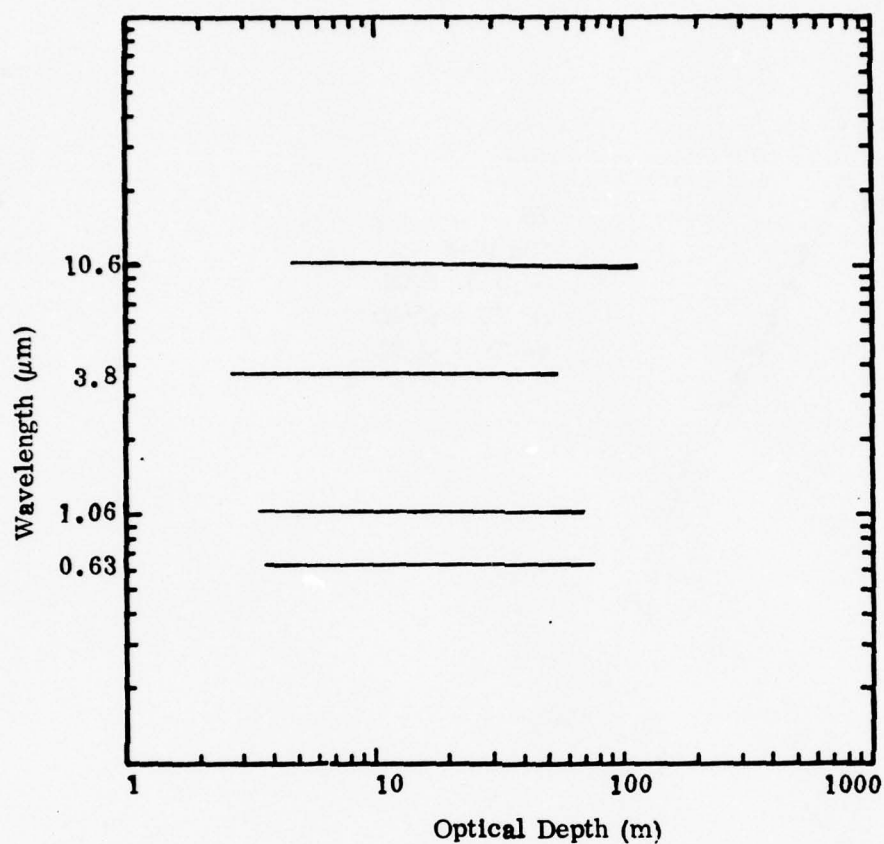
Figure 35. Range of Optical Depth Produced From Sonimist

6.3 The Physics of Droplet Shattering

From the overlay of the various spectra obtained from the Sonimist (Fig. 33) we see that although the number density shifts up and down with different operating conditions, there is little effect on the shape of the spectrum. Furthermore, the total volume of water under the spectrum $\left[\int (dR\ 4/3\ \pi\ R^3\ dN/dR)\right]$ amounts only to a few percent of the total amount of water input to the Sonimist. Therefore most of

the water must go to some large droplets.[*] It is necessary to study the fundamental physics of droplet shattering in order to know the degree of controllability of the particle size distribution in such a process.

The most important parameter governing droplet shattering is the Weber number W_b defined as:

$$W_b \equiv \frac{1}{2} \frac{\rho_\infty U_\infty^2 D}{\sigma} \qquad ,$$

where

ρ_∞ = density of gas stream

U_∞ = relative velocity between droplet and gas stream

σ = surface tension of the liquid

D = diameter of the droplet .

---

[*] Since droplet volume $\sim R^3$, only a small number of large particles is necessary to take up the water. Typical values of mass loading is:

$$\text{mass loading} = \frac{\text{water mass flow rate}}{\text{volume air flow rate of fog chamber}}$$

$$= \frac{40 \text{ gm/min}}{5 \times 10^5 \text{ cm}^3/\text{sec}}$$

$$= 1.3 \times 10^{-6} \text{ gm/cm}^3 \qquad .$$

The mass of a 100 μm diameter droplet is 0.5×10^{-6} gm. Therefore, it would only require 3 droplets/cm^3 to account for most of the water from the Sonimist.

The Weber number is a measure of whether the aerodynamic pressure applied by the gas stream is able to overcome the surface tension of the droplet and thus cause shattering. The critical Weber number reported in the literature[27-29] varies from 3 to 30. Figure 36 shows the shattering velocity required for the breakup of different sizes water droplets. It is difficult to predict the sizes of the small droplets resulting from the breakup except that they are much smaller than the size of the initial droplet. Therefore, the spectrum consists of two parts. There are the droplets which do not breakup further. They peak at around the diameter governed by the critical Weber number. Then there are the small droplets resulting from the breakup. They populate the low end of the spectrum. In most circumstances it is difficult to obtain a shattering velocity higher than sonic. This corresponds to a critical droplet diameter of 30 μm (Fig. 26). Since the Sonimist operates at sonic velocity, the spectral peak of the surviving particles should occur at this diameter. The PMS particle counter only detects particles up to 20 μm diameter. Thus the spectrum observed in the experiment represents the small droplets resulting from the breakup rather than the surviving droplets. Since these droplets are formed in a random manner, the spectrum is insensitive to the adjustment of the Sonimist system parameters, as we observed.

[27] W.R. Lane, "Shattering of Drops in Streams of Air," Ind. Eng. Chem. 43, 6, 1312-1317 (1975).

[28] G. Gordon, "Mechanism and Speedy Breakup of Drops," J. Appl. Phys. 30, 11 (1959).

[29] P. Simpkins and E. Bales, "Water Drop Response to Sudden Acceleration," J. Fluid. Mech, 55, 4, 629-639 (1972).
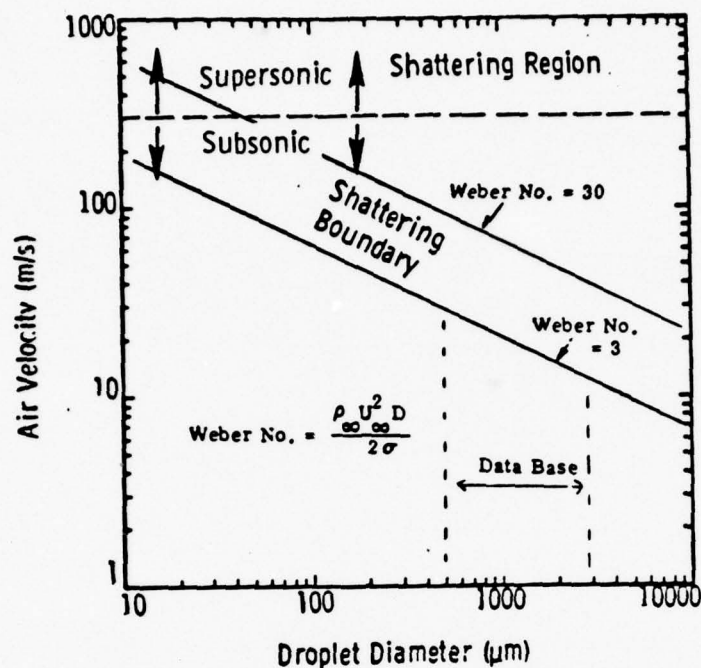
Figure 36. Shattering Air Velocity Requirement

6.4 Summary

The Sonimist spray nozzle produces droplets with a size spectrum that resembles spectra measurements of natural fog. The optical depth of the present artificial fog can be down to 3 m. The spectral shape of the size distribution is found to be insensitive to the Sonimist operating parameters. This is because the observed spectrum is populated mainly by the small droplets randomly formed during the droplet shattering.

7. OTHER METHODS OF GENERATING FOG DROPLETS WITH A CONTROLLABLE SPECTRUM

We studied other means of generating fog droplets with a spectrum controllable in the 0.1 to 10 μm radius range. Preliminary experiments were performed to alter the size distribution of the droplets from the Sonimist by condensing steam onto them and by evaporating them in hot air. Also, growth of large particles from sodium chloride nuclei was carried out.

The generation of monodispersed aerosols was reviewed by Fuchs and Sutagin[30] and more recently by Corn and Esmen.[31] Their review can be summarized in Fig. 37. Atomization does not provide particle radii smaller than 20 μm. In the 1 to 10 μm radius region, droplets of nonvolatile liquids had been successfully grown by the condensation method. However, the growth of water droplets is difficult because of the tremendous latent heat of vaporization and high vapor pressure.

Figure 38 shows the amount of latent heat released from condensing various size droplets at different densities. For example, to condense $10^5/\text{cm}^3$ of 5 μm radius droplets, the heat release amounts to 0.1 J/cm^3. The heat capacity of air is 10^{-3} $\text{J/cm}^3/^{\circ}\text{C}$. Therefore, this heat release amounts to a $\sim 100^{\circ}\text{C}$ increase of the air temperature. To take out this heat, we need to either mix into the initial nuclei-carrying steam/air mixture very cold air or to pass this initial mixture through a cold-wall heat exchanger.

7.1 Condensation of Steam Onto Droplets Produced by the Sonimist

Preliminary experiments were carried out to grow the droplets produced by the Sonimist by mixing first steam into the Sonimist spray and then cold air into the spray.

[30] N. Fuchs and A. Sutagin, "Generation of Monodisperse Aerosols," in _Aerosol Science,_ Ed. by C.N. Davies, Academic Press (1960). Ch. 1.

[31] M. Corn and N.A. Esmen, "Aerosol Generation," in _Handbook of Aerosols_, ed. by R. Dennis, ERDA (1976), pp. 9-39.
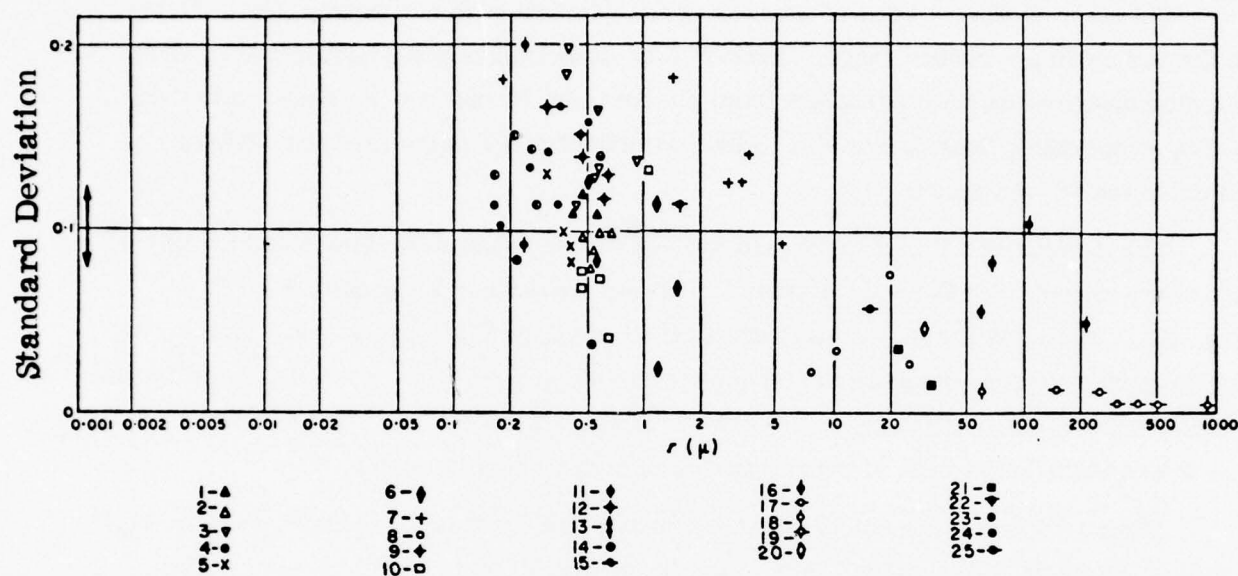
Condensation method: aerosols of DOP, 1[46], 2[13], 3[9], 4[138], 5[119]; DBP, 6[49]; glycerol 7[125]; tetralin, 8[33]; octanoic acid 9[19]; stearic acid 10[143]; linolenic acid, 11[39]; sodium chloride, 12[37]; 13[41]; 14[145]; cadmium, 15[36].

Atomization of liquids: capillary tip in an annular air-jet, water, 16[57], 17[55]; rotating blades, mineral oil, 18[73]; pulsating pressure, water, 19[66]; rotating disc, water, 20[60], DBP, 21[60]; electrostatic atomization, butylbenzoate, 22[78].

Atomization of suspensions: latex, 23[82]; spores of *B. globulis*, 24[144].

Dispersion of powders: lycopodium, 25[105].

Figure 37. Characteristics of Monodisperse Aerosols Generated by Different Methods (from Ref. 30)
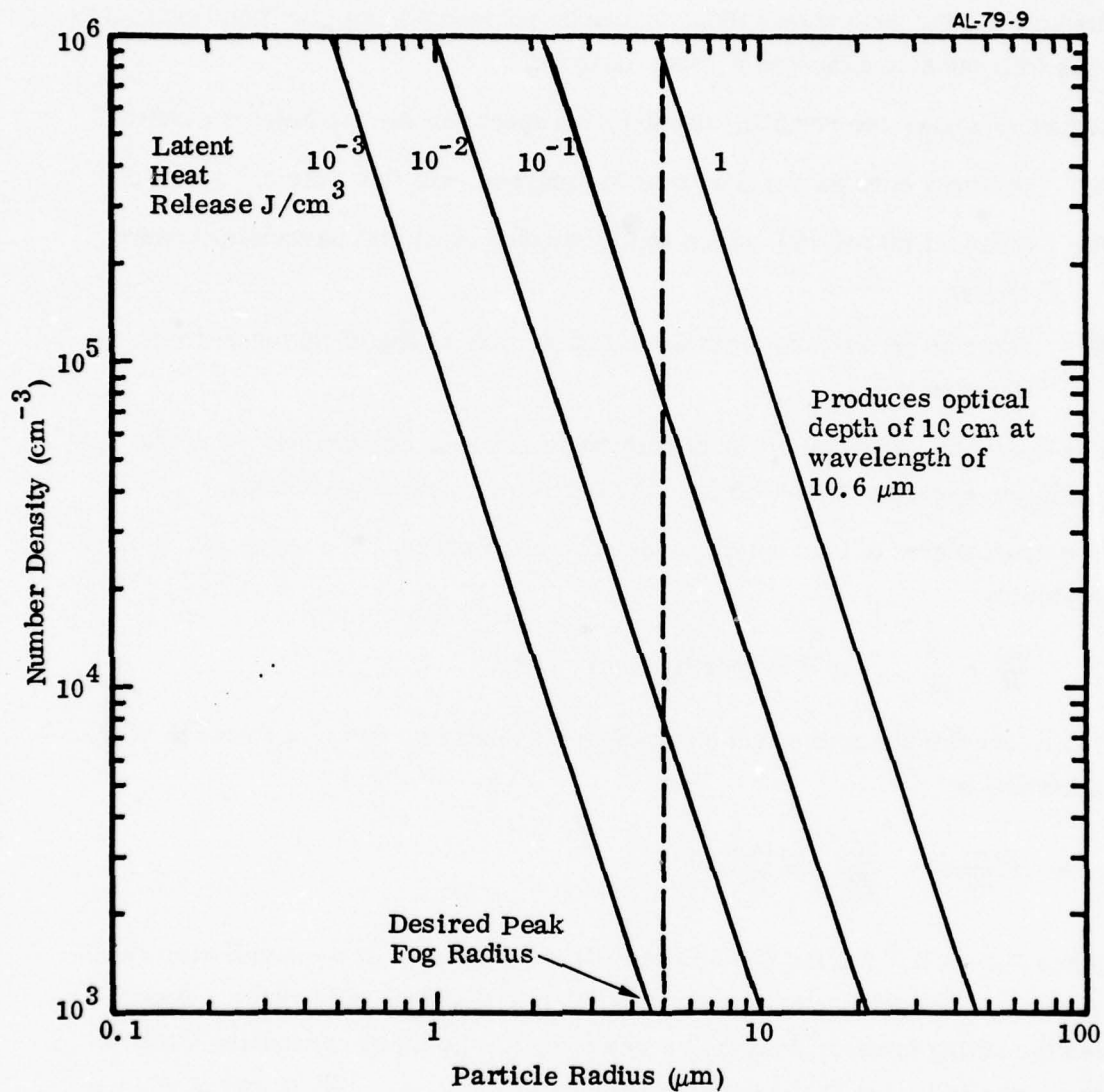
Figure 38. Latent Heat Release From Condensing Various Size Water Droplets at Different Densities (Heat Capacity of Air ~ 10^{-3} J/cm^3/^{o}C)

An equilibrium calculation on the amount of water condensed is reported in Appendix B. A density of $10^5/cm^3$ of $5\mu m$ particle corresponds to a mass loading of 50 gm/m^3. The calculation (Fig. B-2) shows that this can be achieved by mixing liquid-nitrogen-cooled gas with the steam/Sonimist spray mixture.

Figure 39 shows the resulting droplet size spectrum for the following cases:

(1)   Sonimist only (water flow rate 0.5 gm/sec, air flow rate 1.5 gm/sec);

(2)   Sonimist mixed with steam at 0.2 gm/sec (Sonimist parameters same as (1))

(3)   Same as (2) with the addition of 1.2 gm/sec of liquid-nitrogen-cooled nitrogen gas.

The spectrum shows an order of magnitude increase of particles up to the $1 \mu m$ range while the spectrum of the larger size particles remains unchanged.

The droplet growth law in a diffusion controlled process (cf. Appendix B) may be described by

$$\frac{dR}{dt} = \frac{c}{R}. \qquad \text{(c = proportionally constant)} \qquad .$$

Therefore the distortion of the particle size spectrum due to the growth in size of the particles is

$$\frac{dN(R,t)}{dt} = \frac{d}{dR}\left[\frac{cN(R,t)}{R}\right] \qquad .$$

Since $N(R) \sim R^{-6}$ for the Sonimist spectrum, particles in the small size range of the spectrum will grow much faster than those in the large size range. Hence, we observed the tilting towards a steeper slope of dN/dR as more condensing water is available. The following Table computes the ratio $\Delta N_{observed} / \Delta(N_o/R)$ for Cases (1) and (2) where N_o is the spectrum obtained from Case (1).
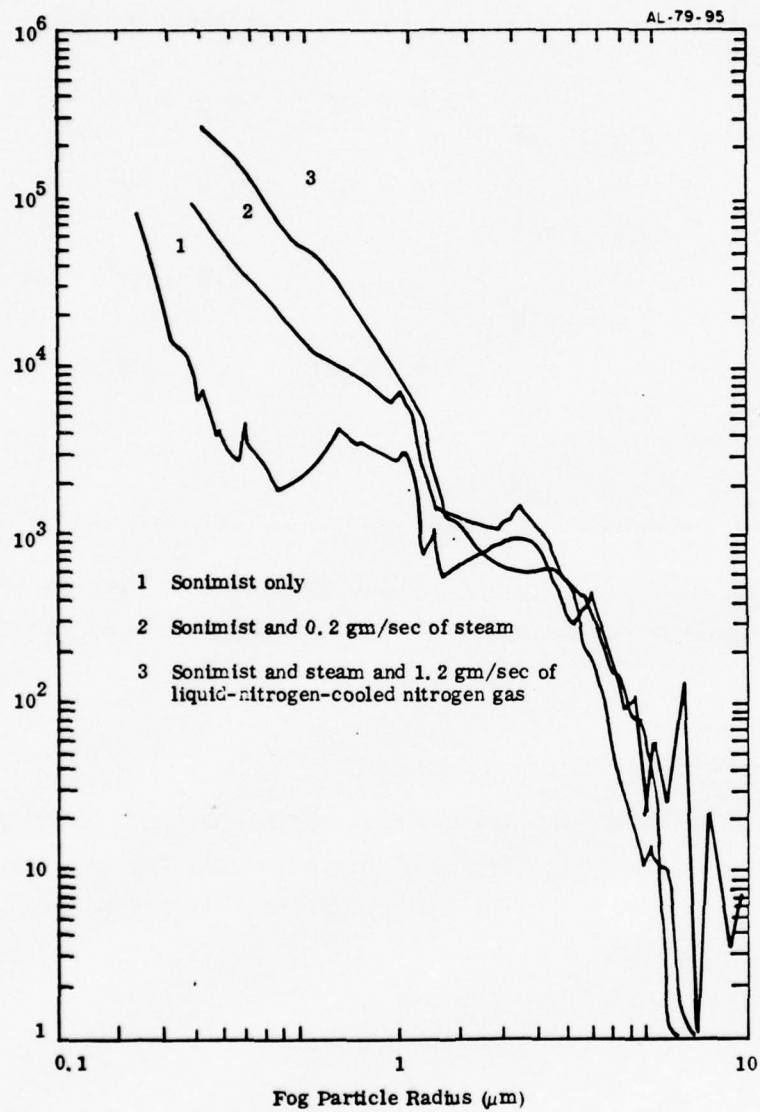
Figure 39. Spectrum From Growth of Sonimist Droplets Showing Effect
of Condensation

Table 3

Ratio of Observed to Calculated Particle Growth

$2R$ (μm)	N_O (μm/cm^3)	$N_O/2R$	$-\Delta\left(\dfrac{N_O}{2R}\right)$	$\Delta N_{observed}$	$\dfrac{\Delta N_{observed}}{-\Delta(N_O/2R)}$
1	5×10^2	5×10^2			
			3.5×10^2	4×10^2	1.1
2	3×10^2	1.5×10^2			
			1.3×10^2	6.5×10^2	0.4
3	7×10^1	2.3×10^1			
			0.05×10^1	0.2×10^1	40
4	9×10^1	2.25×10^1			
			0.45×10^1	0.5×10^2	11
5	9×10^1	1.8×10^1			
			1.2×10^1	1×10^1	0.8
6	3.5×10^1	0.6×10^1			

According to the theory, $\Delta N_{observed}/\Delta(N_O/R)$ should be constant. The data is not accurate enough (especially in regions of low $\Delta(N/R)$) to determine the quantitative validity of the theory.

7.2 Evaporation of the Sonimist Produced Droplets

We also tried mixing the output of the Sonimist with hot air so as to change the spectrum by evaporating the droplets. Figure 40 shows the resulting spectrum from mixing different amounts of hot air with the Sonimist spray. The process is the reverse of the growth process with

$$\frac{dR}{dt} \cong -\frac{c}{R} < 0 \qquad (c = \text{proportional constant}) \quad .$$

Therefore, the small size range of the spectrum shifts down faster than the large size range. At a hot-air flow rate of 150 SCFH (compared with the 200 SCFH air flow rate of the Sonimist), practically all of the particles are evaporated.
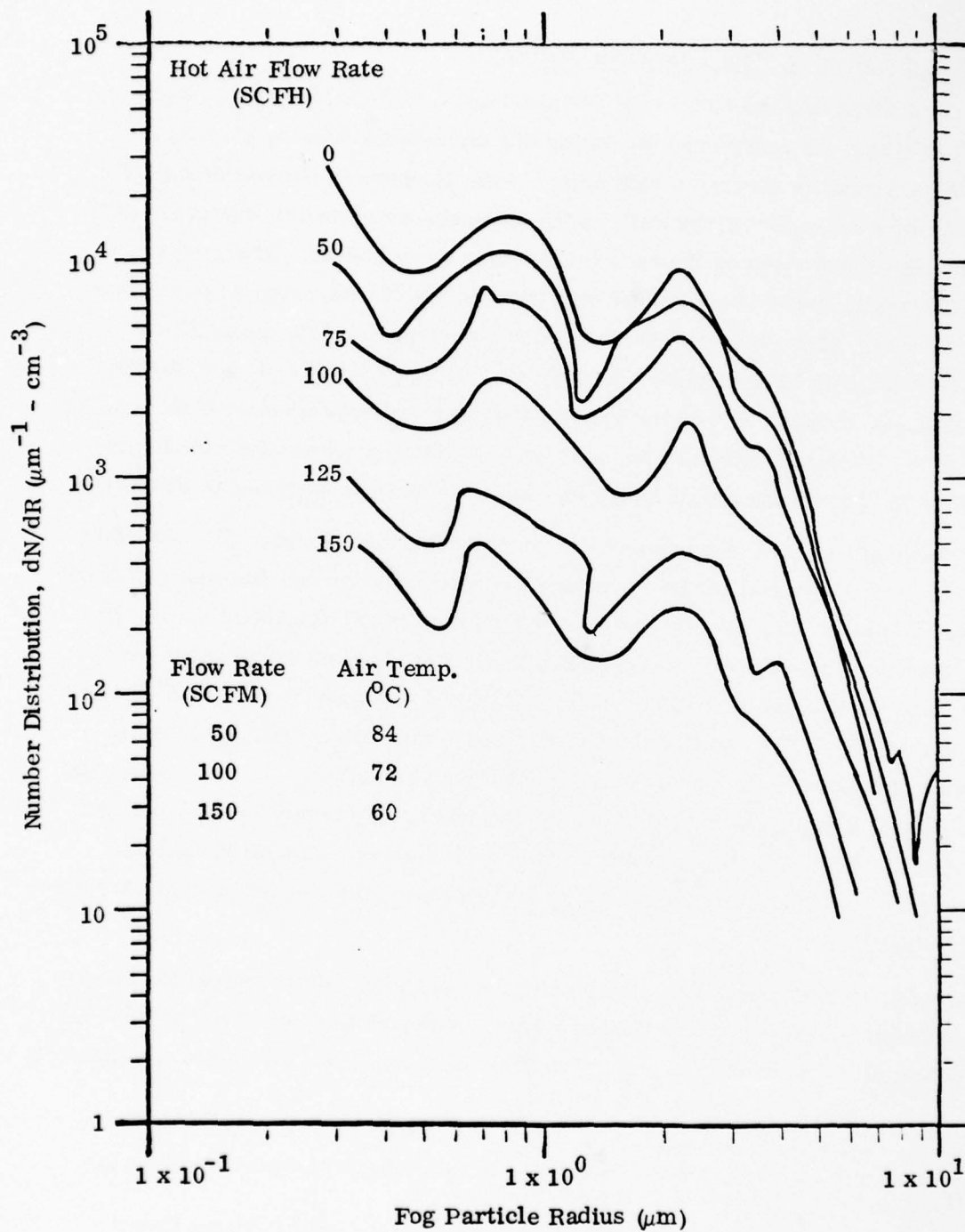
Figure 40. Spectrum Produced by Mixing Hot Air With Sonimist-Produced Fog Showing Effect of Evaporation

7.3 Growth of Droplets by Heat Exchanger Method

Instead of removing the latent heat of vaporization of the condensing water via mixing with cold air, we considered the option of removing the heat by passing the steam/nuclei/air mixture through a cold pipe. In the absence of condensation nuclei, the water will be condensing on the wall. With the presence of nuclei, however, part of the water vapor condenses on the nuclei which then grow in size. The growth process is thermally limited because the only mechanism of heat removal is via conduction to the wall. This method of growing nuclei to large droplets (up to 27 μm radius) was reported to have been successfully employed for liquids of low volatility (Ref. 30 - 33). In Appendix C we look into the feasibility of such a scheme for growing water droplets. From a quasi-one-dimensional calculation it seems feasible to grow particles into the 5 to 10 μm radius range by cooling the wall to very low temperature.

A preliminary experiment was carried out to verify the concept. The set-up is shown in Fig. 41. Hot moist air is prepared by bubbling air through hot water at about 25 cm^3/sec. This air then passes through a heated pipe where the nuclei source is located. The nuclei source (Fig. 42) consists of a grid of number 26 nicrome wire, heavily coated with sodium chloride crystals and heated electrically up to 500°C. The nuclei are generated by the sublimation and recondensation of the sodium chloride. This mixture of moist air and nuclei then flows through a one-inch-diameter pipe with L/D equal to 10. The pipe is cooled by a coolant jacket. Experiments were run both with room-temperature running water and with dry-ice-cooled acetone as coolant. The output particle spectrum is measured by the PMS particle counter using a vacuum-pulled sampling line.

Figures 43 and 44 are the spectra obtained for the two coolant temperatures with the nuclei source heated to various temperatures. Although the data are too crude for absolute quantitative evaluation, on a relative basis they do show that there is growth of a

---

[32] J.Burgoyne and L.Cohen, "The Production of Monodisperse Aerosols of Large Droplet Size,"J. Coll. Sci. 8 , 364-366 (1953).

[33] D.Sinclair and V. LaMer, "Light Scattering As a Measure of Particle Size in Aerosols, "Chem. Rev. 44, 262-264 (1949).

AL-79-77
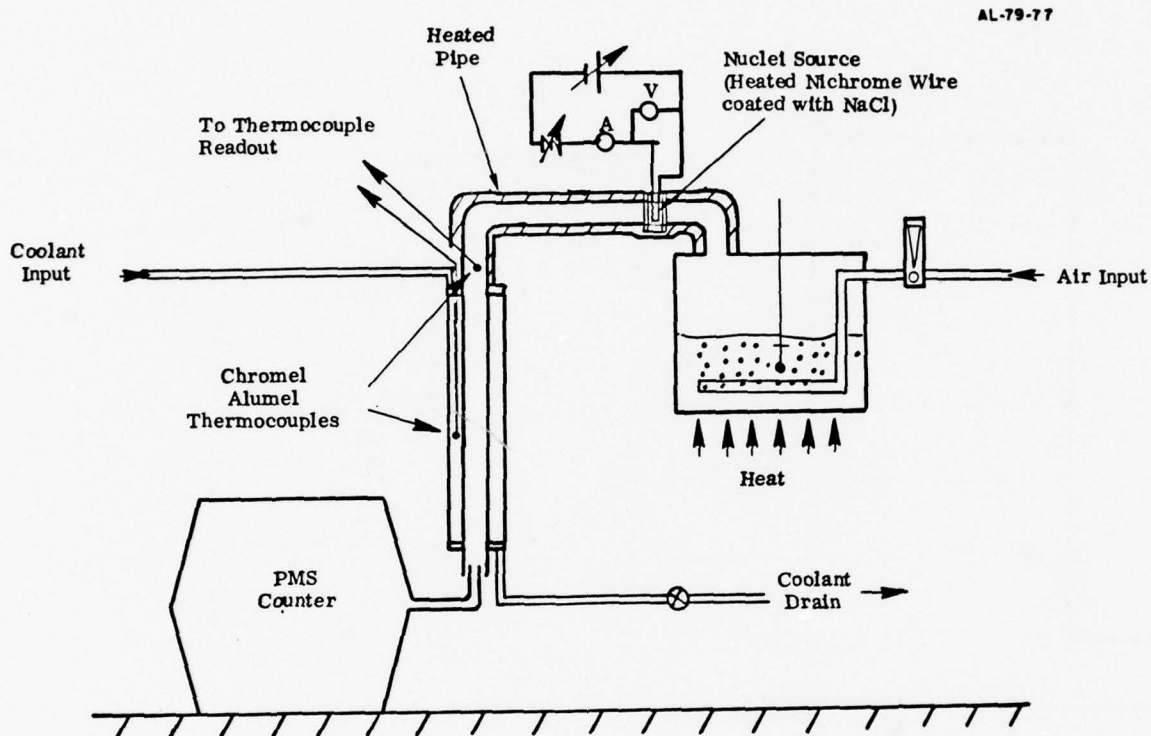
Figure 41. Growth of Fog Particles by Heat Exchanger Method
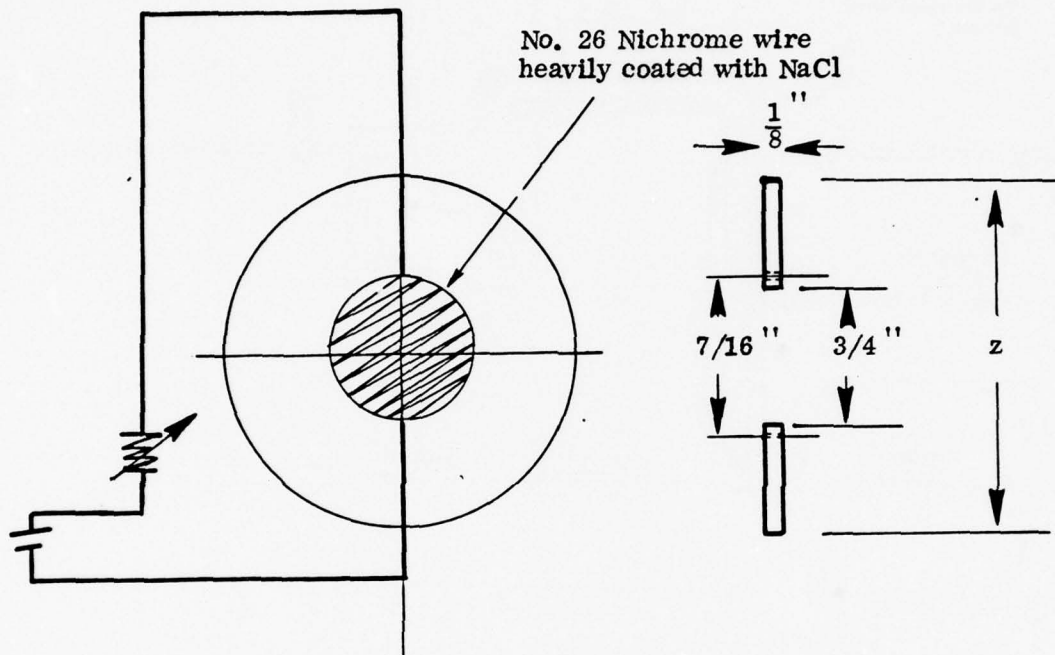
Figure 42. Sodium Chloride Nuclei Generator
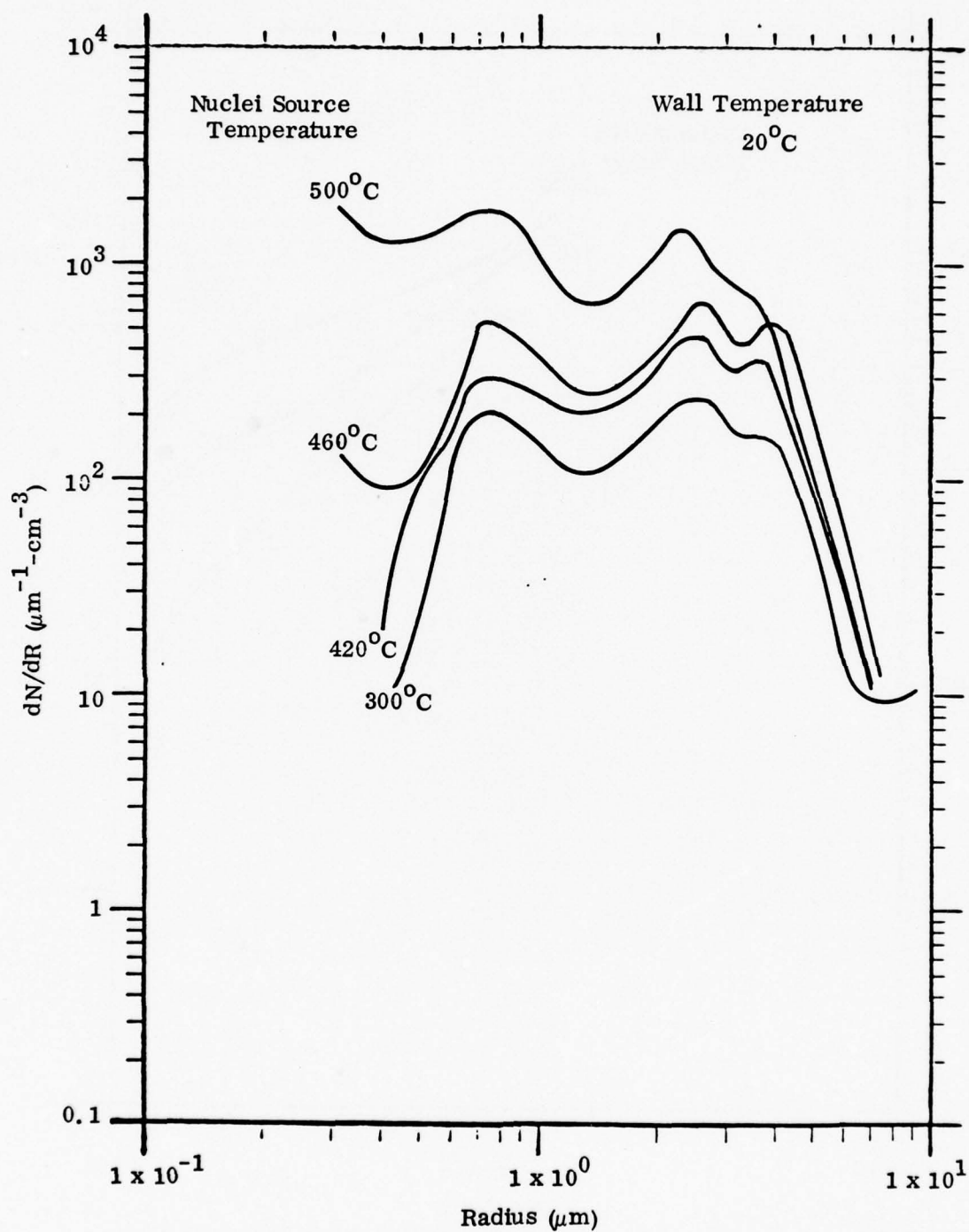
Figure 43. Droplet Spectrum From Nuclei Growth Using Room-Temperature
(T = 20°C) Running Water as Heat Exchanger Coolant

7-11
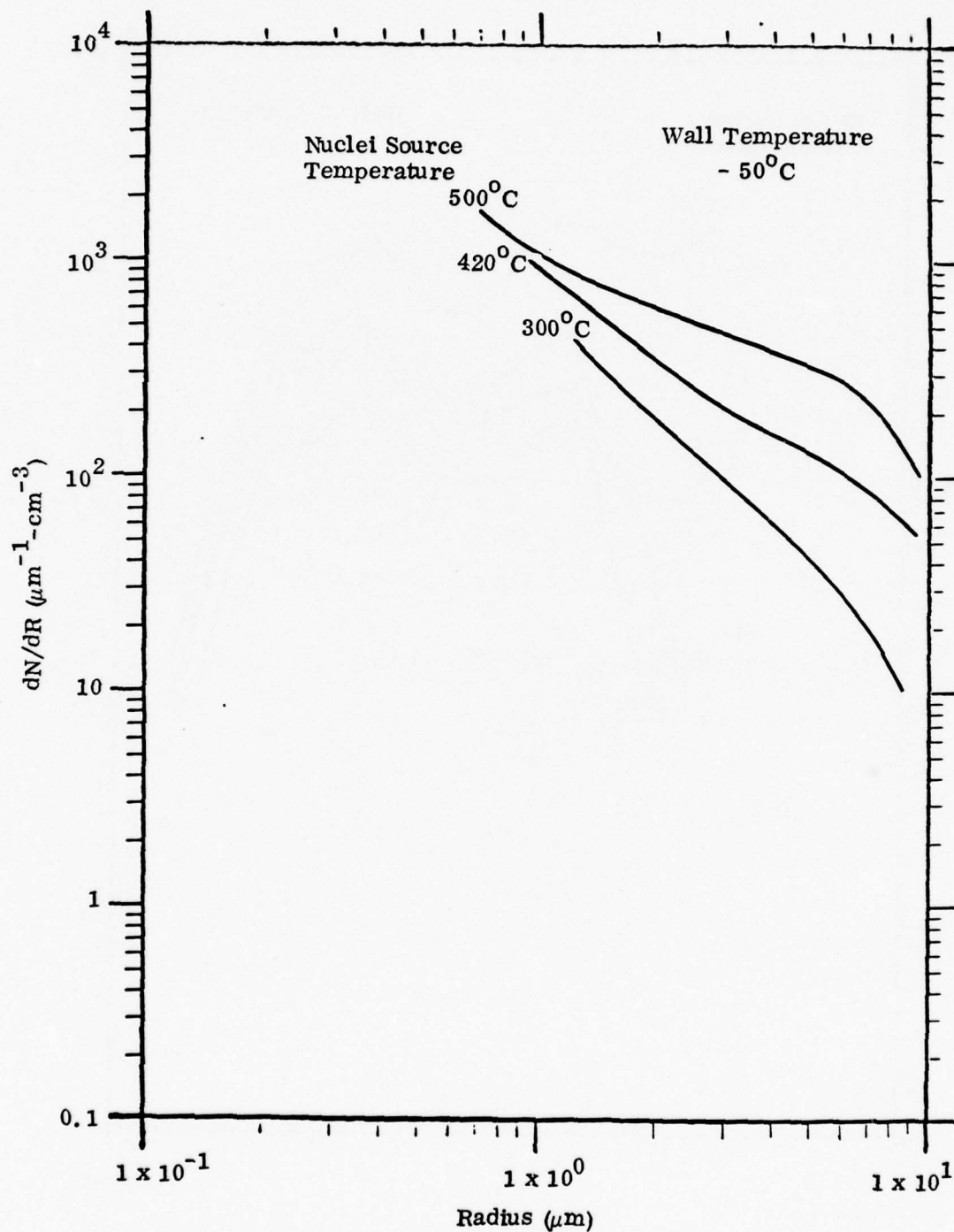
Figure 44. Droplet Spectrum From Nuclei Growth Using Dry-Ice-Cooled
(T = - 50°C) Acetone as Heat Exchanger Coolant

significant amount of large particles. For the room-temperature water-cooled experiment, the spectrum is populated up to 4 to 5 μm radii. For the dry-ice-cooled case, there are significant particles even up to 10 μm radii. The overall particle density is approximately 100 times greater than found with natural fog (Fig. 1b).

7.4 Summary

Preliminary experiments were carried out to produce fog droplets of controllable size spectrum. They are summarized as follows:

Experiment	Result
Growth of droplets from the Sonimist by condensing steam on to them via cold air mixing.	Order of magnitude increase in the number of small particles. Particles with radii greater than 2 μm remain unchanged.
Evaporation of the droplets from the Sonimist by mixing with hot dry air.	Order of magnitude decrease in small particles.
Growth of fog by condensing steam on to NaCl nuclei via a heat exchanger.	Significant amount of large particles (up to 5 to 10 μm radii); density is approximately 100 times more dense than in natural fog.

8. CONCLUSION

A continuous flow fog chamber was built with the fog generated by a Sonimist spray nozzle. The droplet size spectrum produced resembles that of natural fog and is 10 to 100 times denser. An optical depth of 3 to 5m was obtained with the present set up, and it is feasible to decrease the optical depth (i. e., increase the fog particle density) by an order of magnitude by using multiple spray nozzles.

The spectral shape was found to be insensitive to the operating parameters of the Sonimist. Preliminary experiments were carried out to produce fog with a variable size spectrum. The amount of small droplets produced by the Sonimist can be increased or decreased by an order of magnitude by mixing steam or hot air with the spray.

Experiments were carried out to grow sodium chloride nuclei in steam by passing the mixture through a cooled pipe. Preliminary results were very encouraging as a significant amount of large particles (5 to 10 μm radii) were obtained by changing the temperature of the coolant in the heat-exchanger pipe. Fog densities achieved with these controllable, large-particle spectra were up to 100 times greater than natural fog.

9. REFERENCES

1. H.F. Yura, "Optical Heterodyne Signal Power Obtained From Finite Sized Sources of Radiation," _Appl. Opt._ 13, 150-157 (1974).

2. R.F. Lutomirski and R.G. Buser, "Mutual Coherence Function of a Finite Optical Beam and Application to Coherent Detection," _Appl. Opt._ 12, 2153-2160 (1973).

3. J.P. Gollub et al., "Optical Heterodyne Measurement of Cloud Droplet Size Distributions," _Appl. Opt._ 12, 2838-2842 (1973).

4. R.F. Lutomirski and H.T. Yura, "Propagation of a Finite Optical Beam in an Inhomogeneous Medium," _Appl. Opt._ 10, 1652-1658 (1971).

5. A.J. LaRocca and R.E. Turner, "Atmospheric Transmittance and Radiance: Methods of Calculation," IRIA State-of-the-Art Report (June 1975) pp. 30-33, 54-84, 441-467.

6. S.R. Pal and A.I. Carswell, "Multiple Scattering in Atmospheric Clouds: Lidar Observations," _Appl. Opt._ 15, 1990-1995 (1976).

7. J.V. Winstanley and C. Wigmore, "A Multiple Scattering Correction for Lidar Systems," AGARD Conf. Proc. No. 183 (Oct. 1975) pp. 27-1 to 27-13.

8. W.C. Wells et al., "Aerosol Distributions in Maritime Air and Predicted Scattering Coefficients," _Appl. Opt._ 16, 654-659 (1977).

9. H.R. Carlon et al., "Infrared Extinction Spectra of Some Common Liquid Aerosols," _Appl. Opt._ 16, 1598-1605 (1977).

10. V.E. Zuev, "Laser-Light Transmission Through the Atmosphere," _Laser Monitoring of the Atmosphere_, E.D. Hinkley, Ed. (New York, Springer Verlag, 1976).

11. V.E. Zuev, _Propagation of Visible and Infrared Radiation in the Atmosphere_, (New York, Wiley, 1974).

12. V.E. Zuev, M.V. Kabanov, and B.A. Savelov, "Propagation of Laser Beams in Scattering Media," _Appl. Opt._ 9, 137-141 (1971).

13. A. Arnulf and J. Brichard, "Transmission by Haze and Fog in the Spectral Region 0.35 to 10 Microns," _J. Opt. Soc. Am._ 47, 491-498 (1957).

References (Continued)

14. D. Deirmendjian, "Scattering and Polarization Properties of Water Clouds and Hazes in the Visible and Infrared," Appl. Opt. 3, 187-196 (1964).

15 R.G. Pinnick, J.D. Lindberg, and E.B. Stenmark, "Vertical Inhomogeneity in Wintertime Atmospheric Fog and Haze in West Germany and the Effects on IR Transmission," Unclassified report of the Atmospheric Sciences Laboratory, White Sands Missile Range, (1976).

16. V.E. Zuev, Propagation of Visible and Infrared Radiation in the Atmosphere, (New York, Wiley, 1974) pp. 168-177.

17. G. Yamamoto, M. Tanaka, and S. Asano, "Radiative Transfer in Water Clouds in the Infrared Region," J. Atm. Sci. 27, 282-292 (1970).

18. C. Tomasi and F. Tampieri, "Size Distribution Models of Small Water Droplets in Mist and Their Volume Extinction Coefficients at Visible and Infrared Wavelengths," Atm. Environ. 10, 1005-1013 (1976).

19. W.V. Irvine and J.B. Pollack, "Infrared Optical Properties of Water and Ice Spheres," Icarus 8, 324-360 (1968).

20. R.H. Munis and A.J. Delaney, "Simultaneous Measurement of Laser Extinction in Warm Fog at Wavelengths of 0.6328, 1.15 and 10.6 Microns," Army Research Report 343, October 1975, Army Corps of Engineers, Hanover, N.H.

21. R.H. Munis and A.J. Delaney, "Measurements of Laser Extinction in Ice Fog for Design of SEV Pilotage System," Army Research Report 302, August 1972, Army Corps of Engineers, Hanover, N.H.

22. V.E. Zuev et al., "Attenuation of Visible and Infrared Radiation by Artificial Water Fogs," Izv., Atm. and Ocean. Phys. Ser. 1, 509-516 (1965), trans.

23. E. Reisman, G. Cumming, and C. Bartky, "Comparison of Fog Scattered Light and Monochromatic Incoherent Light," Appl. Opt. 6, 1969-1972 (1967).

24. R.G. Knollenberg, Preprint Volume, International Conference on Cloud Physics, (July 1976), Boulder Colorado. Published by the Am. Met. Soc., Boston, Mass.

25. S.K. Friedlander, Smoke, Dust, and Haze (Wiley, New York, 1977).

26. G. Trusty, Naval Research Lab., Code 8586, Washington, D.C. 20375. Private communication, 1978.

References (Continued)

27. W.R. Lane, "Shattering of Drops in Streams of Air," Ind. Eng. Chem. 43, 6, 1312-1317 (1951).

28. G. Gordon, "Mechanism and Speedy Breakup of Drops, "J. Appl. Phys. 30, 11 (1959).

29. P. Simpkins and E. Bales, "Water Drop Response to Sudden Acceleration," J. Fluid. Mech. 55, 4, 629-639 (1972).

30. N. Fuchs and A. Sutagin, "Generation of Monodisperse Aerosols, "in Aerosol Science, Ed. C.N. Davies, Academic Press (1960) Ch. 1.

31. M. Corn and N.A. Esmen, "Aerosol Generation," in Handbook of Aerosols, ed. by R. Dennis, ERDA (1976), pp. 9-39.

32. J. Burgoyne and L. Cohen, "The Production of Monodisperse Aerosols of Large Droplet Size, "J. Coll. Sci. 8, 364-366 (1953).

33. D. Sinclair and V. LaMer, "Light Scattering As a Measure of Particle Size in Aerosols," Chem. Rev. 44, 262-264 (1949).

34. G. Goyer and F. Pidgeon, "Production and Characteristics of Submicron Water Aerosols," J. Coll. Sci. II, 697-703 (1956).

APPENDIX A
TURBULENCE EFFECTS ON DROPLET COAGULATION

A simplified picture of the structure of a turbulent flow is as follows: large scale velocity gradients give rise to flow instabilities which produce eddies with a characteristic scale ℓ_o comparable to that of the gradients, and hence, to the dimension of the duct, jet, or boundary layer producing the gradients. The turbulent velocity u_o characteristic of these layers is some fraction of the mean flow velocity; for instance, in jets and boundary layers, the rms velocity fluctuation is of the order of 5 - 20% of the flow velocity. Now, these large eddies are themselves unstable and tend to break up into smaller ones in times of the order of ℓ_o/u_o. Essentially in one "turn around," their energy being wholly transmitted to these smaller eddies, since, as long as the Reynolds number $R_e = \rho u \ell/\mu$ of the eddies is large, viscous dissipation can be ignored. Here, ρ is the density of the fluid. There is no inherent length scale in the fluid (as long as $R_e \gg 1$), and so the pattern of eddy breakdown and energy transmission to smaller scales repeats itself continuously. The kinetic energy per unit volume associated with eddies of size ℓ and velocity v is proportional to ρv^2, and it gets transmitted down to the next smaller size in time on the order of ℓ/v, so the rate of kinetic energy transmission is:

$$\epsilon = \frac{\rho v^2}{\ell/v} = \frac{\rho v^3}{\ell} \quad , \tag{A-1}$$

and this is the same at all scales below ℓ_o, so that at a scale ℓ the characteristic velocity is:

$$v = \left(\frac{\ell \epsilon}{\rho}\right)^{1/3} = \left(\frac{\ell}{\rho} \frac{\rho v_o^3}{\ell_o}\right)^{1/3} = v_o\left(\frac{\ell}{\ell_o}\right)^{1/3} \quad . \tag{A-2}$$

The viscous dissipation rate $\mu (\nabla v)^2$ then is proportional to $(v/\ell)^2 \sim (\ell^{1/3}/\ell)^2 = \ell^{-4/3}$ and increases as the eddy size decreases. (Here μ is the viscosity.) At some size ℓ_k, the eddy must be able to absorb the energy E being transmitted from ℓ_o, v_o. This size is given by:

$$\mu \left(\frac{v_k}{\ell_k} \right)^2 = \epsilon = \frac{\rho v_k^3}{\ell_k} \quad , \tag{A-3}$$

or

$$\frac{\rho v_k^3 \ell_k}{\mu} = 1 \quad , \tag{A-4}$$

and since $v_k = v_o (\ell_k / \ell_o)^{1/3}$, then

$$\ell_k = \left(\frac{\mu \ell_o^{1/3}}{\rho v_o} \right)^{3/4} \quad \text{(Kolmogorov length)} \quad . \tag{A-5}$$

Physically then, no eddies smaller than ℓ_k are to be found in the turbulent fluid, since viscous effects are then dominant over inertial effects.

For the purposes of assessing the effect of turbulence on coagulation rate, this distance ℓ_k must be compared to the "stopping distance" or "relaxation distance" ℓ_{rel} of a droplet of radius R being shaken by the velocity fluctuation. Consider the drop equation of motion,

$$\frac{4}{3} R^3 \rho_D \frac{dv_D}{dt} = 6 \pi \mu R (v - v_D) \quad , \tag{A-6}$$

where ρ_D is the liquid density and v_D the drop velocity when the fluid velocity in its vicinity is v. This can be written as:

$$\tau_{rel} \frac{dv_D}{dt} = v - v_D \quad , \tag{A-7}$$

where the relaxation time τ_{rel} is:

$$\tau_{rel} = \frac{2}{9} \rho_D \frac{R^2}{\mu} \tag{A-8}$$

A-2

and is the time it would take for viscosity to eliminate a given relative motion of the drop. The characteristic "shaking time" seen by the drop is the eddy time ℓ/v (after eddies of size ℓ) and is:

$$\tau_{eddy} = \frac{\ell}{v} = \frac{\ell}{v_o(\ell/\ell_o)^{1/3}} = \frac{\ell^{2/3} \ell_o^{1/3}}{v_o} \quad . \tag{A-9}$$

Thus, smaller eddies have a higher characteristic "shaking frequency", and, for a given drop size, eddies smaller than a certain size ℓ_{slip} will shake in times shorter than τ_{rel}. Hence the droplets will not be able to follow the motion and will slip relative to the fluid. We find ℓ_{slip} by equating τ_{rel} to τ_{eddy}:

$$\tau_{rel} = \frac{\ell_{slip}^{2/3} \ell_o^{1/3}}{v_0} \quad , \tag{A-10}$$

or

$$\ell_{slip} = \frac{(\tau_{rel} v_o)^{3/2}}{\ell_o^{1/2}} \quad . \tag{A-11}$$

It is clear that if ℓ_{slip} turns out to be less than ℓ_k, no eddy will exist which will shake violently enough to induce droplet slip. The drops are then locked to their local fluid element, and since no two fluids elements can occupy the same position at the same time, turbulence cannot influence the rate of agglomeration. This is true even if ℓ_k is less than the mean distance between droplets; in this case individual droplets may in fact be caught in different eddies and acquire a corresponding relative motion, but still they will "miss" each other as they follow their individual fluid elements (provided the drop size itself is not larger than the eddy size).

For water droplets in air ($\rho_D = 1000$ kg/m^3, $\rho_{air} = 1.2$ kg/m^3, and μ_{air} 2×10^5 kg(m-sec)$^{-1}$, one can calculate ℓ_k and ℓ_{slip} for different u_o, ℓ_o and R. Table A-1 gives these values.

A-3

Table A-1

Calculated Values of ℓ_k and ℓ_{slip} for Water Droplets in Air

ℓ_o(m)	u_o(m/sec)	$R(\mu m)$	$\ell_k(\mu m)$	$\ell_{slip}(\mu m)$
0.1	10	1	26	3.2
0.1	10	2	26	26
0.1	10	10	26	3200
0.1	1	1	147	0.1
0.1	1	10	147	100
1	0.02	1	4900	0.9×10^{-4}
1	0.02	10	4900	0.09

The first five lines in the table refer to conditions typical in the vicinity of the atomizer (small scale, high-energy eddies), while the last two lines refer to conditions in the fog chamber itself. It is clear that the only case for which turbulence would be of importance to agglomeration is that for the largest drops (10 μm) at the highest eddy velocity (10 m/sec and $\ell_o = 0.1$m). Certainly, in the chamber turbulent effects can be ignored.

The dividing line $\ell_k = \ell_{slip}$ is:

$$\left(\frac{\mu}{\rho} \frac{\ell_o^{1/3}}{v_o} \right)^{3/4} = \left(\frac{2\rho_D R^2 v_o / 9\mu}{\ell_o^{1/2}} \right)^{3/2} \quad , \qquad (A-12)$$

which can be rearranged to:

$$\frac{R}{\ell_k} = \frac{3}{\sqrt{2}} \left(\frac{\rho}{\rho_D} \right)^{1/2} \cong 0.074 \quad \text{(water in air)} \quad . \qquad (A-13)$$

A-4

Therefore, if conditions are such as to produce a Kolmogorov length much longer than about 13 drop radii, turbulence agglomeration can be neglected. Figure A-1 summarizes the results of the above analysis.

The mathematical analysis of the spray nozzle and of agglomeration in the jet spray is given below.

Momentum Conservation: $2\pi rh\rho u^2 \simeq A_{exit} \Delta P$

average flow velocity $\sqrt{\overline{u^2}} = \sqrt{\dfrac{A_e \Delta P}{4\pi \tan\alpha \rho}} \dfrac{1}{r}$

turbulent region width $\quad h = 2r\tan\alpha$

For $\quad A_e \simeq 4 \times 10^{-5} \, m^2$

$\tan\alpha \simeq 0.1$

$\Delta P \simeq 10^5 \, N/m^2$

$\rho \simeq 1.2 \, Kg/m^3$

$$\boxed{\sqrt{\overline{u^2}} \simeq \dfrac{1.5}{r}}$$

$$\boxed{h = 0.2r}$$

Take the scale of the turbulence (largest eddies) as

$\ell_o = 0.4h$

$v_o = 0.2 \sqrt{\overline{u^2}} \quad$ (r.m.s. turbulent velocity)

$$\boxed{\ell_o = 0.08r} \qquad \boxed{v_o = \dfrac{0.3}{r}} \qquad ,$$

Then the Kolmogorov length is $\ell_K = \left(\dfrac{u}{\rho} \dfrac{\ell_o^{1/3}}{v_o}\right)^{3/4} \quad ;$

for air $\boxed{\ell_K = 3.4 \times 10^{-4} r}$

The velocity of the Kolmogorov eddies is

$v_K = \dfrac{\mu/\rho}{K} \longrightarrow \boxed{v_K = \dfrac{0.049}{r}}$

A-5
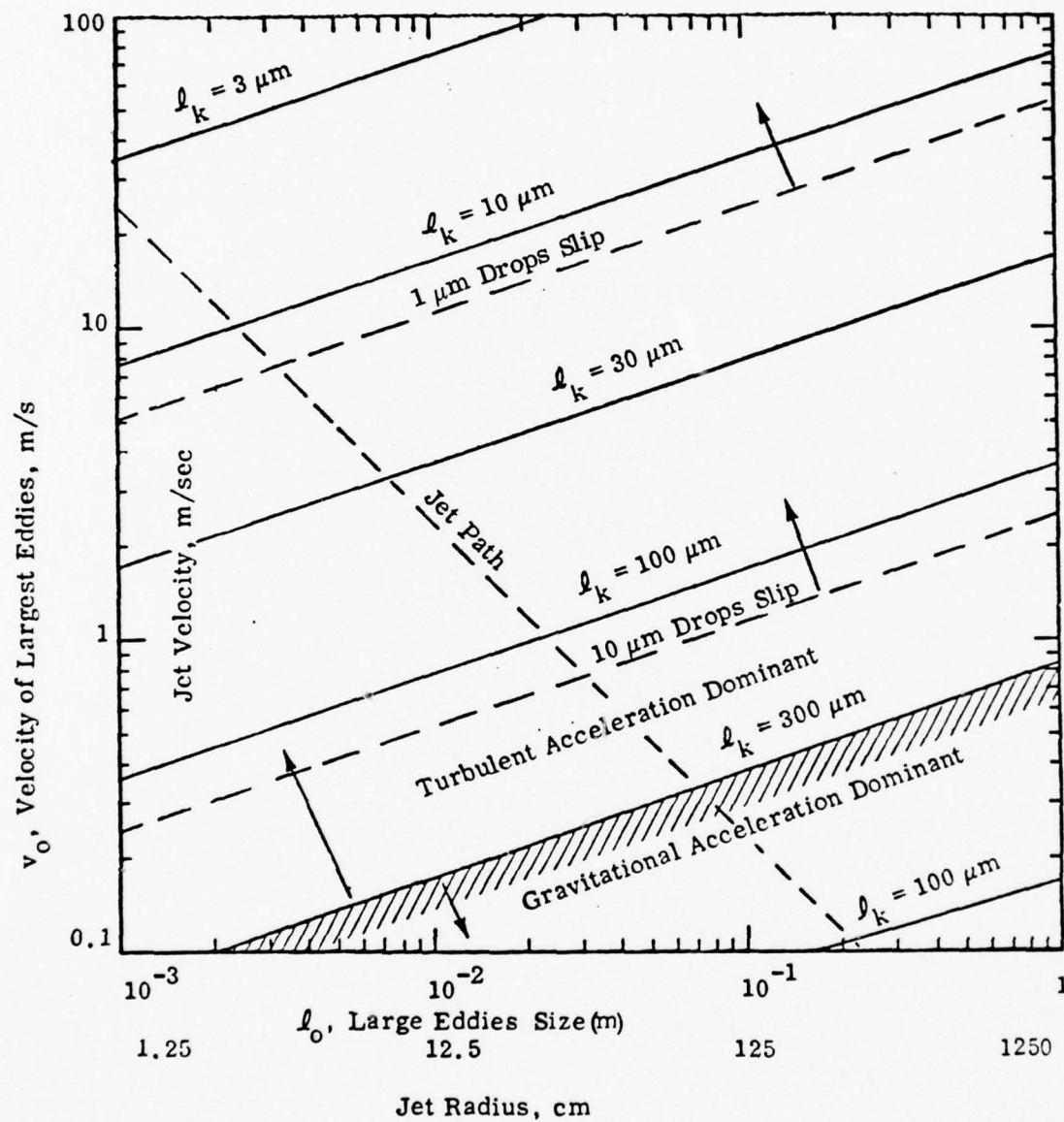
Figure A-1. Turbulent Jet Parameters
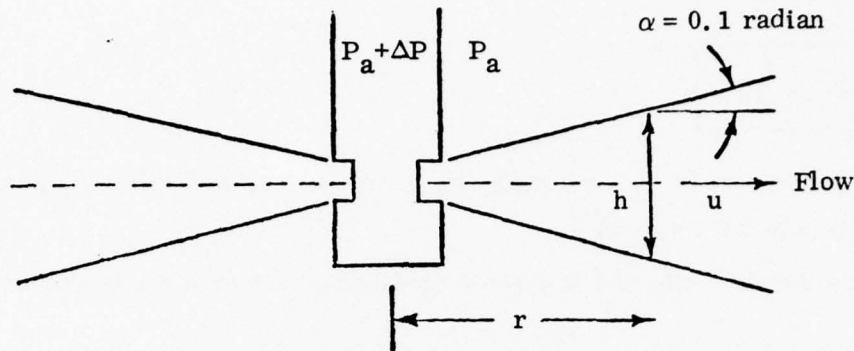
Figure A-2.   Spray Nozzle Schematic

Agglomeration in the Jet

Turbulent shaking dominates over gravitational acceleration if

$$\text{Turb. accel.} \simeq \left(\frac{v^2}{\ell}\right) K \simeq \frac{(\mu/\rho)^2}{\ell_K^3}$$

if more than 9.8 m/sec^2.   This is true if

$$\boxed{\ell_K \lesssim 300 \, \mu m}$$

and this happens for $\boxed{r \lesssim 1 \text{ m}}$.

For a given drop radius R, the drops will slip relative to the small (fast) eddies if their stokes relaxation time

$$\tau_{REL.} = \frac{2}{9} \, \rho_{liq.} \, \frac{R^2}{\mu}$$

is longer than the Kolmogorov eddy time

$$\tau_{EDDY} = \frac{\ell_K}{v_K} = \frac{\ell_K^2}{(\mu/p)}$$

A-7

For air, this implies

$$\boxed{\frac{\ell_K}{R} \lesssim 13.5}$$

For the jet, drops 10 μm or larger slip for $r \lesssim 0.4$m, while drops 1 μm or larger will slip only for $r \lesssim 4$ cm.

Thus, the relative slip of 1 and 10μm drops occurs over a significant section of the jet.

Maximum loss rate of small (1 μm) drops to large (10 μm) drops:

$$-\frac{d\left(\ell n\, N_{small}\right)}{dt} \leq N_{large}\, v_K\, \pi R^2_{large}$$

For $N_{large} = \frac{N_{total}}{100} \simeq 10^{10}\, m^{-3}$, $R_{large} = 10^{-5}\, m$, and $\frac{d}{dr} = \frac{1}{u}\frac{d}{dt}$

$$\boxed{-\frac{d\left(\ell n\, N_{small}\right)}{dr} \simeq 0.1}$$

For $r = 0.6$m

$$\frac{N_{small}}{(N_{small})_o} = e^{-0.06} \simeq 0.94$$

The agglomeration of water droplets in the jet is small.

APPENDIX B

CONDENSATION OF WATER VAPOR BY MIXING WITH AIR
OF LOWER TEMPERATURE

Consider the mixing of a mass, m_1, of air at temperature, T_1, with m_2 of steam at temperature T_2. The equilibrium product will be a mass of m_1 of air, m_v of vapor, and m_w of condensed water all at a final temperature T. From thermal balance we obtain:

$$\frac{m_1}{m_2} c_a(T - T_1) = \frac{m_w}{m_2} \left[L + (c_w - c_v) (T_2 - T) \right] + c_v(T_2 - T),$$

where

c_a = heat capacity of air;

c_w = heat capacity of water;

c_v = heat capacity of water vapor.

With the equilibrium condition that the vapor pressure present at T is given by the saturated vapor pressure, we can solve for m_w/m_2 for a given m_1/m_2 and T_1. The result of the calculation is shown in Fig. B-1 and B-2 for T_1 equal to 20, 0, -50, and -196°C. A density of $10^5/cm^3$ of 5 μm particles amounts to a mass loading of 50 gm/m^3. Figure B-2 shows that this is achievable by mixing in cold air at dry ice to liquid nitrogen temperatures.
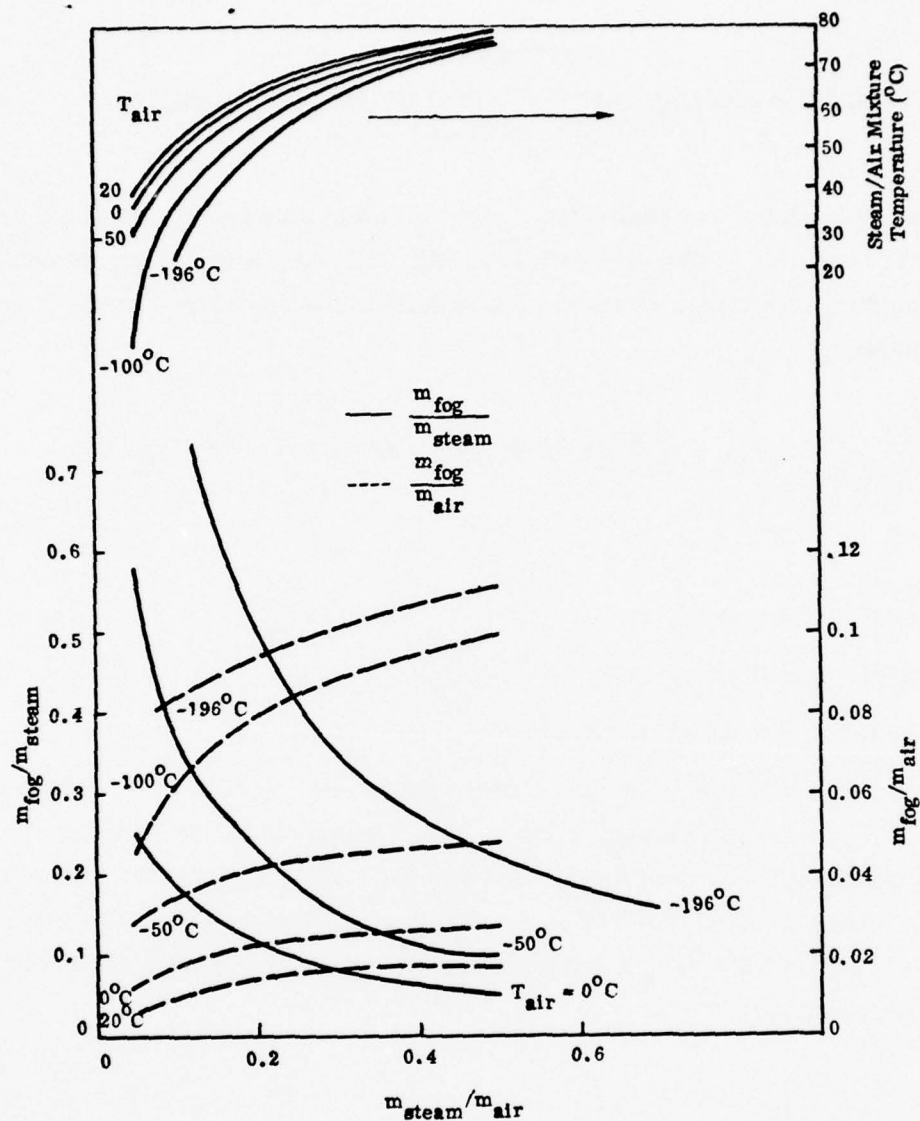
Figure B-1. Plot of Mass Ratios of Condensed Water Vapor (Fog Particles) to Steam and to Air for Different Temperatures of Mixing Air. The Five Upper Curves Give the Temperature of the Steam/Air Mixture. The Three Lower Solid Curves Are the Ratios for Fog/Steam. The Five Lower Dotted Curves are the Fog/Air Ratios.
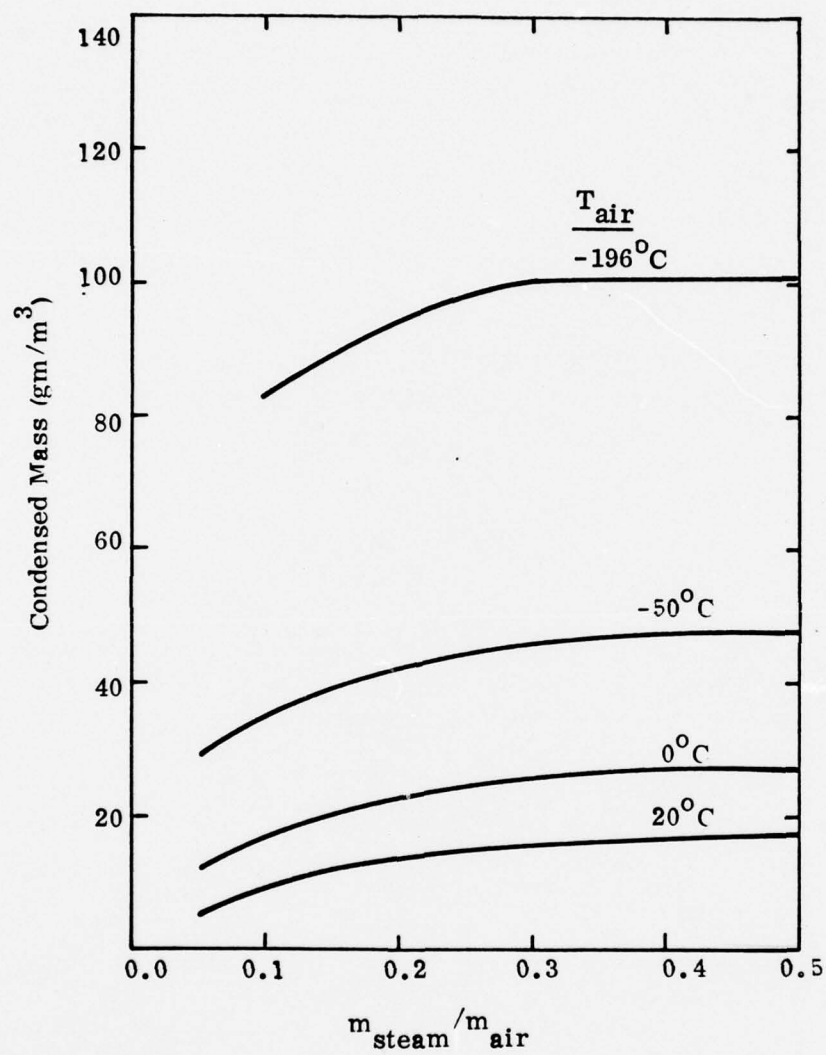
Figure B-2. Condensation of Water by Fog by Mixing With Cold Air.

APPENDIX C

PREPARATION OF FOG DROPLETS BY COOLING OF WATER VAPOR VIA A HEAT EXCHANGER: COMPUTER SIMULATION

We investigated the possibility of growing the small fog particles into larger droplets (~ 10 μm diameter) by heat exchanger condensation methods, i.e., the latent heat of vaporization is removed via a heat exchanger. This method has successfully been used in the past, noticeably in the LaMer Sinclair generator [33] and improved versions of it, for growing droplets of various low-vapor-pressure materials. Growth of submicron size fog droplets were also reported. [34] For the growth of big droplets, however, the high latent heat of vaporization and vapor pressure of water may present a problem. Consider the laminar flow of a vapor (carried by a noncondensible gas) in a cold pipe. In the absence of condensation nuclei, almost all the vapor condenses on the wall. If nuclei are present, however, part of the vapor condenses on them. These nuclei become heated up by the release of the heat of vaporization, and no further condensation takes place until this heat is conducted away to the wall. The process is therefore thermally limited. At the same time, vapor is lost to the wall by diffusion and condensation. The resultant droplet size is determined by the competition between the nuclei and the wall for the vapor.

The process may be modelled by the following equations (here the initial particle size is assumed to be large compared with the mean free path):

Droplet mass balance*

$$\frac{dr_d}{dt} = \frac{1}{r_d} \alpha_v (n_\infty - n_d) v_m \qquad (C-1)$$

---

[34] G. Goyen and F. Pidgeon, "Production and Characteristics of Submicron Water Aerosols," J. Coll. Sci. 11, 697-703 (1956).

* Note that this equation implies faster growth for small particles. Therefore, the particles tend to grow to the same size.

Droplet thermal balance

$$\frac{4}{3}\pi r_d^3 \rho_d C_d \frac{dT_d}{dt} + K_g(T_d - T_\infty)\,4\pi r_d = L\rho_d\,4\pi r_d^2 \frac{dr_d}{dt} \qquad (C-2)$$

Overall mass balance

$$\frac{dn_\infty}{dt} = \frac{-N4\pi r_d^2}{v_m}\frac{dr_d}{dt} + \alpha_v\frac{1}{r}\left(\frac{d}{dr}\,r\,\frac{d}{dr}\,n_\infty\right) \qquad (C-3)$$

Overall thermal balance

$$\rho_g C_g \frac{dT_\infty}{dt} = NK_g(T_d - T_\infty)\,4\pi r_d + K_g\frac{1}{r}\left(\frac{d}{dr}\,r\,\frac{d}{dr}\,T_\infty\right) \qquad (C-4)$$

Vapor pressure relation

$$n_d = \frac{v.p.\ (T_d)}{k\,T_d} \qquad , \qquad (C-5)$$

where

n = vapor molecule density

r_d = droplet radius

α_v = mass diffusivity of vapor

v_m = molecular volume

ρ = density

C = heat capacity per unit mass

K_g = gas thermal conductivity

k = Boltzman's constant

L = latent heat of vaporization of vapor

N = number density of nuclei = constant

Subscripts

    d   = droplet parameters

    v   = vapor parameters

    ∞ = properties far from the drop

    g   = noncondensable carrier gas parameters

The condensation process may be visualized as follows. Initially, say $n_\infty = n_d$ and $T_\infty = T_d$. Then as time progresses, T_∞ goes down because of conduction to the wall (last term in Eq. (C-4)). This process lowers T_d (2nd term in Eq. (C-2)) , lowers n_d (Eq. C-5), and starts the diffusion of n_∞ into the droplet (Eq. C-6)). This diffusion is checked by the latent heat produced (last term of Eq. (C-2)), and further condensation is not possible until this heat is conducted away. While this process is going on, the wall acts as a sink for n_∞ (last term in Eq. (C-3) , reducing the amount of vapor available for the droplet growth.

Equations (C-1) - (C-5) are solved with the following simplifying assumptions. It is assumed that both n_∞ and $(T_\infty - T_w)$ are parabolic profiles. While the exact validity of the assumption is questionable, it does provide the relevant physics of producing constant sink terms for both n_∞ and T_∞.

$$\frac{1}{r}\frac{d}{dr}\left[r\frac{d}{dr}\begin{pmatrix}n_\infty\\T_\infty\end{pmatrix}\right] = \frac{-4}{R^2}\begin{pmatrix}n_\infty\\T_\infty & T_w\end{pmatrix}$$

Therefore a quasi one dimensional treatment is possible. The effective pipe radius R should be interpreted as a boundary layer thickness rather than the actual radius.

The following matrix of design parameters are calculated.

    Inlet condition: Air at 50°, 80°C with R.H.=1

    Wall temperature: 293, 223, 77°K

                   (corresponds to room, dry ice, and

                    liquid nitrogen temperature)

    Nuclei density: 10^4, 10^5, 10^6/cm^3

    Pipe Radius: 1 in.

The results of the computation are shown in the attached graphs. Figures C-1 to C-3 are for initial gas temperature $T_\infty(0) = 50°C$, while Figures C-4 to C-6 are for $T_\infty(0) = 80°C$. Since the controlling time scale is the mass and heat diffusion time to the wall $(t \sim R^2/\alpha)$ (assume Lewis number equals 1), the pipe radius effect is to approximately scale the time as radius squared. Therefore, separate calculations for different pipe radii are not necessary.

The plots of the particle radius as a function of time all show growth $\sim \sqrt{t}$, which is consistent with the diffusion model. The growth time is about 1 to 10 sec. The growth tapers off as the vapor is exhausted. In Fig. C-3 the droplet starts to evaporate after it reaches the maximum size. This effect is solely due to the assumption that there is a constant flux of vapor towards the wall which acts as a sink. Figures C-7 and C-8 are contour plots of the droplet size that can be achieved with various nuclei density and wall temperatures. For an input of 80°C saturated moist air the calculation shows that particles of 5 to 10μm radii can be achieved over a wide range of nuclei concentration if we cool the wall to dry ice temperature (223°K).

C-4

Figure C-1. Droplet Growth Characteristics (see text for discussion)

Figure C-2. Droplet Growth Characteristics (see text for discussion)

Figure C-3. Droplet Growth Characteristics (see text for discussion)
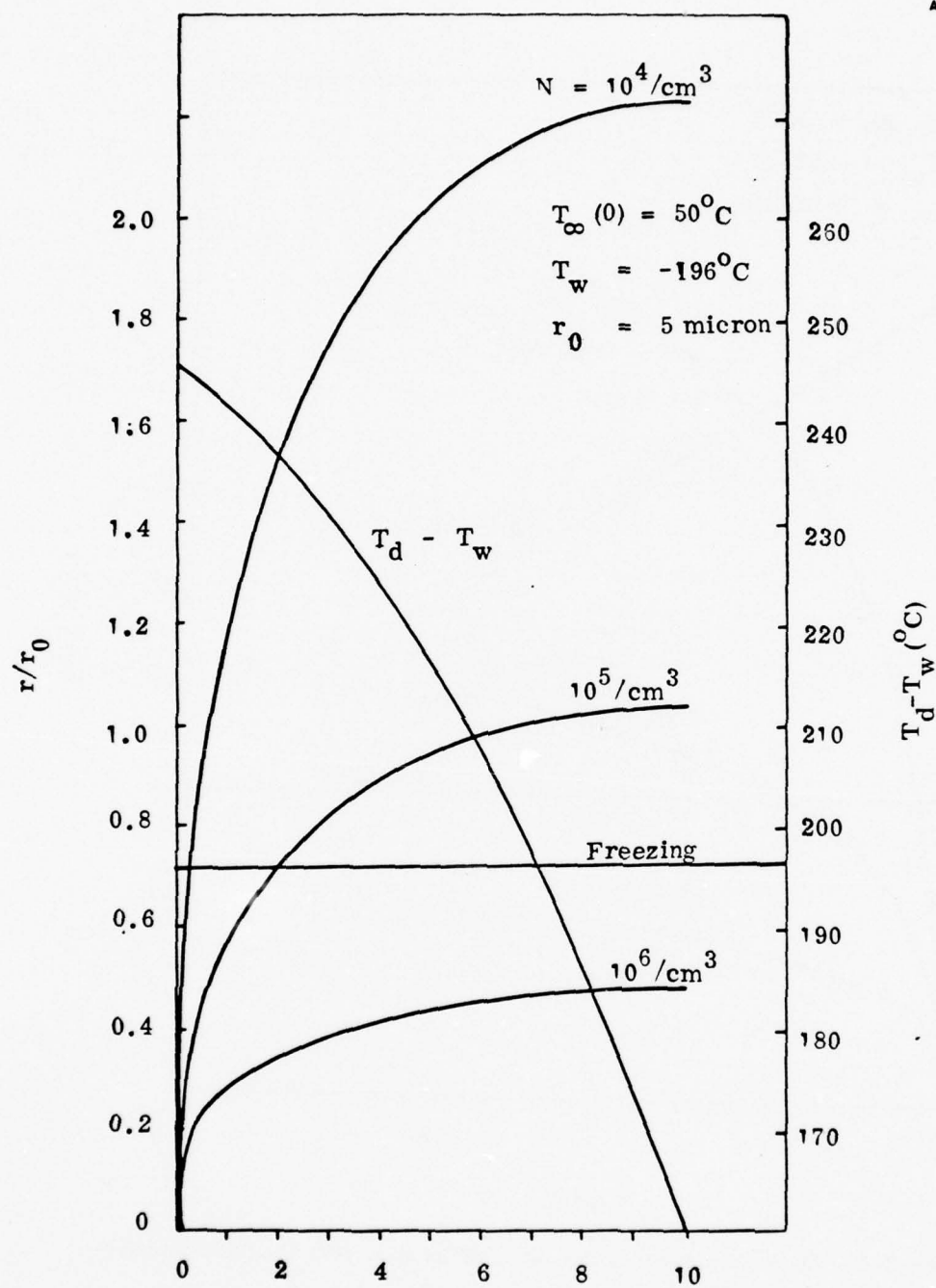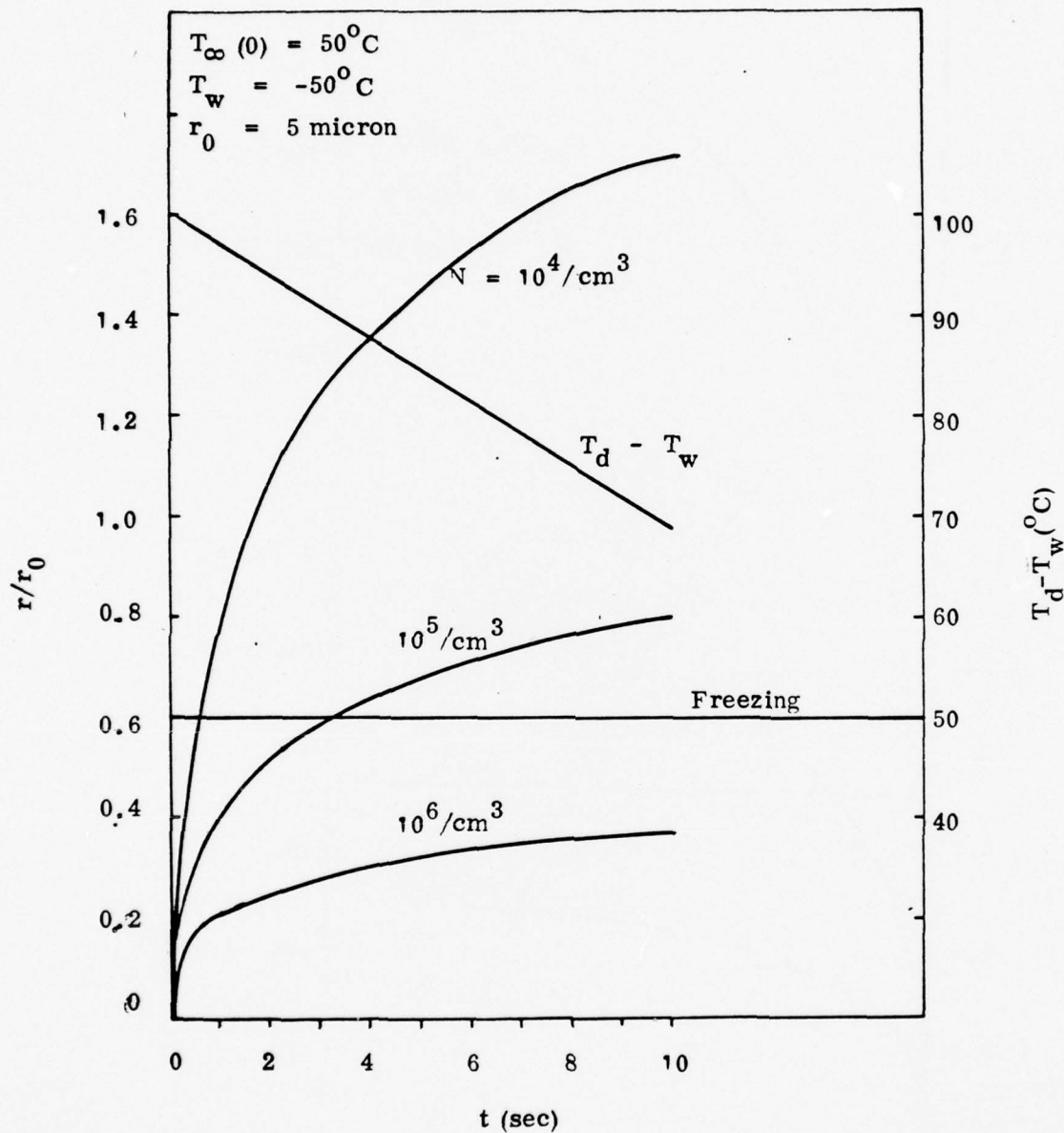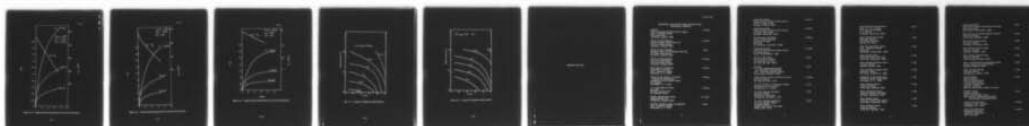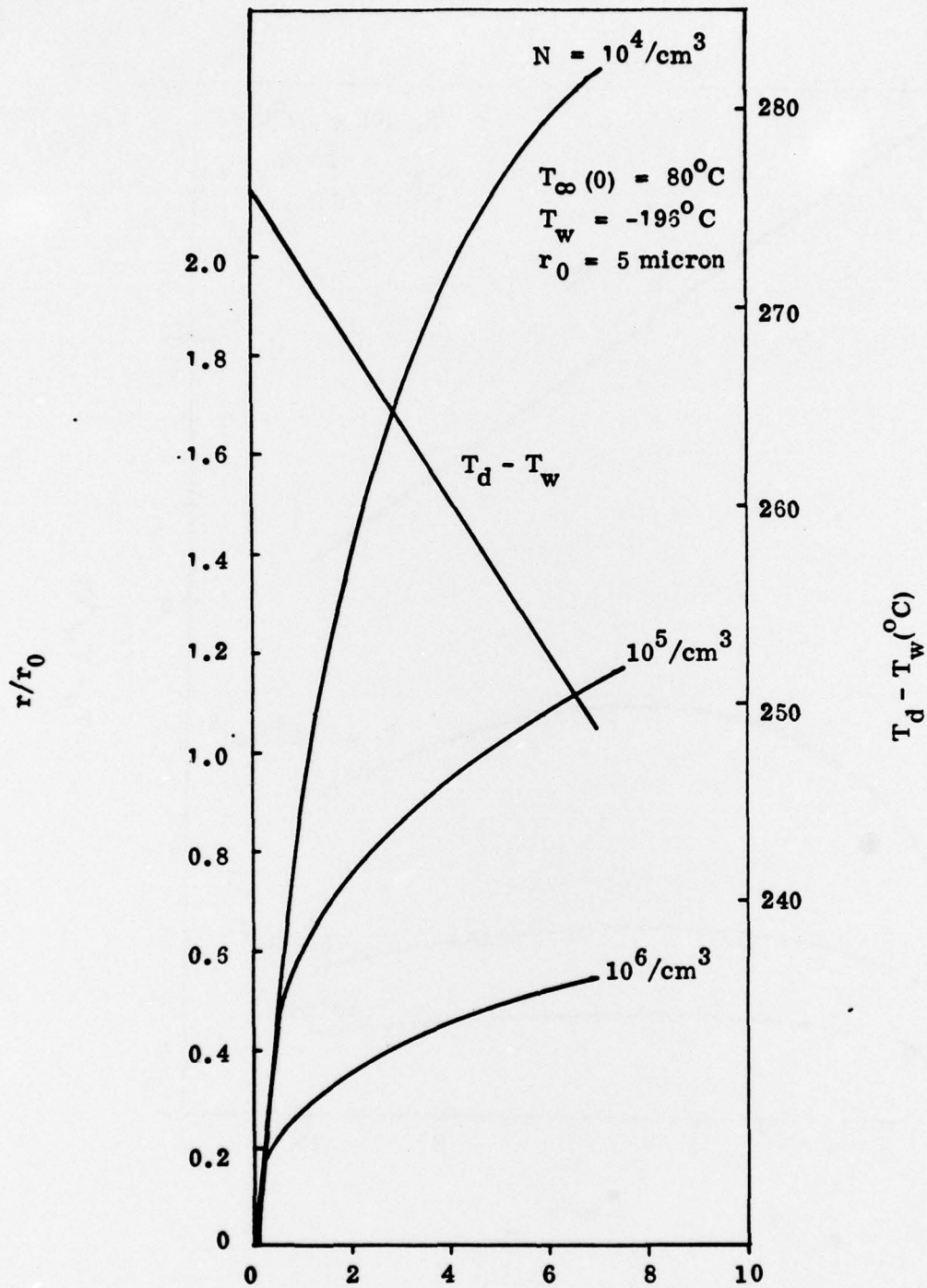
Figure C-4. Droplet Growth Characteristics (see text for discussion)
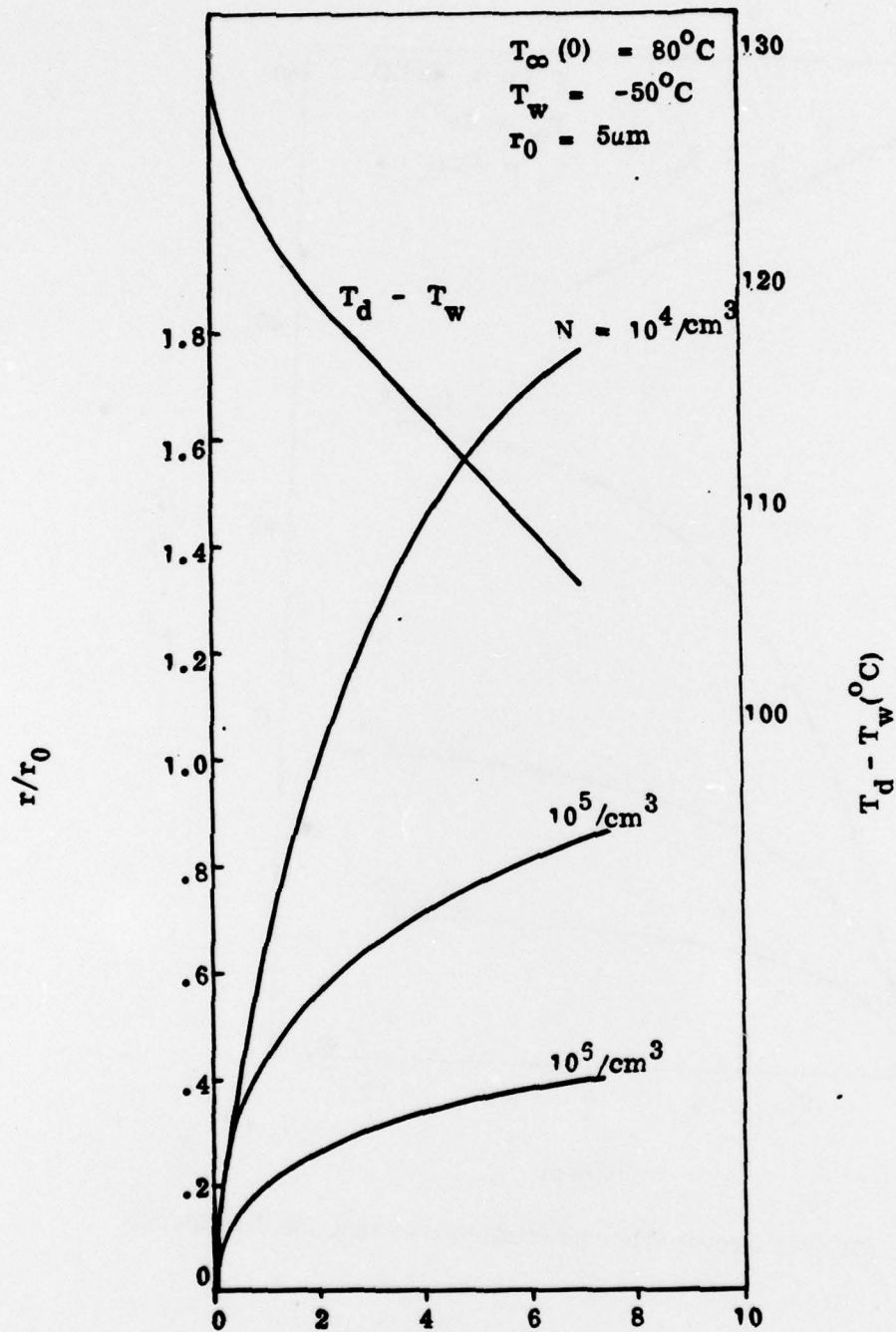
Figure C-5. Droplet Growth Characteristics (see text for discussion)
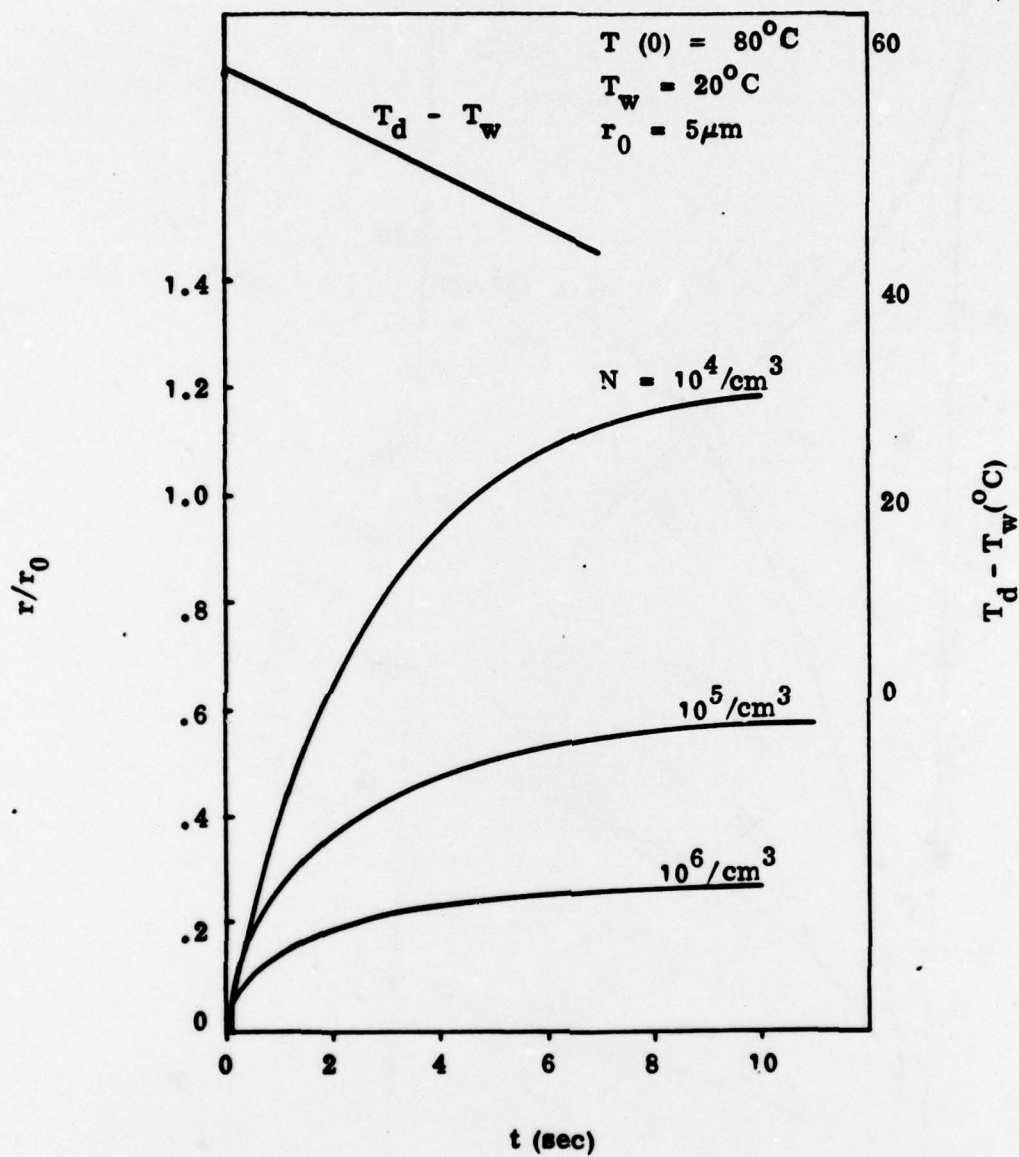
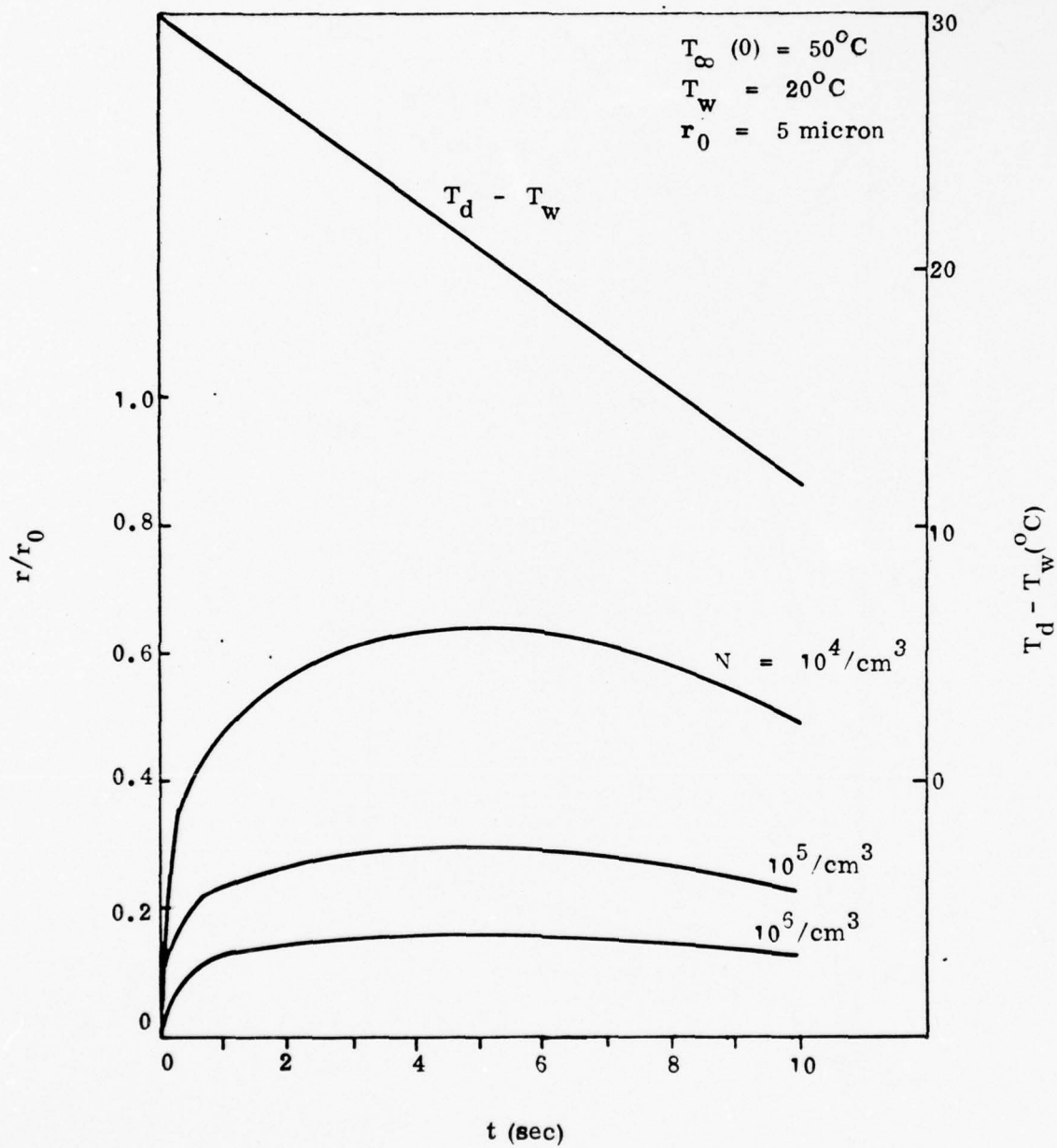Figure C-6. Droplet Growth Characteristics (see text for discussion)
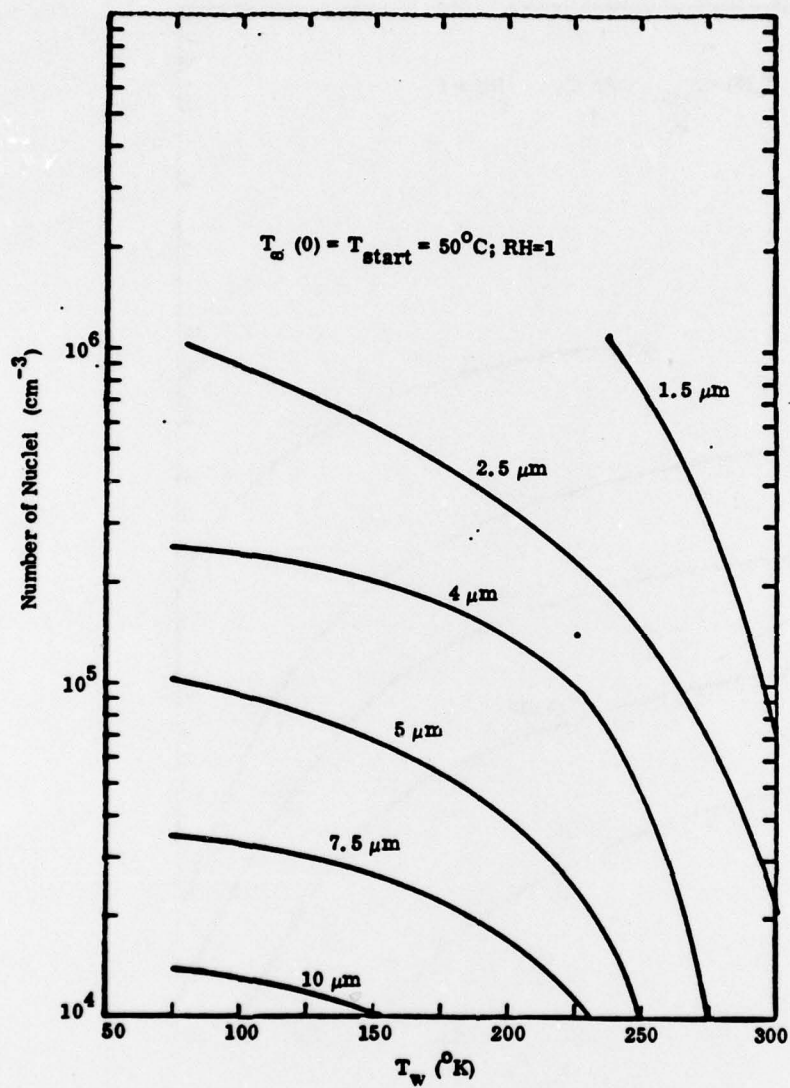
Fig. C-7. Contours of Maximum Radii Obtained

C-11
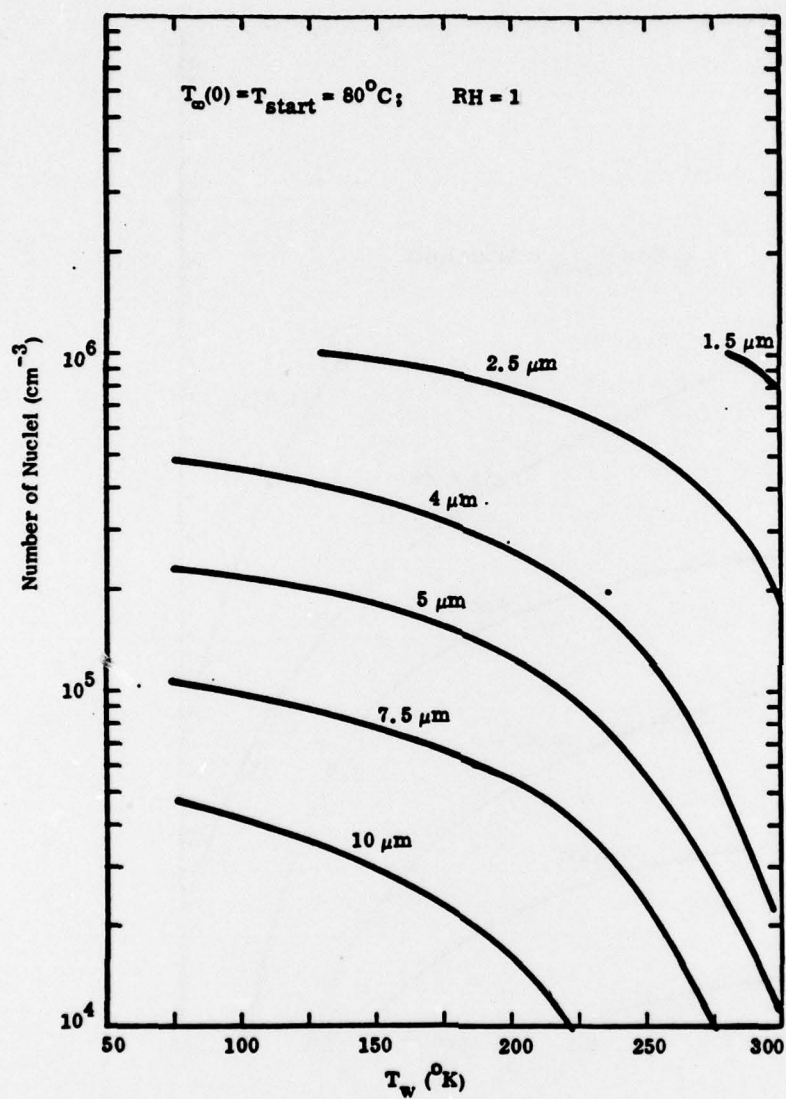
Figure C-8. Contours of Maximum Radii Reached

C-12

DISTRIBUTION LIST

DISTRIBUTION LIST FOR ONR PHYSICS PROGRAM OFFICE
UNCLASSIFIED CONTRACTS

Director   3 copies
Defense Advanced Research Projects Agency
Attn: Technical Library
1400 Wilson Blvd.
Arlington, Virginia 22209

Office of Naval Research   3 copies
Physics Program Office (Code 421)
800 North Quincy Street
Arlington, Virginia 22217

Office of Naval Research   1 copy
Assistant Chief for Technology (Code 200)
800 North Quincy Street
Arlington, Virginia 22217

Office of Naval Research   6 copies
Code 715LD (ONR/London)
800 North Quincy Street
Arlington, Virginia 22217

Naval Research Laboratory   3 copies
Department of the Navy
Attn: Technical Library
Washington, D. C. 20375

Office of the Director of Defense   3 copies
   Research and Engineering
Information Office Library Branch
The Pentagon
Washington, D. C. 20301

U. S. Army Research Office   2 copies
Box 12211
Research Triangle Park
No. Carolina. 27709

Defense Documentation Center   12 copies
Cameron Station (TC)
Alexandria, Virginia 22314

Director, National Bureau of Standards   1 copy
Attn: Technical Library
Washington, D. C. 20234

Commanding Officer   3 copies
Office of Naval Research Branch Office
536 South Clark Street
Chicago, Illinois 60605

Commanding Officer   3 copies
Office of Naval Research Branch Office
1030 East Green Street
Pasadena, California 91101

San Francisco Area Office   3 copies
Office of Naval Research
One Hallidie Plaza
Suite 601
San Francisco, California 94102

Commanding Officer   3 copies
Office of Naval Research Branch Office
495 Summer Street
Boston, Massachusetts 02210

New York Area Office   1 copy
Office of Naval Research
715 Broadway, 5th Floor
New York, New York 10003

Director   1 copy
U. S. Army Engineering Research
  and Development Laboratories
Attn: Technical Documents Center
Fort Belvoir, Virginia 22060

ODDR&E Advisory Group on Electron Devices   3 copies
201 Varick Street
New York, New York 10014

Air Force Office of Scientific Research   1 copy
Department of the Air Force
Bolling AFB, D. C. 22209

Air Force Weapons Laboratory   1 copy
Technical Library
Kirtland Air Force Base
Albuquerque, New Mexico 87117

Air Force Avionics Laboratory   1 copy
Air Force Systems Command
Technical Library
Wright-Patterson Air Force Base
Dayton, Ohio 45433

2

Lawrence Livermore Laboratory   1 copy
Attn: Dr. W. F. Krupke
University of California
P. O. Box 808
Livermore, California 94550

Harry Diamond Laboratories   1 copy
Technical Library
2800 Powder Mill Road
Adelphi, MD 20783

Naval Air Development Center   1 copy
Attn: Technical Library
Johnsville
Warminster, Pennsylvania 18974

Naval Weapons Center   1 copy
Technical Library (Code 753)
China Lake, California 93555

Naval Training Equipment Center   1 copy
Technical Library
Orlando, Florida 32813

Naval Underwater Systems Center   1 copy
Technical Library
New London, Connecticut 06320

Commandant of the Marine Corps   1 copy
Scientific Advisor (Code RD-1)
Washington, D. C. 20380

Naval Ordnance Station   1 copy
Technical Library
Indian Head, Maryland 20640

Naval Postgraduate School   1 copy
Technical Library (Code 0212)
Monterey, California 93940

Naval Missile Center   1 copy
Technical Library (Code 5632.2)
Point Mugu, California 93010

Naval Ordnance Station   1 copy
Technical Library
Louisville, Kentucky 40214

Commanding Officer   1 copy
Naval Ocean Research & Development Activity
Technical Library
NSTL Station, Mississippi 39529

Naval Explosive Ordnance Disposal Facility   1 copy
Technical Library
Indian Head, Maryland 20640

Naval Ocean Systems Center   1 copy
Technical Library
San Diego, California 92152

Naval Surface Weapons Center   1 copy
Technical Library
Dahlgren, Virginia 22448

Naval Surface Weapons Center   1 copy
Technical Library
Silver Spring, Maryland 20910

Naval Ship Research and Development Center   1 copy
Central Library (Code L42 and L43)
Bethesda, Maryland 20084

Naval Avionics Facility   1 copy
Technical Library
Indianapolis, Indiana 46218

Scientific Officer   1 copy
Physics Program
Office of Naval Research
800 North Quincy Street
Arlington, Virginia 22217
Attn: Dr. Bob Junker
Reference Contract No: N00014-77-C-0591

DCASMA, Boston   1 copy
666 Summer Street
Boston, Massachusetts 02210
Attn: James P. Edwards/DCRB-DBGB-1
        Administrative Contracting Officer

Director, Naval Research   6 copies
Laboratory, Attn: Code 2627
Washington, D.C. 20375

Office of Naval Research   6 copies
Department of the Navy
Arlington, Virginia 22217
Attn: Code 1021P

4